Development of 664GHz Sub-harmonic Mixers

Paul Richard Wilkinson

Submitted in accordance with the requirements for the degree of Doctor of Philosophy

April 2014

The University of Leeds, School of Electronic and Electrical Engineering, Institute of Microwaves and Photonics

STFC Rutherford Appleton Laboratory, Millimetre-Wave Technology Group

The candidate confirms that the work submitted is his/her own, except where work which has formed part of jointly authored publications has been included.

The contribution of the candidate and the other authors to this work has been explicitly indicated below. The candidate confirms that appropriate credit has been given within the thesis where reference has been made to the work of others.

The primary jointly authored publication is "A 664 GHz Sub-Harmonic Schottky Mixer - Paul Wilkinson, Manju Henry, Hui Wang, Hoshiar Sanghera, Byron Alderman, Paul Steenson and David Matheson - International Symposium on Space Terahertz Technology – Oxford University, March 2010."

This is primarily the work of the candidate as featured in Chapters 3 & 4 of this thesis, design support was given by M Henry and H Wang, diode fabrication was completed by H Sanghera, device assembly and supervision given by B Alderman, supervision by P Steenson and D Matheson was the group leader and provided overall guidance.

The second design paper from the UK/Europe-China workshop (full details on page 5) is similar to the first mentioned above but only based on the work in Chapter 3.

Acknowledgements

First of all I would like to thank my primary academic supervisor, Paul Steenson for all of his help and support over the years.

I would also like to thank the rest of the team at the University of Leeds School of Electric and Electronic Engineering especially the cleanroom support staff for their assistance.

The Millimetre Wave Technology team at STFC's Rutherford Appleton Laboratory were a big help and welcomed me into the team during the 20 months that I spent with them. Their expertise in the area really helped me build up knowledge of the field. Peter Huggard, Byron Alderman, Manju Henry, Hui Wang and Simon Rae deserve a special mention as do the teams from the Diode Facility and the Precision Workshop who fabricated most of the devices.

The team at Radiometer Physics (Germany) require a mention for their assistance in measuring the performance of the final designs and for other helpful input too.

Without ESA and the project portfolio of Peter de Maagt the project would not have received the funding which made this research possible.

The informal support and encouragement of many friends has been indispensable, and I would like particularly to acknowledge the contribution of Jonathon Fuller and Owen Jackson.

Final thanks must go to my (now) wife, Claire, for her understanding and support during the preparation of this thesis.

Abstract

Due to demand from Earth and astronomical sensing applications a sub-harmonic Schottky diode based mixer is designed and optimised to work at a receiver frequency of 664GHz. Practical work is undertaken to lower the junction capacitance of the diodes by fabricating them with smaller anode sizes by using electron beam lithography instead of ultra-violet photolithography.

The diode topology is optimised focusing on the diode fingers themselves to improve performance at this frequency by studying the component electrical characteristics of the diode and then optimising the inductance of the diode fingers. This is the major novel activity in this body of work and shows that subtle changes in the design can have a large positive effect on the performance of the diodes at these ultra-high frequencies.

The optimised diodes are used as the basis of a sub-harmonic mixer design which is designed to work at a centre frequency of 664GHz. After initial difficulties and a re-design the conversion loss of the mixer is measured at 15-16dB with a noise temperature of 9000K which whilst below the target performance is still a significant achievement. The optimised diodes in a separate mixer also operating at 664GHz are shown to give a performance of 11dB conversion loss and around 3500K noise temperature. The diodes and this second mixer (designed by RPG) are now available commercially.

Publications relevant to work completed during this PhD

A 664 GHz Sub-Harmonic Schottky Mixer – Paul Wilkinson, Manju Henry, Hui Wang, Hoshiar Sanghera, Byron Alderman, Paul Steenson and David Matheson – International Symposium on Space Terahertz Technology – Oxford University, March 2010

The Design of a 664 GHz Sub-Harmonic Mixer – Paul Wilkinson, Manju Henry, Hui Wang, Hoshiar Sanghera, Byron Alderman, Paul Steenson and David Matheson – 2nd UK/Europe-China Workshop on Millimetre Waves and Terahertz Technologies – RAL, Oct 2009

Schottky Diode Technology at the Rutherford Appleton Laboratory – B. Alderman, H. Sanghera, M. Henry, H. Wang, P. Wilkinson, D. Williamson, M. Emery, and D. N. Matheson – RAL. Oct 2009

High Power Frequency Multipliers to 330 GHz – Byron Alderman, Manju Henry, Alain Maestrini, Jesús Grajal, Ralph Zimmermann, Hosh Sanghera, Hui Wang, Paul Wilkinson, and David Matheson – 5th European Microwave Integrated Circuits Conference – Paris, Sept 2010

The diode optimisation work detailed in this thesis could not be published due to commercial sensitivity issues.

Contents

List of tables and illustrations

Abbreviations used in this Thesis

AC – Alternating Current

ADS – Advanced Design System (Agilent)

ALMA – Atacama Large Millimetre Array

DC – Direct Current

ESA – European Space Agency

HFSS – High Frequency Structural Simulator (Ansoft)

HIFI – Heterodyne Instrument for the Far Infrared (on board ESA's Herschel telescope)

IF – Intermediate Frequency

IV – Current Voltage

LO – Local Oscillator

MHS – Microwave Humidity Sounder (instrument on MetOp satellite)

PMMA – Poly(methyl methacrylate)

RAL – Rutherford Appleton Laboratory

RF – Radio Frequency

RPG – Radiometer Physics GmbH

SEM – Scanning Electron Microscope

STFC – Science and Technology Facilities Council

Chapter 1 - Introduction

Passive millimetre wave detection has a growing market especially with security interest in mm wave imaging systems and with radio astronomy. All passive mm wave detectors operate somewhere between 30 GHz and 3000 GHz (wavelengths between 10mm and 0.1mm)and detect naturally occurring radiation. Particular areas of interest for this project are 330 GHz and 660 GHz as around these frequencies there are absorption peaks of interest from commonly found molecules in the atmosphere and space. There are other applications around these frequencies including molecular spectroscopy, security imaging and radar systems.

This area of the spectrum has not yet been fully exploited but advancements have been made driven by scientific applications in remote sensing and astronomy (e.g. ALMA, HERSCHEL HIFI, MetOp MHS). In remote sensing the 664GHz channel can be used for detecting cirrus clouds and cloud ice path measurements which are in turn used to calculate cloud ice content measures that can be used to refine climate models.

The choice of frequency is due to a combination of the science needs and the fact that relatively few results have been reported at 664GHz and there is an opportunity to demonstrate novel performance. There is a limited availability of components, system and test hardware up to 1000GHz but this is improving and should not be an issue for the project.

Direct detection of these frequencies is not possible at sufficient spectral resolution, with high sensitivity and low noise and a large instantaneous bandwidth, to be useful with any existing technology. Other useful attributes for a direct mm (or submm) wave detector are being simple, inexpensive, rugged and compact. The last three of these attributes are useful as often this sort of instrument is flown at high altitude on light aircraft, balloons or even satellites in order to meet the science needs. This is because there is a lot of interest in atmospheric observations using mm wave frequencies.

Indirect detection of these frequencies is a far better method. Heterodyne receivers mix the desired input signal with a fixed known signal called the local oscillator which is usually near or in the desired frequency range of the input signal. This gives a mixed output signal which contains several product signals. The two main products come from multiplying together two sinusoidal waves using a common trigonometric identity.

$$\sin(A) \cdot \sin(B) \equiv \frac{1}{2}\left[\cos(A-B) - \cos(A+B)\right]$$

$$v_1(t)v_2(t) = \frac{A_1 A_2}{2}\left[\cos 2\pi(f_1 - f_2)t - \cos 2\pi(f_1 + f_2)t\right]$$

This clearly shows the two main products come from the sum of the original frequencies *(f_1+f_2)* and the difference between them *(f_1-f_2)*. As mixers are not perfect, the input frequency and the local oscillator can also normally be detected in the output signal from the mixer, but once the mixer is in a system, all but the most useful part of the output is usually filtered out. The most useful part is the difference signal as this can be detected with good spectral resolution and high instantaneous bandwidth (usually limited by the bandwidth of the mixer) as it is usually well under 50GHz. Existing detector technology at these frequencies is readily available, such as vector network analysers.

1.1 Types of Detection

Direct Detection

There are several types of direct detector available at high frequencies (anything over 150GHz). Bolometers are about the only sensitive method of direct detection available, but they operate over a broad spectral range and although they can achieve good spectral resolution, they have a small instantaneous bandwidth as a result of the use of a Fabry-Perot filter. Fabry-Perot filters work by internal reflections between two surfaces where the distance is variable. The distance can be changed to tune the frequency response of the filter and to sweep it across a large range of frequencies. The small instantaneous

bandwidth of these filters make measurements over a large range of frequencies time consuming.

Heterodyne Detection

Use of a nonlinear component (such as a Schottky diode junction) in a heterodyne detector (e.g. mixer) can provide both a fine spectral resolution and a potentially large instantaneous bandwidth. However, they are generally more complicated devices and require a high frequency local oscillator signal which can be difficult to obtain for sub-mm operation.

The main high sensitive heterodyne receiver types are those based on superconducting tunnel junctions, hot electron bolometers and Schottky barrier diodes. SIS (superconductor-insulator-superconductor) junctions have achieved record sensitivity and low noise [1]levels and are the first choice for radio astronomy applications. Hot electron bolometers also show good sensitivity, but they suffer from the same limited bandwidth problems as direct detection bolometers. Both SIS and bolometer based systems require cryogenic cooling which increases their complexity and therefore cost for design, assembly and ongoing use. Both systems also require very low LO power, typically under 1μW. This means that it can be more practical to get a LO signal for such sub-systems, especially at very high frequencies (>500GHz).

Heterodyne receivers using Schottky diodes have the advantage of working well at room temperature (although if they are cooled to cryogenic temperatures, sensitivity improves). This means they are simpler to integrate into compact airborne or space based instruments and they are also ideal for taking measurements over longer periods of time as the running costs are a lot lower. They do require larger LO powers at room temperature though, in order to get the required sensitivity. Applying a DC bias to the junction can also improve sensitivity but at the expense of additional noise.

The requirement for much larger LO powers at ever increasing frequencies has led to the development of constantly improving frequency multipliers and multiplier chains in order to provide good LO signals resulting from more easily available signals. In general the power available at a given frequency is inversely proportionate to the frequency, so as you increase the frequency the power drops.

One way of alleviating this problem is to use sub harmonic mixers. In fundamental mixers the LO signal is around the same frequency as the frequency being detected, but in a sub harmonic mixer the LO is around half the frequency with a trade-off with conversion efficiency and LO power requirement. This means that a higher powered LO source will more likely be available. Sub harmonic mixers do require a higher powered LO source than their fundamental equivalent although a sub harmonic mixer would be simpler than a multiplier and mixer combination if the LO was not readily available.

Generation of LO

Direct generation of THz frequencies across the whole mm wave range is not possible and the gap widens further when you require the signal at room temperature to drive a Schottky based multiplier. There are two primary directions from which to approach the problem, electrical and optical and presently both are not without problems.

From the electrical side devices such as Resonant tunnelling diodes and Gunn diodes are capable of producing signals of up to about 0.75 THz, but at very low power levels [2]. They can be used in arrays to increase the power output, but high frequency arrays have not yet been demonstrated [34].

From the optical side, Quantum cascade lasers are an area of current development and are approaching 1THz operation [56], but still at low powers and they require cryogenic temperatures. Devices at the lowest frequencies (i.e. a few THz) also operate in pulsed modes and not continuous wave.

Other techniques such as stacking Josephson junctions and shaping the stacks into resonant cavities has produced small powers up to 0.85THz but the devices are still in relatively early stages [7].

In order to get higher power at the relevant frequencies the most common practical options are electrical up-converting from lower frequencies or down-converting from higher optical ones.

Up-converting uses a non-linear element (such as a Schottky diode) which is excited to generate harmonics. One of the harmonics is then extracted and used as the LO. The extracted harmonic is usually of a higher frequency than the input signal and these devices are usually referred to as Schottky multipliers. They are usually realized as doublers or triplers and can be combined into chains to multiply further.

Down-converting signals into the THz region can be done by photomixing of two lasers. This relies on a similar principle to heterodyning and has produced signals a few mW in strength, but the stability of the lasers remains a major problem.

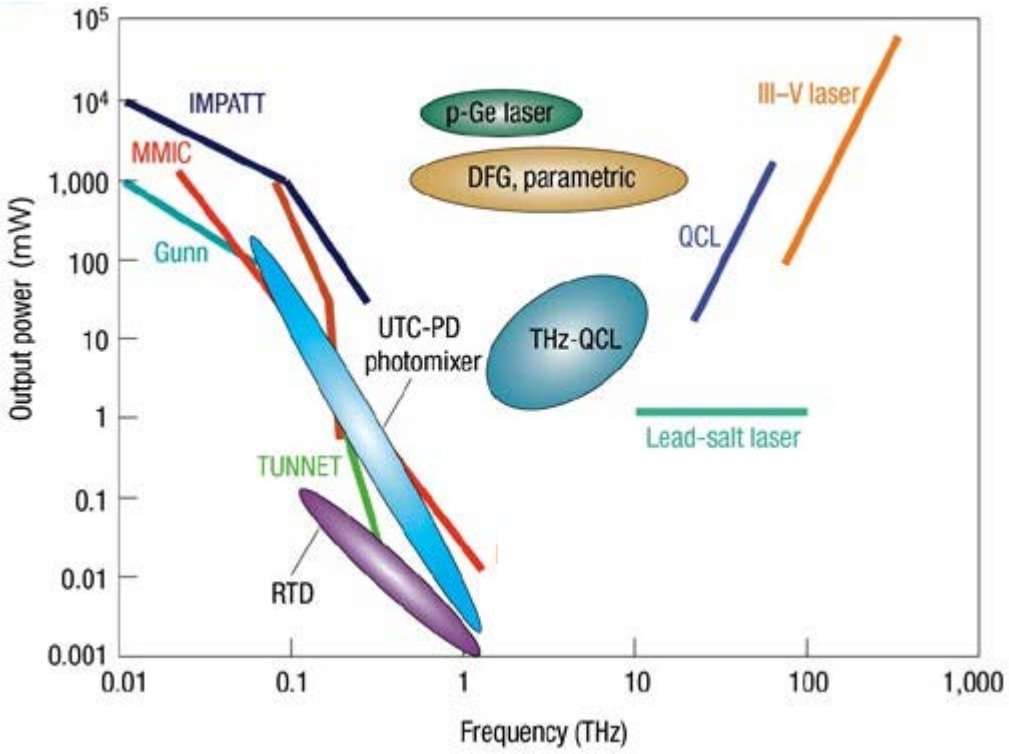

Figure 1-1 (reproduced from [8]) - THz-emission power as a function of frequency. Solid lines are for the conventional THz sources; IMPATT diode stands for impact ionization avalanche transit-time diode, MMIC stands for microwave monolithic integrated circuit, TUNNET stands for tunnel injection transit time. Ovals denote recent THz sources. The values of the last two are indicated by peak power; others are by c.w. power.

In Figure 1-1 the devices below 1THz are mainly limited by parasitic capacitance and transit time limits. Those above 1THz are limited by inter or intra band bandgaps.

Quasi Optical Systems

There are two main types of sub-mm wave Schottky diode receiver systems. These are based around quasi-optical and waveguide systems.

The initial quasi-optical design was the corner cube antenna. This uses a 90° corner reflector (like 3 adjacent sides of a cube) with a wire antenna coupled to the Schottky chip. They are quite a mature technology and have been built at frequencies up to a few Terahertz. The main disadvantage of quasi optical systems is the relatively poor main beam efficiency. In the case of the corner cube antenna [9]this reduces the amount and

quality of the signal that even makes it into the device. Other antenna forms in quasi-optical systems have been tried, including double slot and thin membrane approaches but they are generally outperformed by waveguide structures.

Waveguide Systems

In waveguide structures the signal is coupled into the waveguide using a corrugated feed horn and nearly perfect coupling efficiency can be achieved [10] by such approaches. Waveguide structures have become the most common form of Schottky diode receivers especially with the growth in planar diode technology and control and reproducibility of embedding impedances.

Both types of system, waveguide and quasi-optical, can be built using either whisker contacted or planar Schottky diodes, although planar diodes are becoming by far the dominant type mainly due to their robustness, although the parasitic capacitances are somewhat higher than for the whisker contacted junctions.

Whisker Diodes

The modern day whisker contacted geometry uses an array of holes in oxide which sit over preformed metallised Schottky contacts on the epitaxial layer. This metallised area is then contacted with the metal whisker. This provides a very low parasitic contact to the diode which is the main reason for its high performance and therefore use at submillimeter wavelengths. Another benefit is that the whisker can be used to couple power into the diode, where it acts as a mono-pole antenna and in a corner cube this appears as an array of mono-poles (5 reflections) due to the multiple reflections of the primary whisker in the three faces.

The biggest problem with whisker contacted diodes is that they are not very reliable when it comes to vibration and shock tests. They can be made rugged enough for airborne or space operation, but this becomes more difficult as the anode is made smaller because

the whisker has to be kept larger which in turn leads to increased parasitic capacitance due to the metal overlap. It is also very difficult to make receivers using more than one diode.

Planar Diodes

Planar Schottky barrier diodes are a newer development and address the main issues with whisker diodes, because they are fully fabricated using well established lithography techniques. They can also be easily integrated with filters or coupling circuitry on chip too. The fabrication techniques mean the contact is much more rugged and reliable and hundreds of diodes can be fabricated reproducibly and reliably on a single 1cm square wafer. They can also be produced on chip in line with transmission line filters.

1.2 Schottky Diodes

The Schottky diode (named after German physicist Walter Hermann Schottky who first predicted the Schottky effect) is a semiconductor diode which uses a metal-semiconductor junction as a Schottky barrier. This rectifying barrier results in very fast switching times and low forward voltage drop. The fast switching times are a result of the Schottky diode's being majority carrier devices, which means they only utilise one charge carrier. This is in contrast to PN diodes which rely on the recombination of electron-hole pairs which limits the switching speed.

The IV relationship for a Schottky diode can be shown by the Shockley ideal diode equation.

$$I_D = I_S \left(e^{qV_D/NkT} - 1\right)$$

Where,

I_D = Diode current in amps

I_S = Saturation current in amps (typically 1×10^{-12} amps)

e = Euler's constant (~ 2.718281828)

q = charge of electron (1.6×10^{-19} coulombs)

V_D = Voltage applied across diode in volts

N = "Nonideality" or "emission" coefficient (typically between 1 and 2)

k = Boltzmann's constant (1.38×10^{-23})

T = Junction temperature in degrees Kelvin

Figure 1-2 [11] - Shockley ideal diode equation

This diode equation is derived with the assumption that the only processes giving rise to current in the diode are drift (due to E), diffusion and thermal recombination-generation. It doesn't describe the levelling off of the I-V curve at high forward bias due to the internal resistance of the diode.Even for small forward bias voltages the exponential is very large so the subtracted 1 becomes negligible and can be ignored. The equation can

be further simplified by combining the constants into what is called the thermal voltage, V_T.

$$I = I_S e^{V_D/(nV_T)} \quad \text{where} \quad V_T = \frac{kT}{q},$$

Figure 1-3 – Ideal diode equation, simplified.

The ideality figure, n, is usually between 1 and 1.4. As n increases, the non-linearity of the diode decreases and virtually all aspects of a mixers performance become worse. For this reason ideality is often used as a general indicator of a diodes quality and performance.

Ideality is affected by several mechanisms. Surface imperfections at the barrier interface are a major cause of non ideal behaviour. Much care is taken during fabrication to ensure that between the final etching of the anode hole and the deposition of the metal into the hole to create the Schottky contact the clean, fresh semiconductor surface is not affected. This is difficult though, as it takes a finite time for the metal evaporation chamber to pump down between the sample being etched and loaded into the evaporator and the metal being evaporated. One way to improve this is to use a load lock on the vacuum chamber so the entire chamber does not require pumping down to a low enough level.

Despite the prominence of temperature in the equation its effect on mixer efficiency is small [12].

Quantum tunnelling across the Schottky barrier is another current mechanism that deviates the performance of the diode away from ideal behaviour.

The skin effect alsoalters the high frequency resistance associated with the diode as it is the tendency of an AC current to distribute itself so the current density at the edge is higher than that in the centre. This is due to eddy currents created by the AC current and causes the resistance to increase with the frequency of the current.

One area where no evidence can be found is the choice of III-V semiconductor used. Due to it's higher mobility, InP may be a better choice than GaAs, but no extensive studies have been found relating to improved mixing performance of Schottky diodes based on InAs or InP.

Capacitance

In order to operate at THz frequencies the anode must have a diameter of less than 1um. This reduces capacitance of the junction as the capacitance at the anode is directly related to the surface area of the depletion region. It is necessary to reduce the capacitance as high frequency signals cannot effectively modulate the active regions of junction devices with a certain maximum capacitance. This basically manifests itself as a cut off frequency.

The depletion region is formed when the metal is brought into contact with the semiconductor. When this happens electrons from the semiconductor spontaneously move from the semiconductor to the metal due to differences in the Fermi energies. This leaves behind ionised donor locations in the semiconductor. The area containing these ionised donors is called the depletion region as it is free of mobile charge carriers [13].

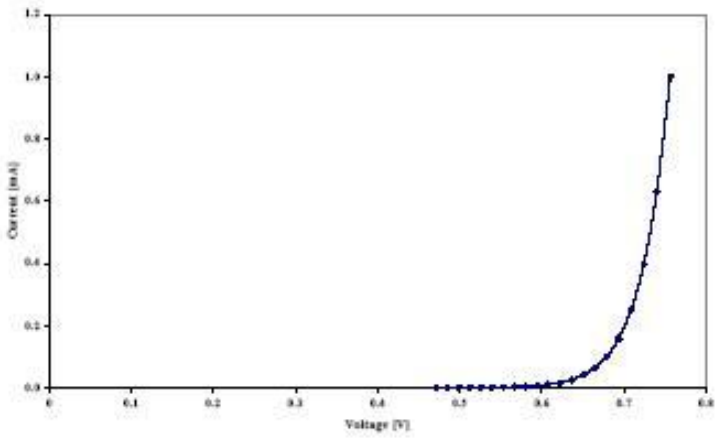

Figure 1-414 - The IV performance of a Schottky Barrier

The junction capacitance is due to the structure and doping of the device, but the overall capacitance of the diode (as measured) is much greater. This is mainly due to the

additional parasitic capacitance between the two metal pads that are used to contact the device however there are other sources of capacitance in such a complicated structure. These capacitances (other than the junction capacitance) are known as parasitics. The only way the junction capacitance can be isolated is by calculation using the junction area and doping densities to calculate the amount of charge separation that takes place.

$$C(V) = \frac{C_{j0}}{(1 - \frac{V}{\phi_{bi}})^{1/2}}$$

Figure 1-5 – An equation relating capacitance to zero junction bias capacitance, Cj0 , built in potential and voltage.

Using the zero bias capacitance and the series resistance of the diode (which can be determined by DC measurements) it is possible to calculate an indicative cut-off frequency for the diode. This makes several assumptions though, including negligence of the skin effect, which affects the resistance of the device at high frequencies.

$$f_c = \frac{1}{2\pi R_s C_{j0}}$$

Figure 1-6 – Equation for calculating the cut-off frequency

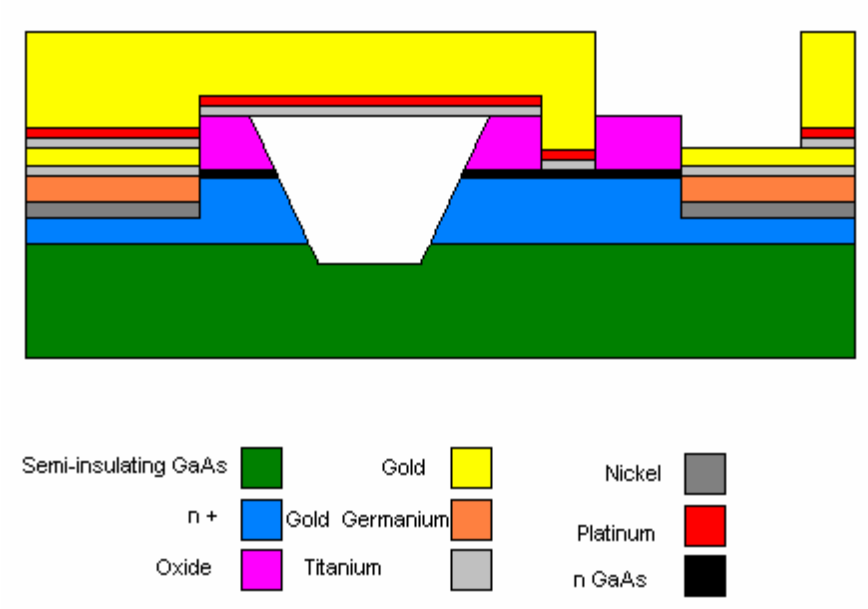

Figure 1-7 [14] – A schematic of a cross section of a diode

Resistance

Series resistance in a Schottky diode structure is caused mainly by the doped semiconductors at the metal interfaces i.e. the ohmic contacts and the Schottky contact. At higher currents the voltage drop across the ohmic becomes significant.

The series resistance can be calculated from the equation show below. ΔVd is the difference in voltage between the measured IV characteristic and the Ideal Diode performance at a particular current.

$$R_s = \frac{\Delta V_d}{I_d}$$

Figure 1-8 – Series resistance

This leads to a larger problem, not with the diodes, but with how they are described. The series resistance measured by this method depends on the current so it can be made to look smaller (and hence the diodes look better) by making the measurements at higher

currents. There is not at present a standard current for characterising diodes and as such across Europe and indeed the world it can be difficult to compare diodes from different manufacturers in literature as they often don't quote the current that the measurements were made at.

Equivalent Circuit

These main components that describe the diode behaviour can be combined into an equivalent circuit and to predict the behaviour of a Schottky diode when used in a mixer or multiplier.

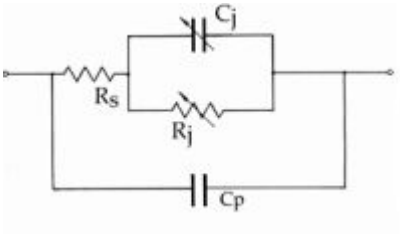

Figure 1-9 [15] – Schottky diode equivalent circuit – C_j is the parasitic capacitance of the depletion region of the junction, R_j is the nonlinear resistance of the Schottky barrier, R_S is the series resistance of the substrate and contacts and C_p is the parasitic capacitance including that between the ohmic contacts.

The performance of the diode ultimately affects the performance of the overall mixer, but other factors, such as impedance matching are also important in the mixer design and fabrication. You can make a bad mixer with a good diode but you can't make a good mixer without a good diode.

1.3 Mixer Circuits

The previous section deals with the characteristics of discrete diodes. This section deals with the characteristics of systems which contain the diodes. This includes losses and noise, which are the most often quoted figures when it comes to mixer performance.

The focus will be on Schottky heterodyne waveguide mounted mixers operating at frequencies of 100GHz and above. Multipliers for similar frequencies will also be discussed.

Harmonic or fundamental Mixers

The difficulty in producing sufficient LO power at higher frequencies has led to the development of subharmonically pumped mixers. The performance of a mixer at higher frequencies may be limited by the lack of sufficient LO power, or by excess LO noise. In these cases it can be better to use a mixer that is pumped at half the required LO frequency and use the second harmonic, produced in the diodes, to mix with the incoming signal. These mixers are based on fairly mature technology and whilst theoretically they cannot match fundamentally pumped mixers of the same frequency, in practice they are not that far behind.

A fundamentally pumped balanced mixer is an attractive option as it avoids the need to inject the LO though a coupler in front of the mixer due to the natural isolation between the LO and the signal within the diode structure. This would make it easier to incorporate in instrumentation. It is practical in general communication mixers, but due to the high frequencies involved in this project is not straightforward. The diode would be feasible to manufacture although would require significant development first, but the LO requirements would be much more difficult to meet because at least two diodes need to be pumped by power generated at the signal frequency and there is nothing available.

A fundamental mixer (single-ended) would have good sensitivity but due to the LO power being coupled with the signal optically or using a lossy waveguide couple more LO power would need to be generated than is required by the mixer and this is not available.

For a given frequency it is usually easier to subharmonically pump a mixer than to use the same source to drive a frequency multiplier. This is because the additional loss in the doubler is higher than the loss from using a harmonic to drive a mixer. At frequencies over 500GHz subharmonic mixers [16] are about twice as good as the latest frequency multiplier [17] driven mixers. With developments in the production of mixer diodes less power is needed but this affects both types of mixer (subharmonic and multiplier driven fundamental mixers) equally, so they both get better. One problem with harmonic mixers is the output bandwidth which is limited by higher IF impedance. Sub-harmonic mixers of this type also give good separation between the signal, LO and IF as the frequencies can be well separated by simple filters in the waveguide cavity.

It is possible to achieve subharmonic mixing with a single diode mixer but the fundamental mixing response is usually much greater than the second harmonic response, which makes the device very inefficient in this form. A much better solution is the use of an anti-parallel diode pair, and if the diodes are identical then there is no fundamental mixing response.

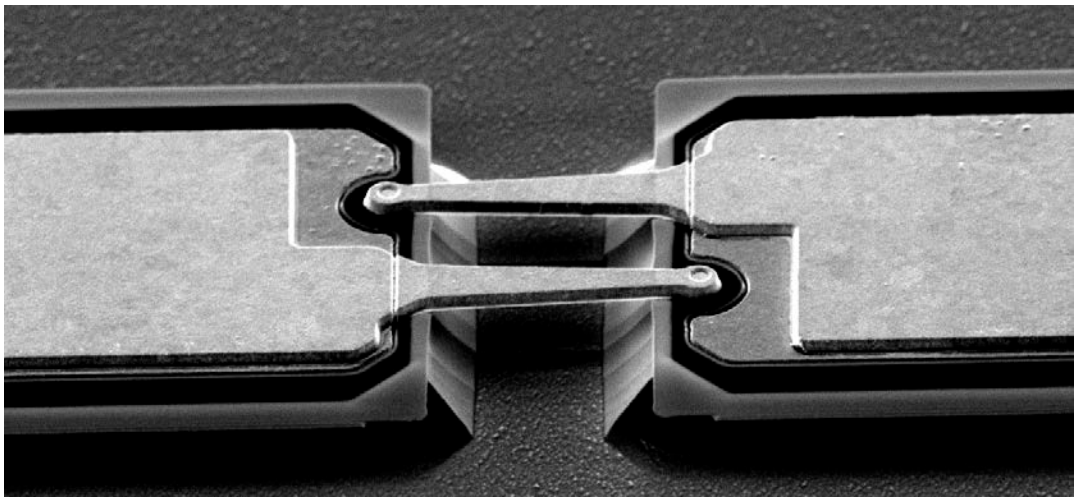

Figure 1-10 - An anti-parallel diode pair produced at RAL. Single diodes can be made using the same process by only exposing and etching one of the anodes before the Schottky contact is made.

Noise

The noise in a mixer has two main components: noise arising from the diode and noise arising as a consequence of noise on the LO/RF signals. The second part of this is fairly straightforward – if you put a noisy signal into a simple mixer you can expect a noisy signal to come out of it. One exception to this is that a well-designed (good diode match) subharmonic mixer will reject LO noise in generation of the harmonic and therefore gives a very clean signal to mix with the RF.

Noise in a diode is dominated by shot noise and thermal noise for low frequency mixers but at higher frequencies noise is created by hot electrons, intervalley scattering and traps at the metal-semiconductor interface [18], [19].Shot noise is caused by the statistical fluctuation in the number of electrons crossing the Schottky junction. Thermal noise is due to the random thermal motion of the charge carriers. Hot electrons are caused by high electric fields in semiconductors and are electrons which are not in thermal equilibrium with the lattice. Intervalley scattering and interface traps are both noise mechanisms which are caused by irregular movement of carriers.

The thickness of the epitaxial layer and the quality of the ohmic contacts to the device have also been shown to affect the noise properties of a Schottky diode [20].

The most common figure given for the noise performance is the double sideband noise temperature. This is a measure of the noise in the system both above and below the carrier frequency. The noise of a device is measured by presenting hot and cold loads to the system.

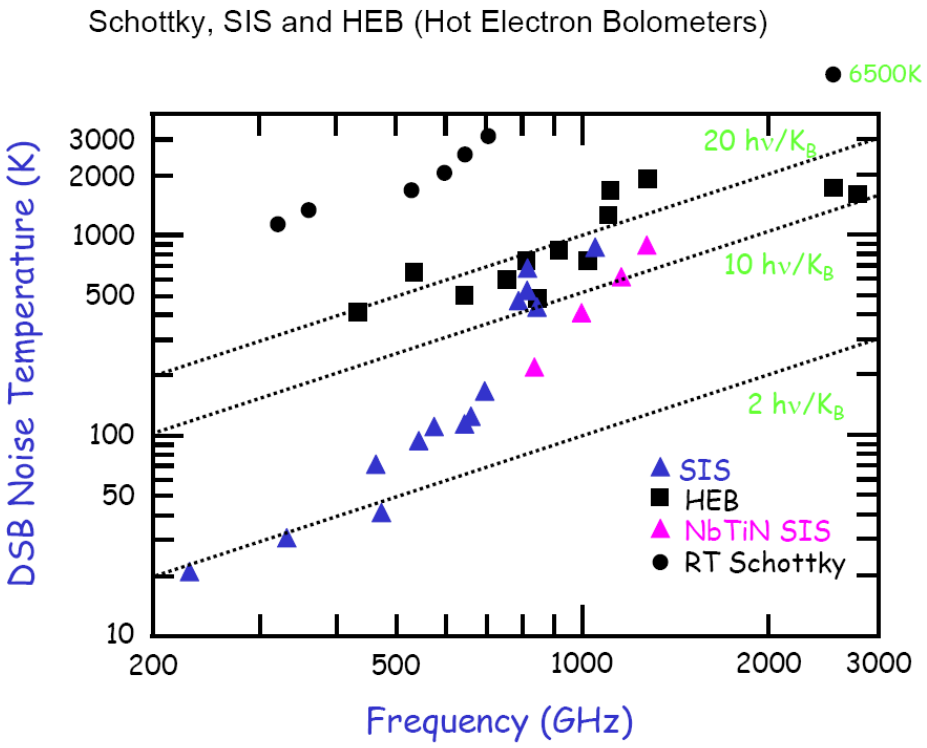

Figure 1-11 – Noise performance of different heterodyne systems (reproduced from [21])

Bias

One way that it is possible to reduce the LO power needed is to bias the diode junction. This means that the signal does not have to drive the oscillation all the way to the knee of the IV curve of the diode. The bias brings the midpoint of the signal closer to the knee so smaller signals can drive the diode to the non linear part of the response, but for back to

back diodes arranging for each to have a separate bias, whilst being closely coupled at millimetre wave frequencies is very challenging.

Integrated diode circuits and Substrate techniques for performance improvement

Traditionally, discrete Schottky diodes have been flipped and soldered onto filters that are mounted in the mixer blocks. Now it is more common to define the transmission line filters as part of the lithography process which means that they are directly coupled to the diodes as the filters are part of the same metal layer as the metal deposited on the diodes and the diodes and filters are then supported by strips of dielectric, such as undoped GaAs or quartz. This helps to reduce the resistance in the device which reduces the losses of the mixer.

Another way of decreasing some of the parasitics in the device is to etch the structure from behind and to either use the membrane that is produced or to transfer this thin structure on to a quartz structure [22], [23].

Performance of existing Devices

Mixer Performance

Actual data on fundamental Schottky diode mixers above 300GHz is scarce, mainly due to the difficulty in generating sufficient LO power, and the competition from SIS mixers. The competitive nature of funding generally from space agencies also makes publication less likely when work is completed.

Type	Frequency (GHz)	When	Who	LO Power (mW)	conversion loss (dB)	dsb noise (K)	Bandwidth (%)	anode size (um)	anode area (um^2)	series resistance (ohms)	diode ideality
sub harmonic WG	183	Jun-07	RAL		4.7	600		2 round	3.1	10.6	1.172
fundemental	640	1998	JPL		8.1	1640		0.4x2	0.8	7	1.31
fundemental WG	585	Sep-00	Virginia		8	1200		0.9 round	0.6	11	1.32
QO	258	Jan-93	Michigan	2.5	7.2	1310	10	1.2 round	1.1	10	1.13
sub harmonic WG	600	1996	JPL	10	12	4200	3	0.4x2	0.8	5.8	1.26
	585	1997	Virginia	1.16	7.6	2380	18	1.2 round	1.1	14	1.17
	690	1997	Virginia	1.04	9.2	2970		1.2 round	1.1	14	1.17
	258	1994	Michigan		7.8	1600		1.5 round	1.8		
sub harmonic WG	665	1992	Massachusets			5100		virginia type 1L8		15	
fifth harmonic WG	650	2004	Helsinki	10dBm (130GHz)	27			virginia type SC1T5			

Sub harmonic WG	340	2012	RPG			1300		unknown			
Sub harmonic WG	448	2012	RPG		5.9	1100		Unknown			
Sub harmonic WG	664	2012	RPG			1500		unknown			
Sub harmonic WG	525	2011	Virginia	2-3	n/a	2000		Unknown			

Figure 1-12 – A table showing high frequency Schottky diode mixer performance [24], [25], [26], [27], [28], [29], [30]

Multiplier Performance

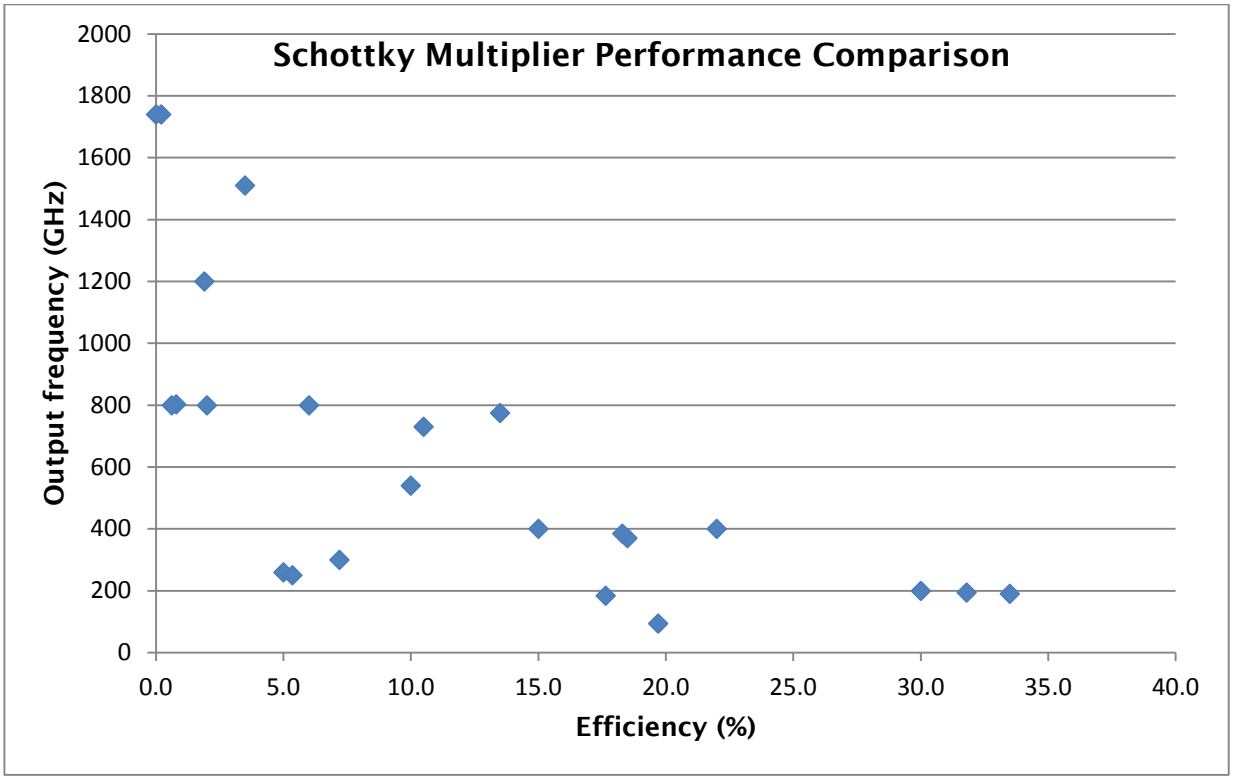

Figure 1-13 – The performance of existing Schottky Multipliers [31], [32], [33], [34], [35], [36], [37], [38]

The above graph shows the difficulty in producing sufficient power to use as LOs to drive mixers at high frequencies as the efficiency plummets even in state of the art devices. The higher frequencies shown are actually multiplier chains. The efficiency combined with the input powers of one or two hundred milliwatts at most explains the microwatt outputs which are insufficient to drive mm wave Schottky mixers.

Availability of Devices

There are only a few sources for obtaining Schottky devices used at frequencies above 100GHz around the world. The main research groups in the field are at Jet Propulsion lab (USA), Technical University of Darmstadt (Germany) and Rutherford Appleton Laboratory (UK). The main commercial suppliers of devices are Virginia Diodes (USA), Radiometer Physics GmbH (Germany) and Teratech (a spin out of the RAL research group – UK). Due to the specialist nature of this work and the competitive interests involved both commercially and academically it is not common for the groups to publish their work in order to protect their intellectual property.

Other on-going projects in the same frequency range

There are 3 projects underway in Europe alone targeting a similar frequency range which shows the demand for such devices is expected to grow. 2 are funded by the European Space Agency and one by the European Union's Framework Programme 7. These are competitive in nature as described above, with the best performing devices likely to be selected for future use in ESA missions.

Modelling of mixer circuit components

This part of the report deals with the various mixer circuit component modelling that has been completed both at the University of Leeds (Microwave office) and Rutherford Appleton Laboratory (ADS and HFSS).

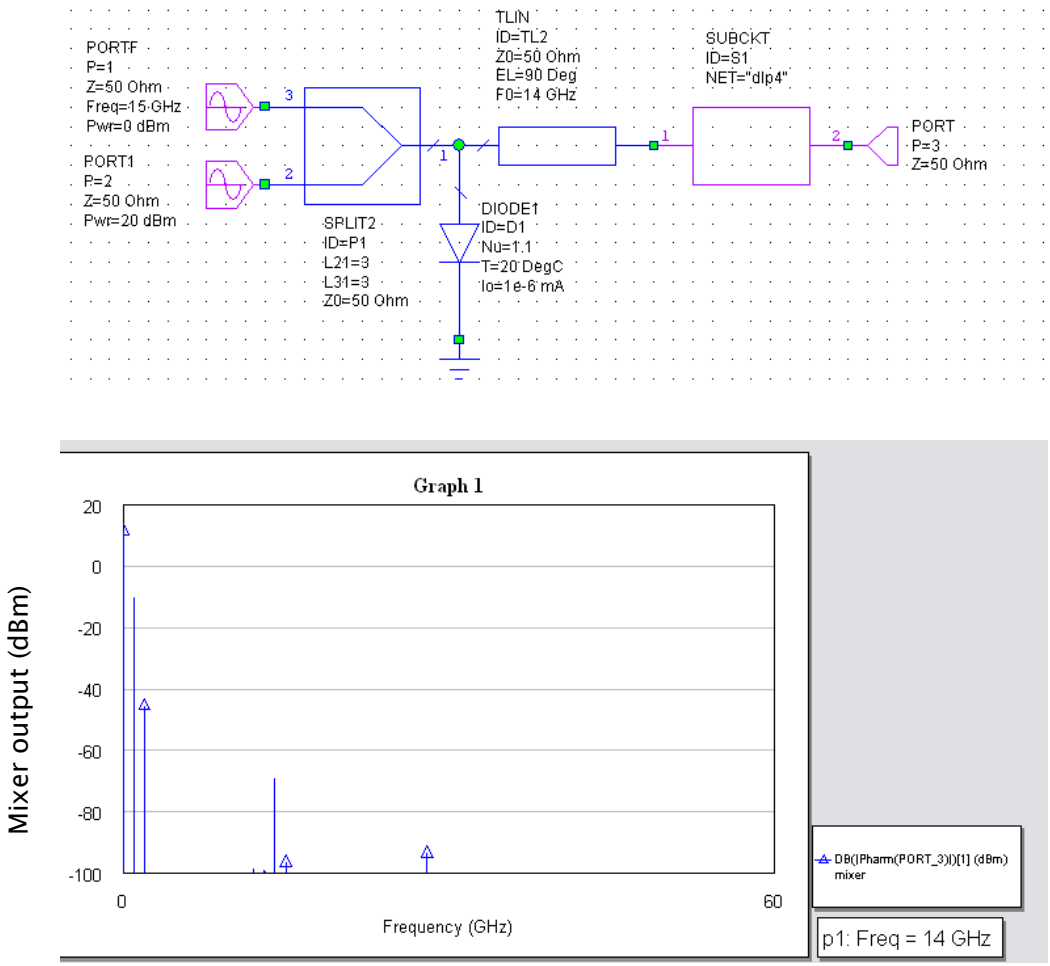

Figure 1-14-Microwave office mixer circuit and output graph showing a typical simulated mixer output spectrum

HFSS familiarisation

The first step of mixer simulations is learning the basics of Ansoft's HFSS (high frequency structural simulator) and Agilent's ADS (Advanced Design System). The first step was familiarisation with HFSS through two tutorials; "Getting Started with HFSS: A Waveguide T-junction" and "Getting Started with Optimetrics: Optimizing a Waveguide T-junction Using HFSS and Optimetrics". These tutorials introduced the basic building blocks of the

software like constructing a device and adding ports before running simulations and graphing the results. The second tutorial started to look at optimising design parameters in order to meet specific performance targets.

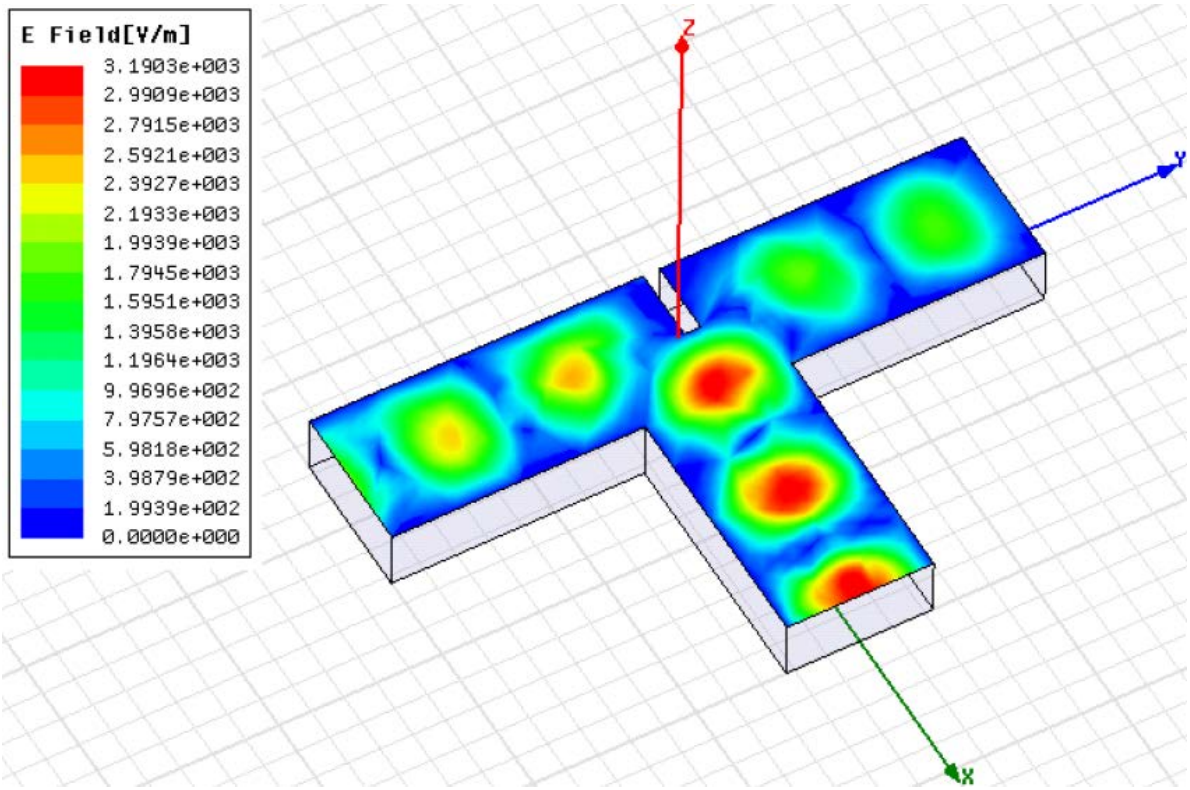

Figure 1-15 – The waveguide T-junction with the E field overlaid showing the field after the design has been optimized to give a 1/3 to 2/3 split in signal by moving the septum.

The optimetrics part in this design was set to vary the distance of the septum from the centre of the T until the output to one port was twice the output to the other port. This is very simple in HFSS as everything can be parameterised and this sort of optimisation then takes the form of a simple equation which the software tries to solve by changing allowed parameters.

Filter Design and Simulation

The next stage was to leave behind waveguides and design a basic microwave band pass filter and simulate it in HFSS and ADS. It was important again to parameterise as much as

possible to make any changes to the designs easier. It was also very important to make sure both designs were identical, but unfortunately global parameters couldn't be exchanged between the two programs. This is what the filter looked like in both programs.

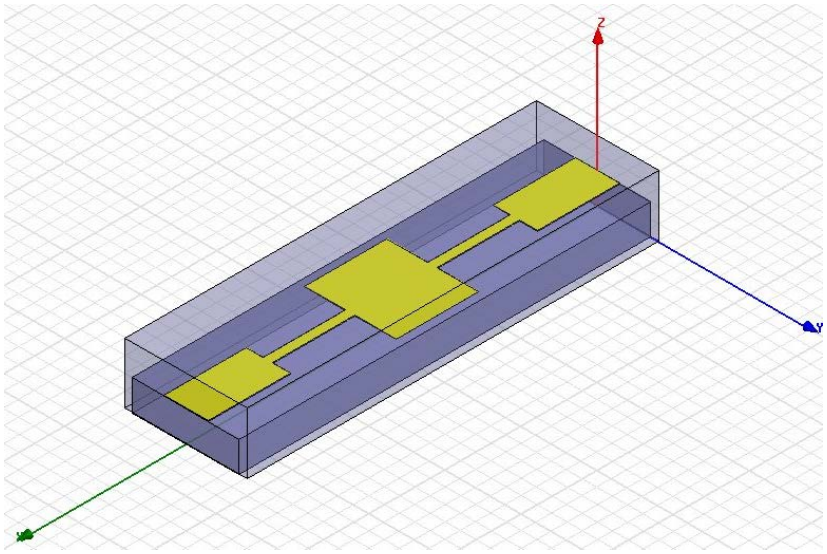

Figure 1-16 – 3D model of filter design in Ansoft HFSS

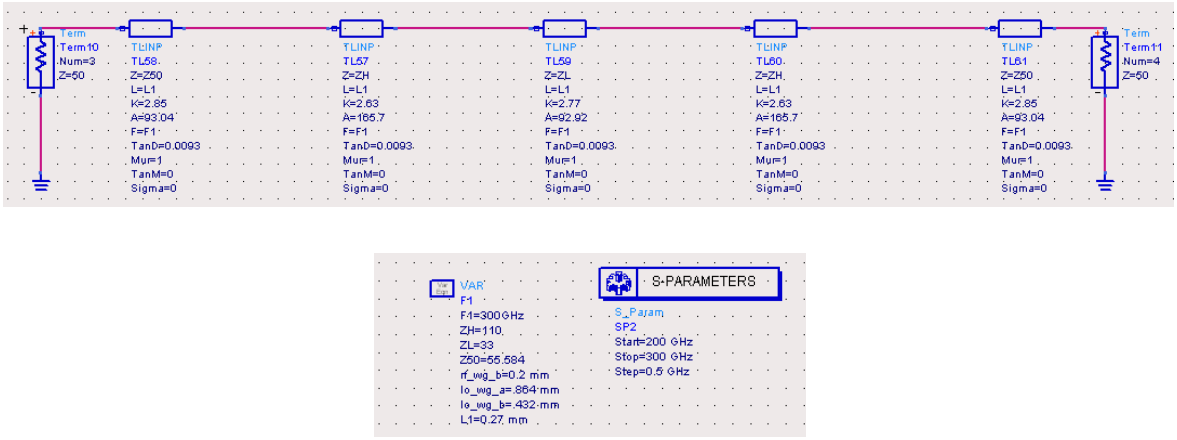

Figure 1-17 – Schematic view in Agilent's ADS of simple filter design without step discontinuity models

This chart compares dBS(1,1) and dBS(1,2) outputs of both initial filters in the range of 170 to 210 GHz.

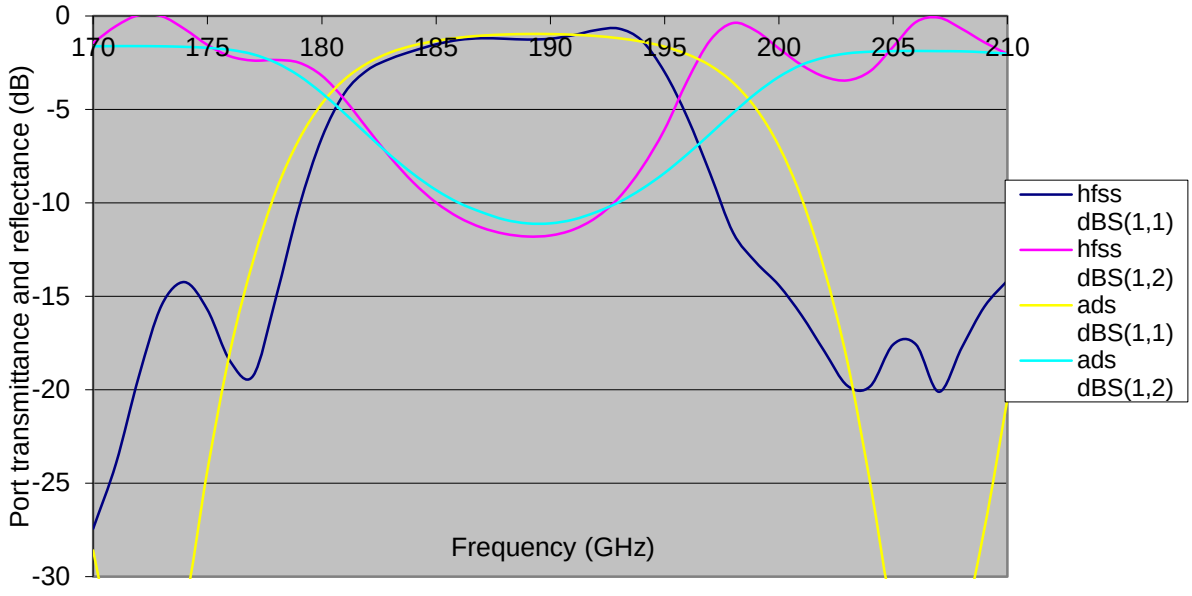

Figure 1-18 – Graph comparing output of initial models

As you can see there is broad agreement from the two different simulations in the band stop area used. A big difference is visible in the reflected signal loss around 175 and 205 GHz with the ADS simulation showing a lot more loss, -15 to -20 for the HFSS trace is still a fairly big loss and whilst not perfect it is acceptable for a filter of this type.

The best way to increase the accuracy of the ADS simulation is to insert junction s parameters between the transmission line elements to simulate the change in width of the lines more accurately. Theses junction s parameters are simulated in HFSS then exported and linked into the ADS project.

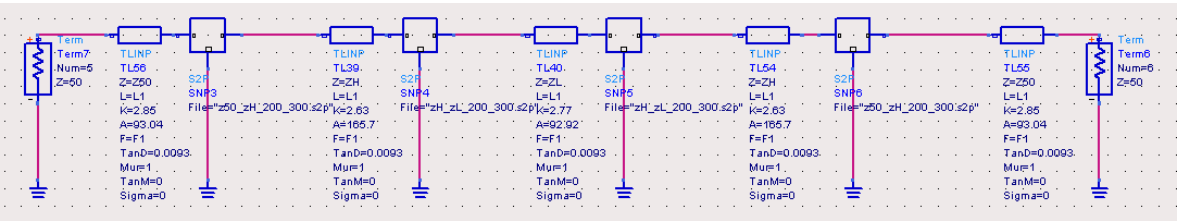

Figure 1-19 – The ADS project design including the junction s parameter blocks

This step brought the results a bit closer (especially after the junction blocks were orientated the right way round). Adding a 50ohm tline at each end of the design in ADS

instead of just telling it there were 50ohm ports at each end also improved the similarity of results (which means the filter ends were not 50 Ohms therefore causing unwanted reflections), but there was still room for improvement. In order to improve the HFSS simulation, the design was checked over thoroughly and boundary conditions were added. The simulation was also changed to include more passes for refinement of the results and more interpolation points on the results graph. This seemed to improve the alignment of the bandpass areas at 175 and 205GHz, but it also shifted the whole band stop area a couple of GHz to the right.

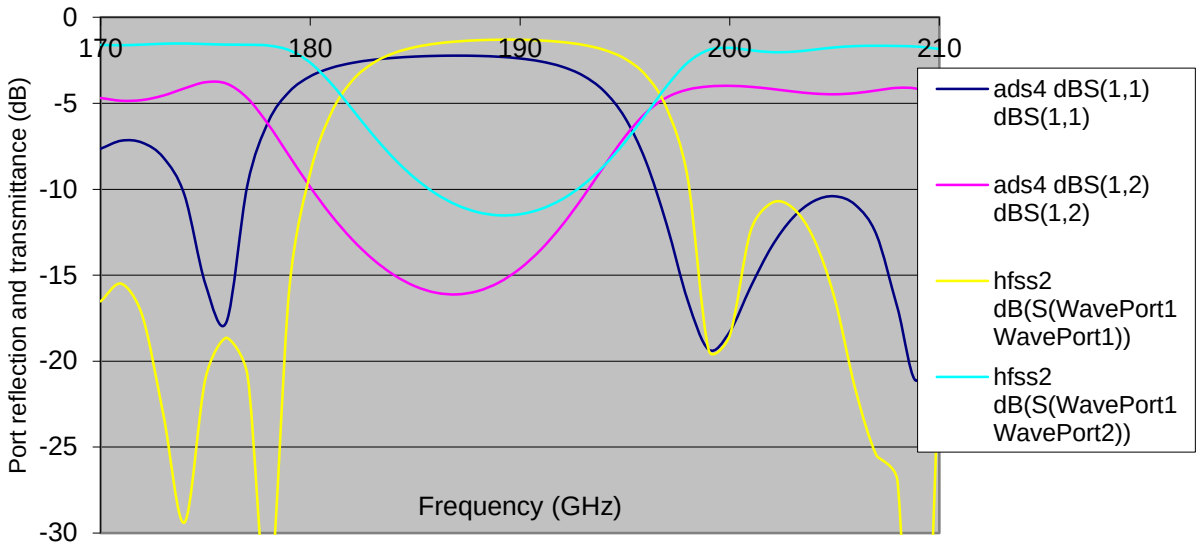

Figure 1-20 - improved HFSS and ADS results

These results were acceptable, but not as close as they should be despite the two totally different approaches that these two pieces of software use.

In an attempt to improve things further the length of each different width of gold was changed from 33mm to 27mm to make it more like a quarter of a wavelength. The design was also rebuilt in both programs from the ground up now that substantially more experience in the programmes had been gained since the designs were initially attempted. The frequency range was also increased to 1-300GHz. There are lots of similarities between the graphs (especially the S(1,1) traces) but the band stop area is significantly

wider in the ADS trace and also has sharper edges. The first minimum after the stop area in each S(1,1) trace also occurs at a very similar magnitude and the overall shape of the graph below 100GHz is very similar for both S(1,1) traces.

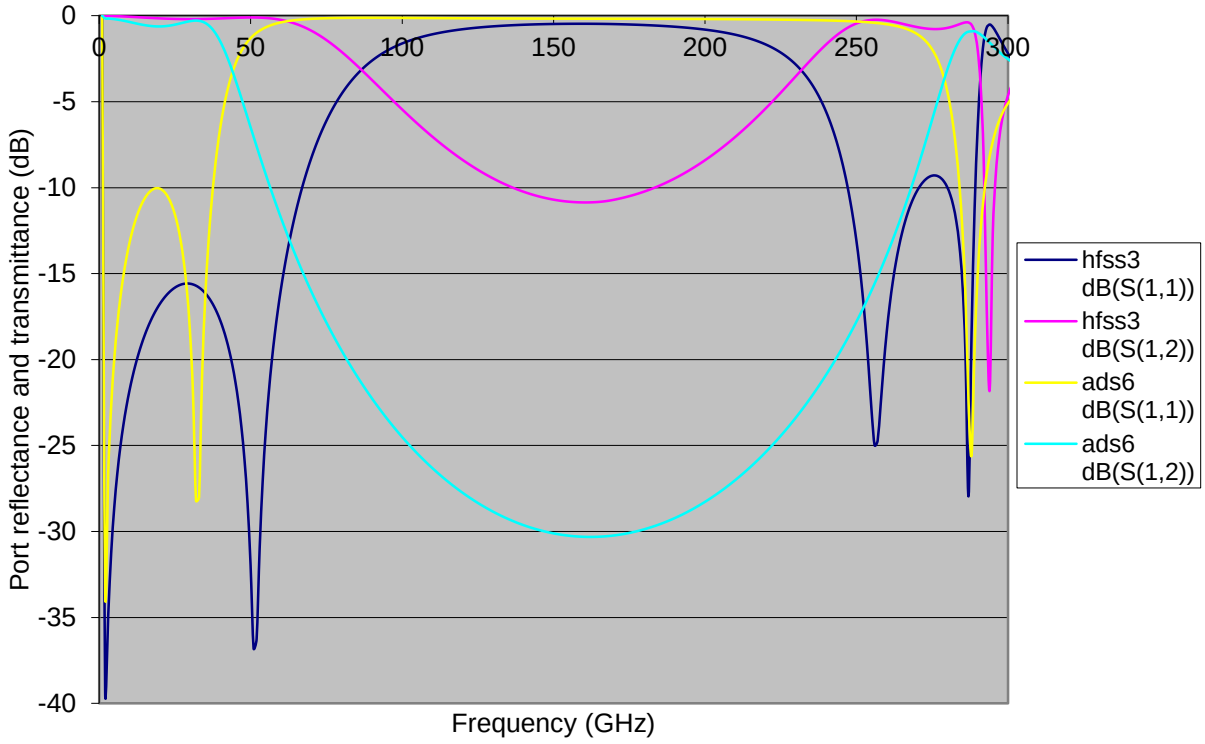

Figure 1-21 - Final HFSS and ADS comparison, over larger range

1.4 Summary

The aim of the project is to design and produce Schottky based fundamental mixers that work at high frequencies (around 330GHz and 660GHz). All practical work so far has tended towards improving the fabrication of existing diodes and decreasing the anode size by using an electron beam lithography (EBL) step instead of a UV photolithography step. This step involves defining the anode area with the E-beam lithography then etching through a 250-300nm oxide layer using RIE to prepare for the overlay finger photolithography stage. The E-beam resist is stripped and then the sample is recoated with new UV-sensitive resist, then the finger and pad are exposed and this also opens a clear area over the EBL exposed anode and the remaining 50nm or so of oxide is etched before the Schottky metal contact is deposited on the finger and anode area. To improve on the diodes produced by photolithography, the anodes must have a diameter of less than 1um. This should be easily possible using EBL and anodes with diameters as small as 100nm should be possible. Smaller anodes enable higher frequencies to be mixed as they reduce some of the parasitics in the diode. One aspect of the future work, besides that of the mixer circuit design and implementation (i.e. membrane or substrate-transfer etc), will investigate the effects on performance of sub-micron anodes and the ratio of the perimeter to area – where the suspicion is that the smallest perimeter to area ratio will give the lowest leakage and noise figure.

Oxide and Resist Etching

The first tests were based around the etch rate of a layer of SiO_2 and the etch rate of the resist (495A8 PMMMA). These tests were necessary in order to ensure that the resist layer was robust enough in the RIE process to mask the areas of the oxide that are not meant to be etched while the 300nm deep holes are etched where they are not covered in resist and under where the anodes are to be deposited. This resist was chosen to provide a thick layer that would be suitable for use in the relatively harsh environment of a plasma etching system.

The resist thickness is also an important factor in the minimum feature size that can be exposed on the electron beam system. In general you can't produce features that are much smaller than the thickness of the resist (typically <0.5 of the resist thickness) but in this case it's not a problem as the anode areas will be larger than 500nm diameter at first.

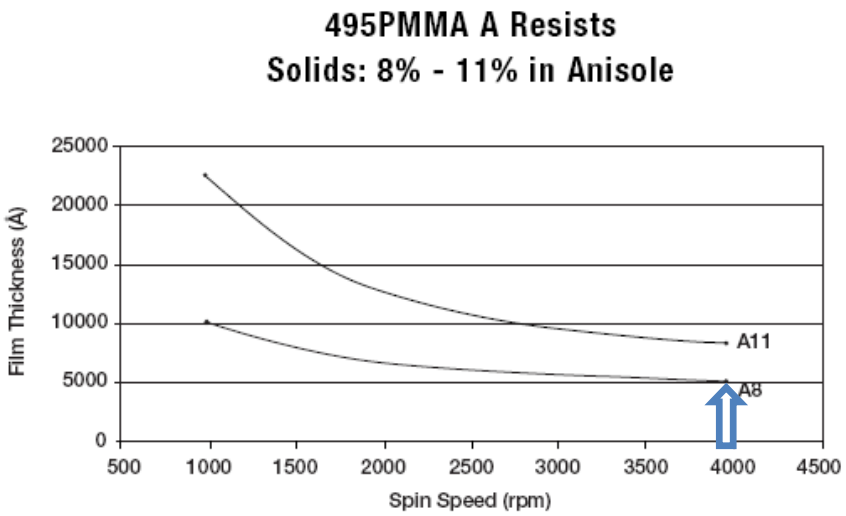

Figure 1-22 – PMMA was spun using this graph from the data sheet as a reference. The arrow shows the desired thickness and spin speed used.

The actual resist thickness varied somewhat, and tended to be on the thicker side of the desired 500nm which was fine as the aim was the thickest possible single layer resist using the resists already available. All resist thickness heights (and etch heights mentioned later) were measured with an Alpha Step IQ Surface Profiler which has a guaranteed 0.1% step height repeatability.

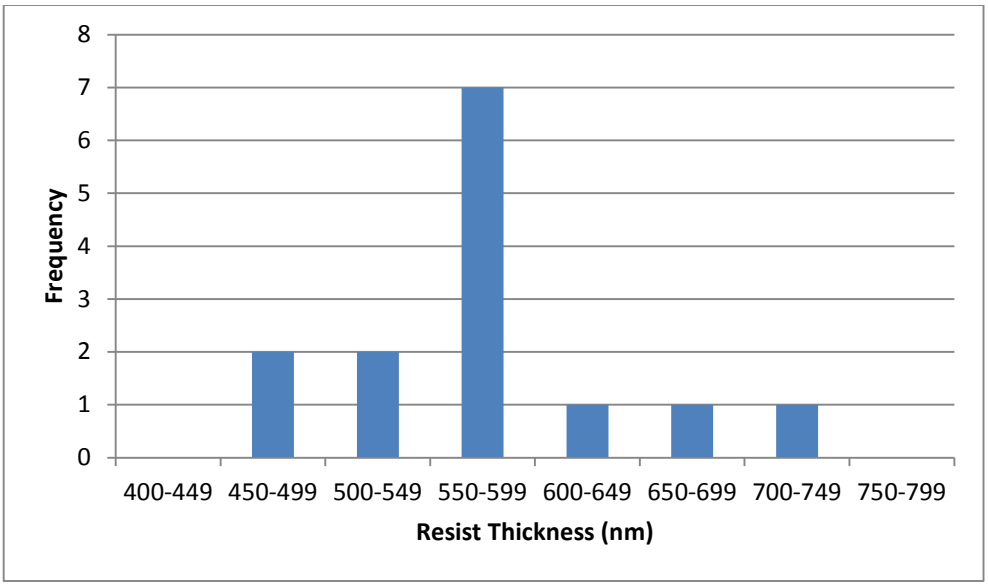

Figure 1-23 – Resist Thickness Variance of PMMA495A8

In the CHF_3 system used at Rutherford Appleton Laboratory (RAL) the resist was etched at the same speed as the underlying SiO_2. This was done using the standard planar Schottky diode process which is 20°C, 30sccm CHF_3, 6sccm Argon, system pressure of 50mTorr, 150W power (with 0W reflected) for 5 minutes. For the first sample (*squares.a*) the step height of the resist before etching was 645±7nm, and the step height after etching was 654±10nm. After cleaning (in acetone, then IPA, then water then dried) the step height was 226±3nm. From this the etch rate of the SiO_2 was calculated to be $0.75nms^{-1}$ and the etch rate of the resist is very similar. After optical inspection on *squares.a* it appeared that the SiO_2 layer had been etched all the way through to the underlying GaAs layer (which is not etched at the same rate as the SiO_2). Because of this result, i.e. the similarity between the PMMA and SiO_2 etch rate the etch rate indicated by the alpha step is not reliable, so another sample (*squares.b*) was etched using the same conditions as the first.

For *squares.b* the resist thickness was 707±4nm, the step height after etching was 731±6nm and the step height after cleaning and removal of the PMMA was 164±9nm. This gave an etch rate of $0.68nms^{-1}$ which is different to the first, but not by very much.

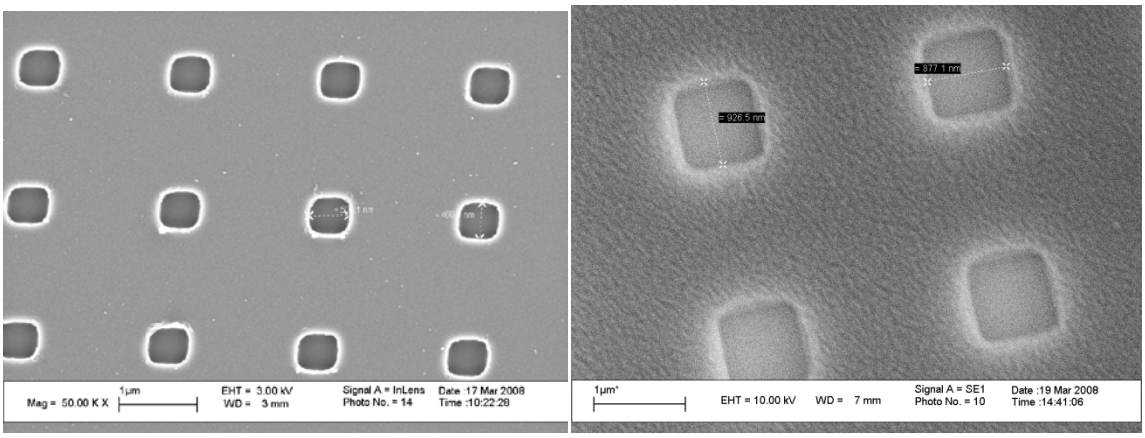

Figure 1-24 – Images showing the difference in image quality between a FEGSEM (left) and an ordinary tungsten filament SEM (right)

The same experiments were carried out in the CH_4 system at the University of Leeds under the following conditions – 100W, 0W reflected, 90sccm CF_4, 10sccm O_2, 24 ℃, 30mTorr, 150V DC. This gave a SiO_2etch rate of 0.97nms^{-1} and the resist etched about 2.5 times faster than the SiO_2. The enhanced etch rate of the PMMA in the system at Leeds is thought to be due to the presence of oxygen in this process as similar gas mixtures are also used for cleaning processes due to their ability to etch hydrocarbons. It is worth pointing out that at Leeds there is no CHF3 process at present. The consequence of the PMMA being etched at 2.5 times that of the SiO2, is that a much thicker layer would be required compared to the process of using CHF3 at RAL. Although relatively straightforward this finding took some time and many process runs to confirm.

Effect of Chamber Pressure on Reactive-ion etching

There are many variables to consider when using an RIE step in a microfabrication process as can be seen in the list of conditions used above. Power and gas flow rates generally affect the rate of the etch, as does temperature, DC bias, overall system pressure, gas ratios and sample size (referred to as chamber loading effect). The gas mixture can affect the rate of the etching and the nature of the etching that occurs (chemical or sputtering) can be affected by the system pressure and DC bias. The type of etching that occurs also

affects the surface roughness of the areas that are etched, and as mentioned earlier, this can also be affected by the DC potential that is built up between the two electrodes, which in turn affects the kinetic energy or momentum of the etching species. The chamber pressure can affect all of these attributes as well as the isotropy of the etch. The isotropy is of interest as RIE is often used primarily because of the high degree of anisotropic etching that can be achieved compared to wet etching which tends to be isotropic (although it can sometimes be controlled by changing which face of the crystal structure that is being etched). The high aspect ratio anisotropic etching is desirable for many applications where the vertical sidewalls that are created are needed for the device being produced.The high anisotropy results from balancing the formation of an organic polymer and the sputtering and chemical etching components of the etching. In essence, a thin polymer layer is formed on the newly etched surface and where this surface is perpendicular to the bombarding Oxygen and CF4 ions then the sputtering, which results from the momentum transfer arising from the DC electric field, wears away this thin polymer. However, on the side-walls of the feature to be etched the ions impinge obliquely and the sputter etch rate is reduced to the point where the polymer still shields the edge-walls from the reactive ion etching.

The pressure was varied whilst the other variables were all kept constant in an attempt to characterise the effects of changing the chamber pressure alone.

At RAL the chamber pressure was varied from 25mTorr to 100mTorr which showed that increasing the pressure from 25mTorr to 65mTorr increased the wall verticality and after that it didn't appear to get any more vertical. It is difficult to judge the angle accurately without mounting cross sections of the samples properly in the SEM, but there was not sufficient time or need to do this, so the samples were coated with a thin layer of metal then imaged with an SEM using a tilted stage to look at the profile of the etch at the exterior corners. This gave the best view of the etch sidewall angle.

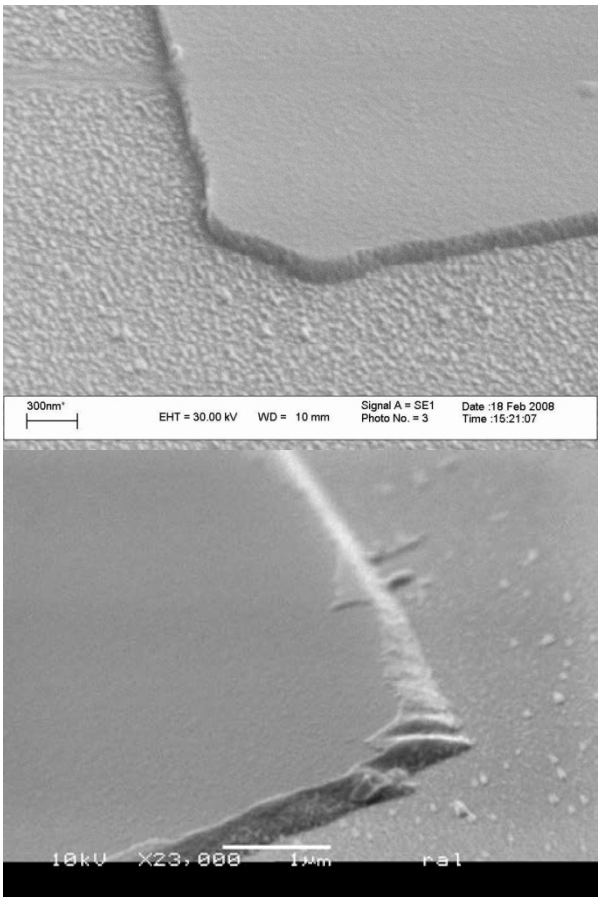

Figure 1-25 – Etch profile at 65mTorr (left) and 25mTorr (right) showing increase in wall verticality.

Electron Beam Lithography exposure

The next stage was to characterise the electron beam exposure required to expose the layer of 495A8 PMMA which would be suitable as a resist mask for CF_4 or CHF3 plasma etching of SiO_2 on GaAs. This was initially done using the Raith (E-beam machine manufacturer) demo pattern, which contains automatic dose test areas and then using some custom patterns to check that the dose was correct for holes of the appropriate size. This is a potentially complex process as the ideal exposure depends on the surrounding feature sizes in a non trivial way, which is referred to as the proximity effect. It was found that for small dots, a dose of 200% of the standard doseof 100uC/cm^2(at 10kV) was the correct dose. This means that a dose of 200 uC/cm^{2}is required for areas exposed.

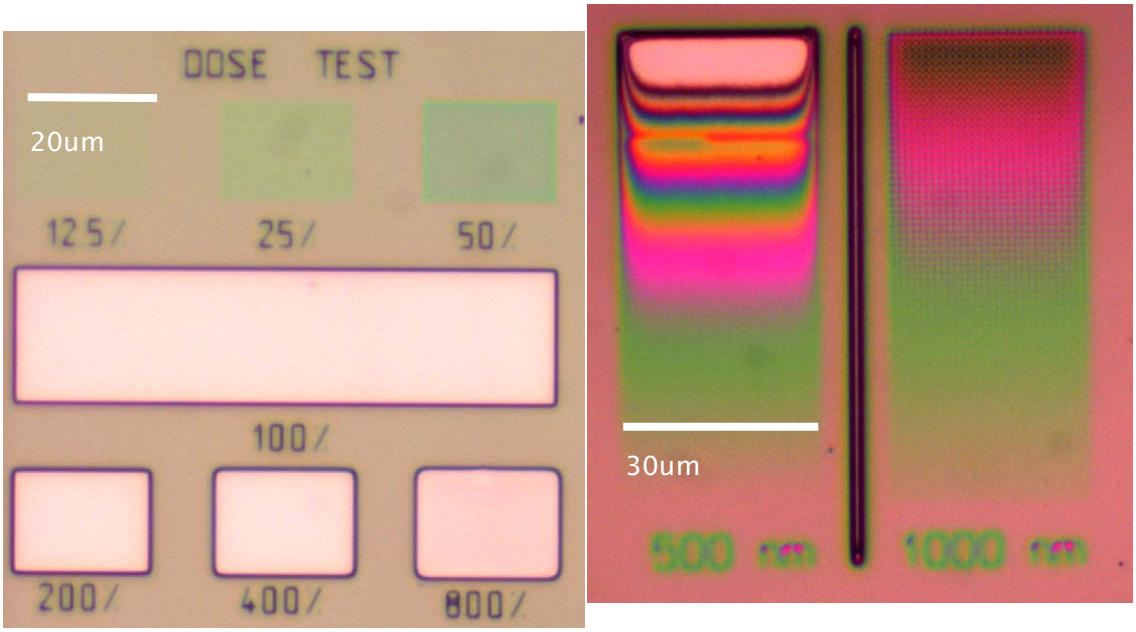

Figure 1-26 – Raith software demo pattern for area exposure dose test (left) and spot exposure does test (right)

Fabricating diodes with small anodes

The results from testing the dose on a thick layer of PMMA and the oxide etch testing were combined in an attempt to fabricate diodes with anodes smaller than 1um diameter. First to prove that it was possible the holes were etched in blank oxide. The holes were spaced far enough apart so that there would be no proximity effects on these patterns when the exposure was carried out.

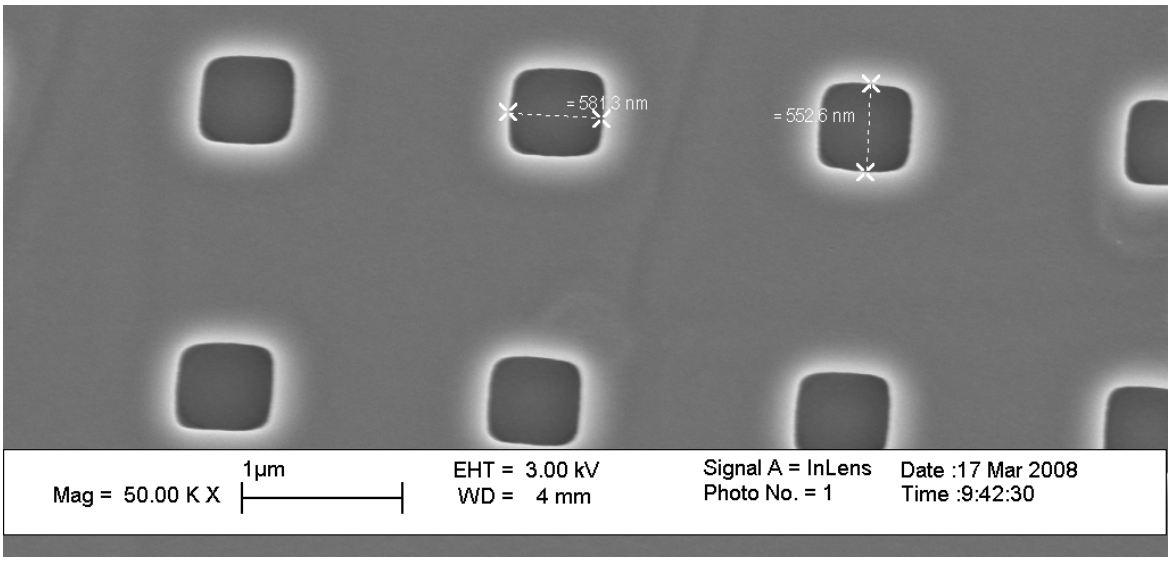

Figure 1-27 – 500nm holes patterned in 250nm thick SiO_2 on GaAs

This testing showed that it was quite possible to reliably etch holes as small as 220nm in the oxide layer to the required depth as shown in Figure 1-28 and Figure 1-29.

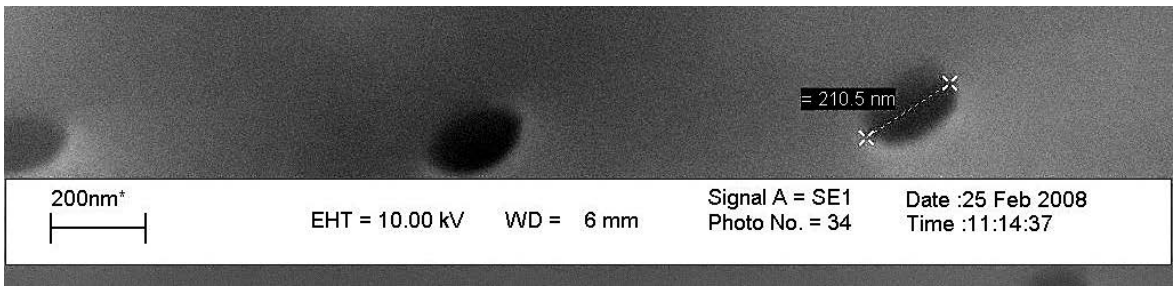

Figure 1-28 – 210nm hole etched in oxide layer.

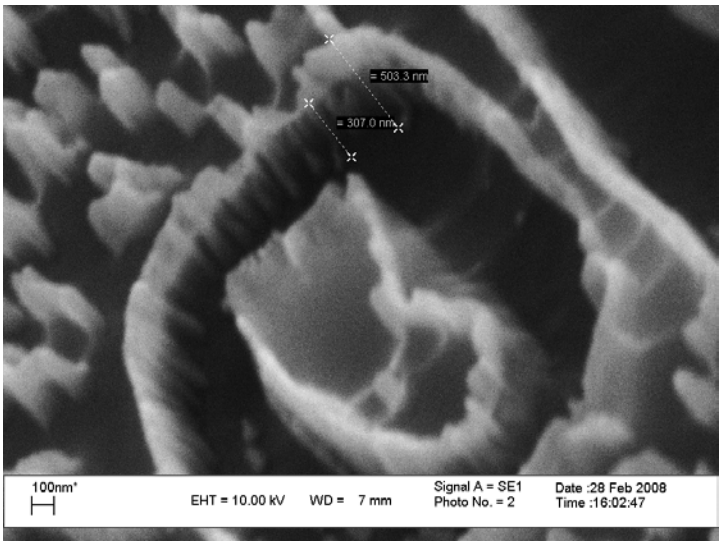

Figure 1-29 - Image showing the depth of small features etched in a layer of oxide.

The next step on receiving a part processed sample from RAL was to pattern the holes in the resist so that they can be etched and then the metal deposited to form the Schottky barriers.

The first step was to convert the dxf file from RAL into a GDSII database for use in the electron beam system. This turned out not to be straightforward and resulted in the hierarchy being lost, so the new E-beam compatible file was used to create a totally new design file that was hierarchy based. This enabled changes to the design (and especially the alignment linescans) to be made much more easily.

The alignment step has proved to be much more difficult than expected. This is believed to be in part due to the shape of the alignment marks on the part processed sample which are 4-5um wide squares. Investigations to look at the effect of changing these squares to 10um crosses, which are the recommended alignment marks for the Raith alignment software could be tried in the future, as well as other measures which are described later but these would imply making a new optical mask set, which may be inevitable. In Figure 1-29 the very small squares are the 4-5micron alignment markers which are simply too small for the alignment algorithm to find them accurately and extract the required data.

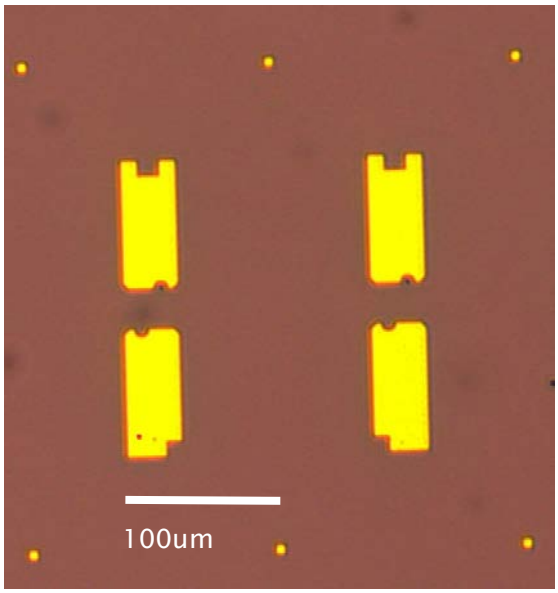

Figure 1-30 – Optical microscope photo showing the ohmic contacts and the small square alignment marks of the sample from RAL

A different approach was tried. Instead of using the predefined alignment marks, the ohmic contacts themselves were used to gather the alignment data to align the anodes. Due to their size, the E-beam software picked them up a lot more easily and a successful alignment could be made (positions shown in Figure 1-31). After adjusting the decision thresholds in the alignment algorithms used for detection, it was possible to do a fully automatic exposure, where the software takes line scans of the ohmic contacts to establish where they are, then calculates the new positions for the exposed patterns and, in this case, exposes the anodes in the right place accordingly (as seen in Figure 1-32).

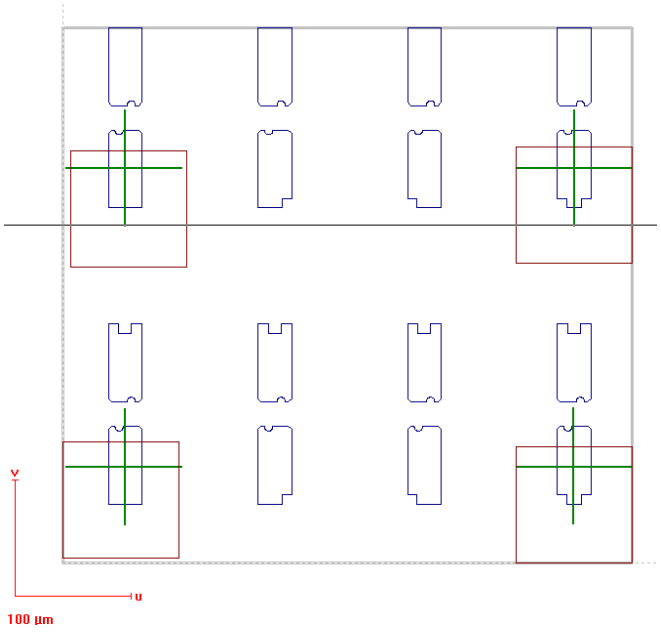

Figure 1-31 – The design of the repeat unit with the alignment linescans shown (in green)

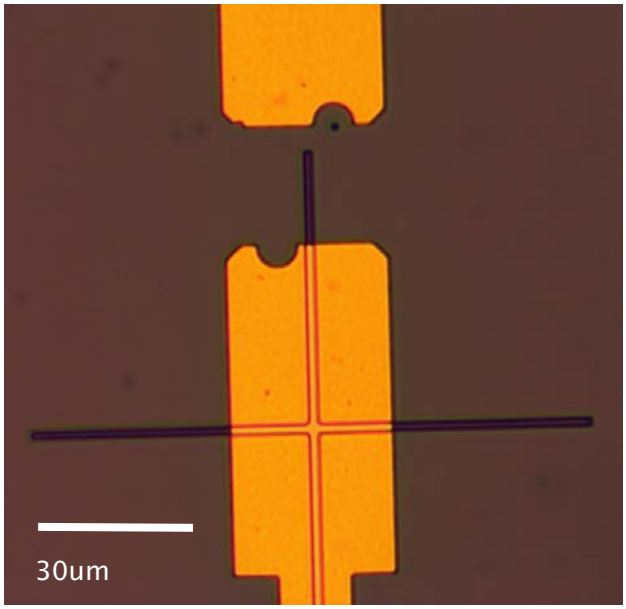

Figure 1-32 – an almost perfectly positioned anode hole developed in the resist layer.

At first, the consistency of the automatic alignment was not very good, and after some further studies has been improved, by, a) increasing the number of points on the line scans and b) the number of line scans the software does before averaging and then determining the position of the feature. Adjusting the threshold and decision points of the

algorithm that determines the position of the feature has also lead to increased consistency.

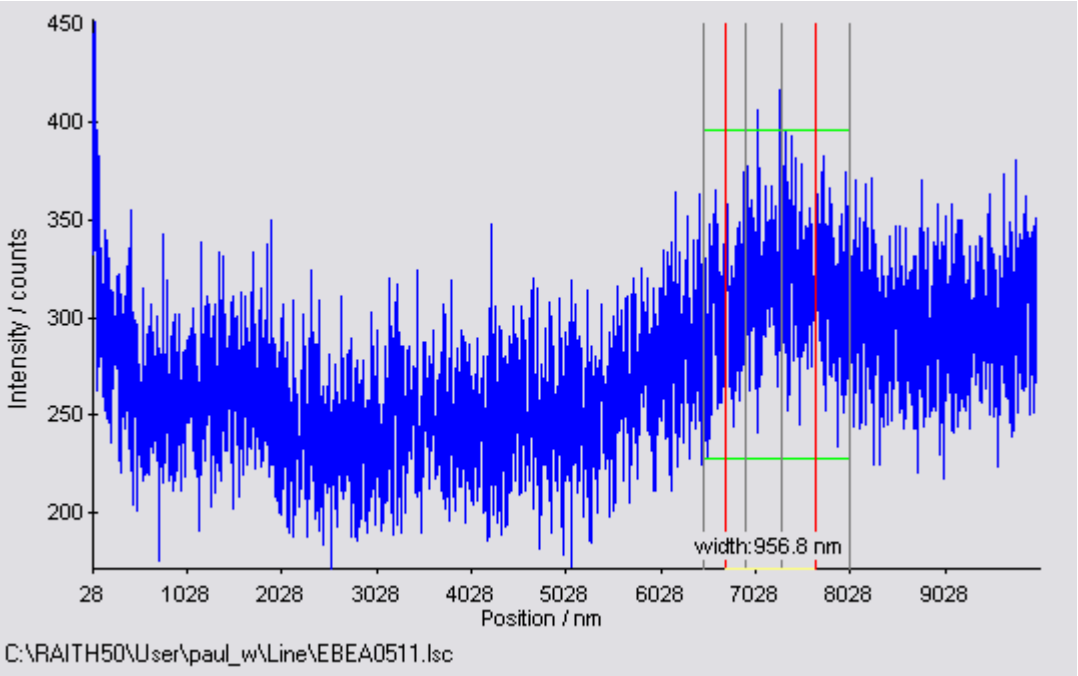

Figure 1-33 – A line scan before the algorithm optimisation that shows nothing, but the algorithm has picked up a feature incorrectly

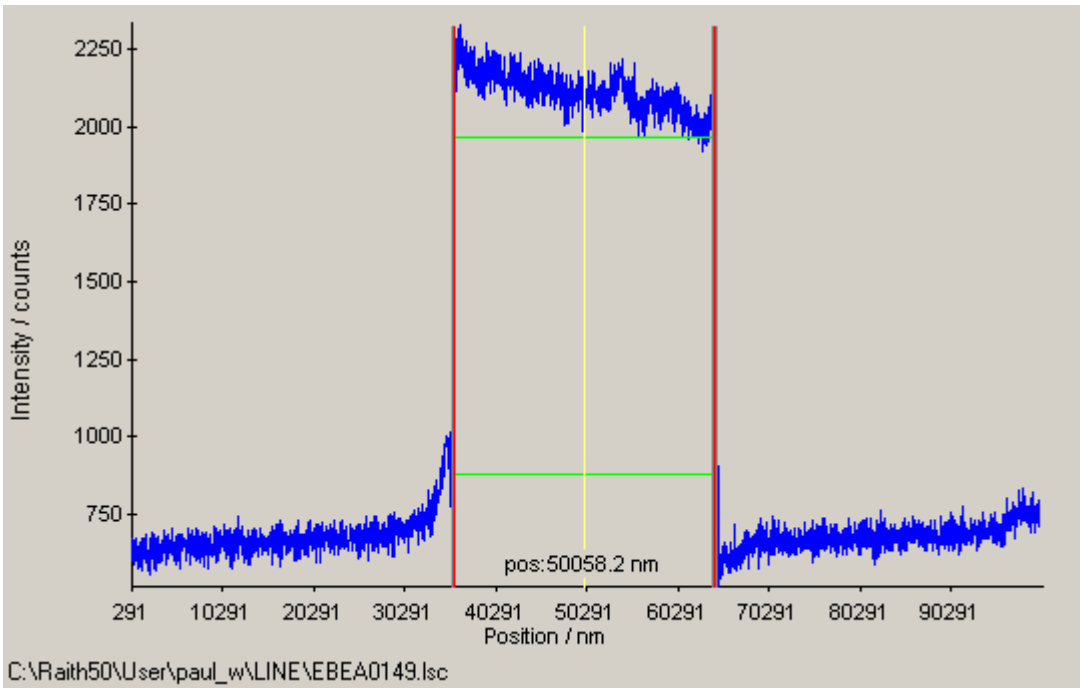

Figure 1-34 – A line scan showing a correctly identified and positioned feature after changes to the algorithm. It would also no longer detect features like those found in Figure 1-33.

The downside of these more accurate scans is the cross that is seen in Figure 1-32. This is because the line scans are a large enough dose so that when the sample is developed, the resist where the line scans were performed is developed away. Fortunately, it is not expected to have a significant effect on the finished diodes because these will be later covered by resist and before the fingers are exposed and developed. At present the anode alignment step yield is estimated to be around 50%. This will be known better when the fabrication of the sample has been completed at RAL and the diodes have been fully characterised.

The line scan identification algorithm still needs improving. In the example below, the edge on the right has not been as tightly identified as the edge on the left. This is merely a result of the incorrect thresholds being set in this case, which can be improved upon. However, there are often trade-offs such that setting these decision points is not always simple or straightforward. For example they can be strongly affected by the beam characteristics used (i.e. 10kV versus 30kV), as well as the microscopic properties of the

metal pattern edges used for the alignment markers. Due to the small size of the anode (in the case of Figure 1-32) compared to the size of this feature (the width of the ohmic contact) an error of this size in the calculated position of the ohmic will result in the anode being exposed up to 2um away from where it should be, which is unacceptable for an anode that is only around 1um across.

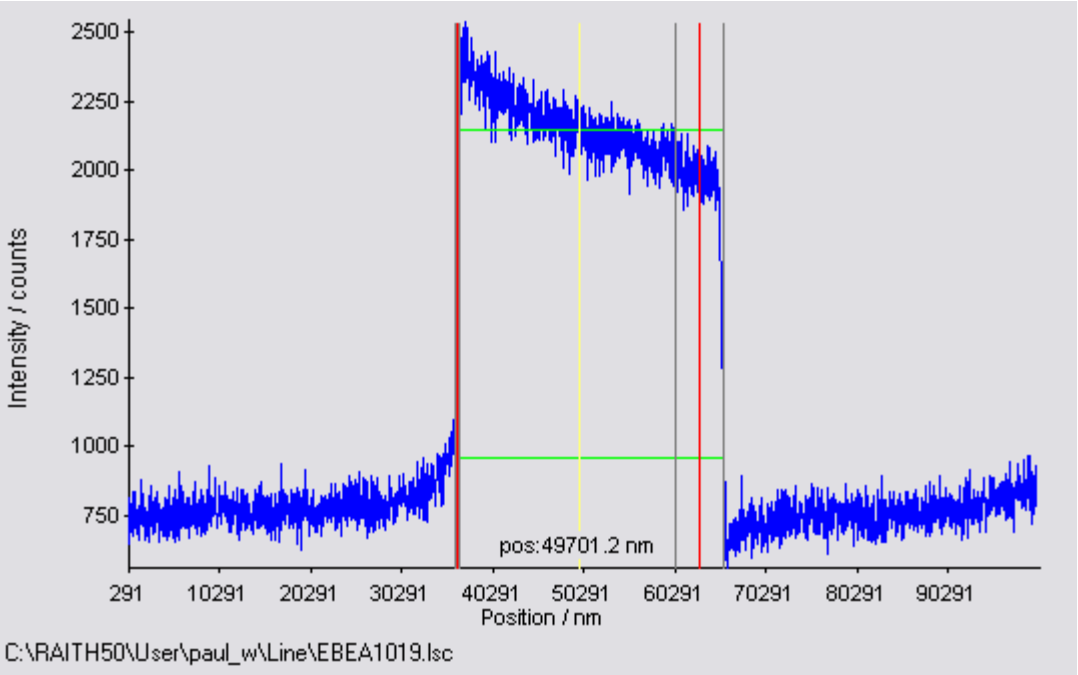

Figure 1-35 - Line scan 1019 showing error in position

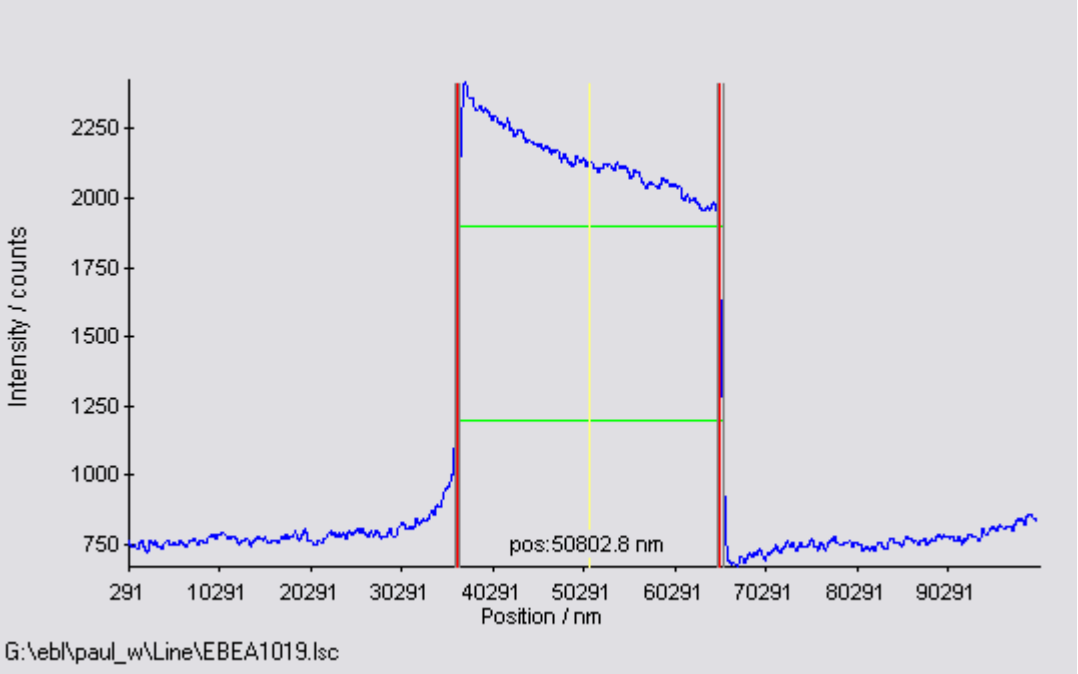

Figure 1-36 - Line scan 1019 after noise reduction and improvement in algorithm accuracy

After the algorithm has been further improved the scan is accurate enough to enable exposure of the anode in the correct position. Because successful exposure depends on all line scans in a write field being correct then there are certain optimisations that can be made to increase the chances of a successful exposure. One major limitation of the accuracy in this case was the shape of the pattern and the shape of the writefield. The instrument can only accept square writefields in a regular non-overlapping array. In this case, the repeat unit of the diode pattern was slightly non square, which meant there were always problems in one direction with getting the writefields to overlap with the repeat unit of the pattern.

This could be improved by creating a new mask where the repeat unit was a square, so the writefield of the ebeam could be exactly matched to the pattern.

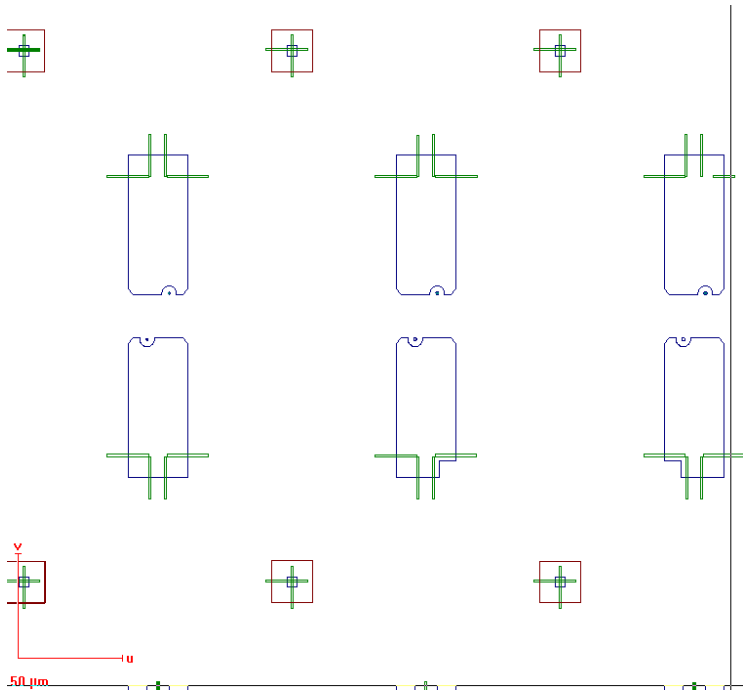

Figure 1-37 – part of the current repeat unit showing alignment marks (small blue squares) and linescans for alignment (green lines)

Each writefield requires 4 alignment marks for optimal accuracy, one in each corner of the writefield. There are two options for this in a new square based pattern. The first option would be to have a mark in each corner of the repeat unit of 8 diodes, however this would mean that if one mark was not scanned perfectly then the position of the anodes in 8 diodes would be compromised. If the writefields were made a lot smaller so that there was only one diode per E-beam writefield, with an alignment mark in each corner, then this would mean that one scan imperfection would only compromise the accuracy of one diode. This is the preferred patterning approach. This should improve the yield across the chip, but would result in a longer exposure time because there would be 8 times the number of linescans. This may also cause problems due to beam drift in the E-beam machine, but it is unlikely as the whole exposure would still be under about 4 or 5 hours.

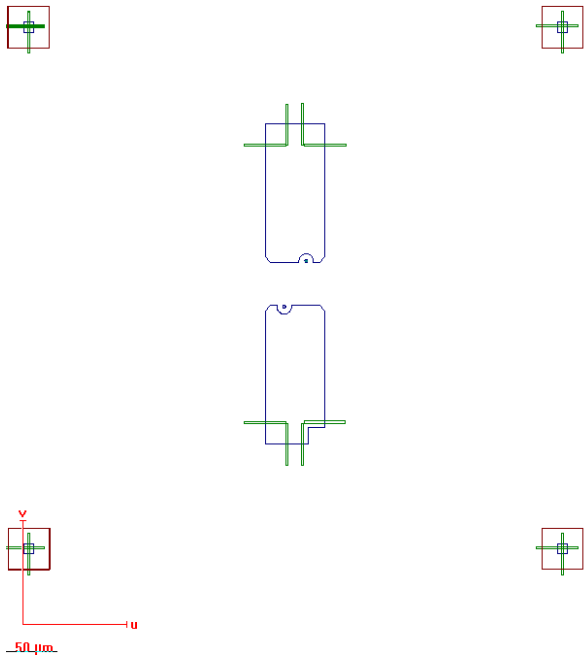

Figure 1-38 – a proposed design for a smaller writefield

Another way of increasing the reliability of the scans would be to change the shape of the alignment marks. When the pattern is first aligned to the sample, it is done manually with 3 points on the sample in the chamber being matched to their respective points on the design file in the software using the machine as a conventional SEM albeit with a very accurate stage to read the positions. This can be done to an accuracy of less than a couple of microns over the whole sample. The E-beam machine uses this manual alignment to decide where it should do the linescans for the exposure alignment. If these manual alignments are not perfect (i.e. to within 1-2um) then the linescans will miss the small square alignment marks used in the original pattern, which will result in misalignment for that writefield.

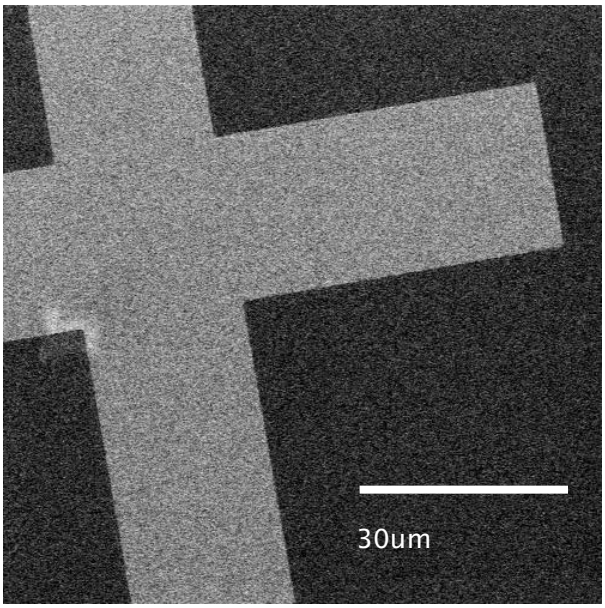

Figure 1-39 – marks used at the edge of the chip for manual alignment

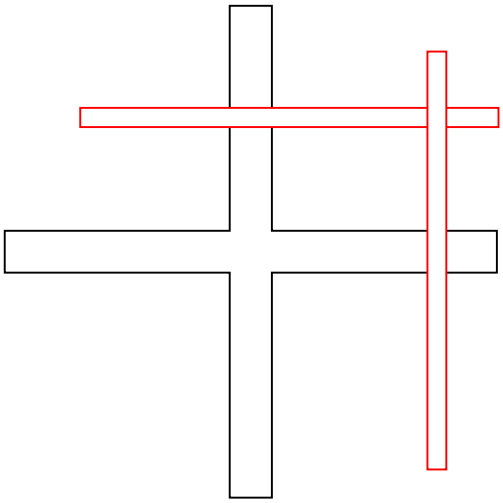

Figure 1-40 – Proposed idea for a new alignment mark showing linescans for alignment (in red)

One straightforward way this can be improved is by changing the shape of the alignment marks. If they are changed to crosses (or "L" shapes) that are 10um along, and if each line is 2 or 3 um wide then these patterns are much easier to find. The linescans are then arranged in an offset cross and the chances of the linescan hitting the cross during its scan are much higher than with a small square.

The developmental challenges of exposing and etching small anodes in Schottky diodes has been described but has not yet produced satisfactory results. In order to prove the performance benefits to the diodes of using small anodes a sample needs to be fabricated with an overall yield of above 90% so the diodes can be tested and adequate statistics gained.

The initial focus during the first year was on the fabrication of the diodes, but the majority of the work in years 2 and 3 was on the design of the diode and mixer, which is focussed on in the next chapters.

Diode characterisation experiments

RAL is working with the GaAs foundry United Monolithic Semiconductors (UMS) to mass produce a working Schottky diode for high frequency work using a modification of the existing UMS BES diode process. There have been some problems with the initial wafer run and the one that was characterised is the difference in anode size and therefore current in each direction. The graph below in Figure 1-42 shows that there is a repeatable and measurably larger current in one direction (the blue data points which are the top diodes as per the image below) of the pair than the other.

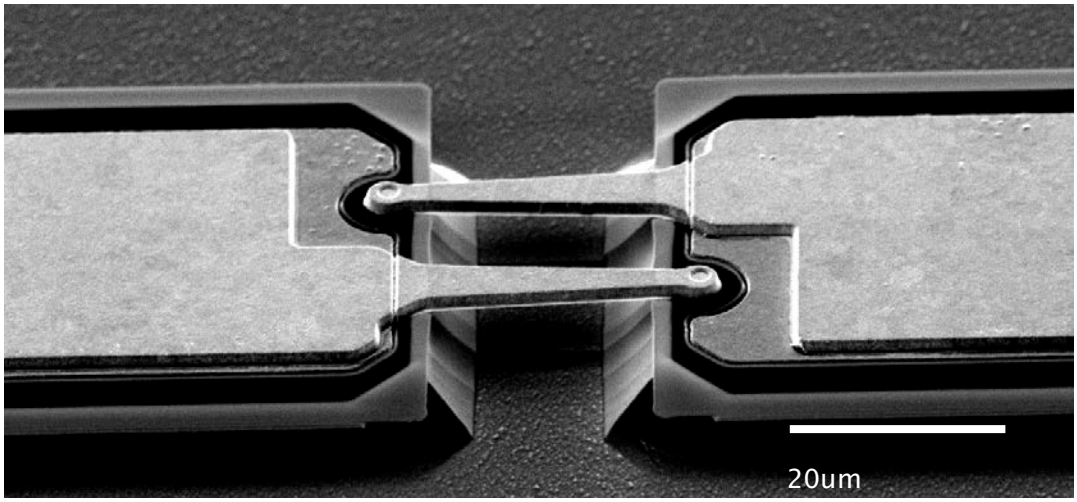

Figure 1-41 - A completed Schottky diode pair produced using the RAL UV photolithography process

This is attributed to differences in the anode area which are caused during the isolation step in the fabrication. This is because the diodes are isolated by ion implantation instead of a deep mesa etch step (as in Figure 1-41). The angle of the substrate during the ion implantation has affected the anode size slightly.

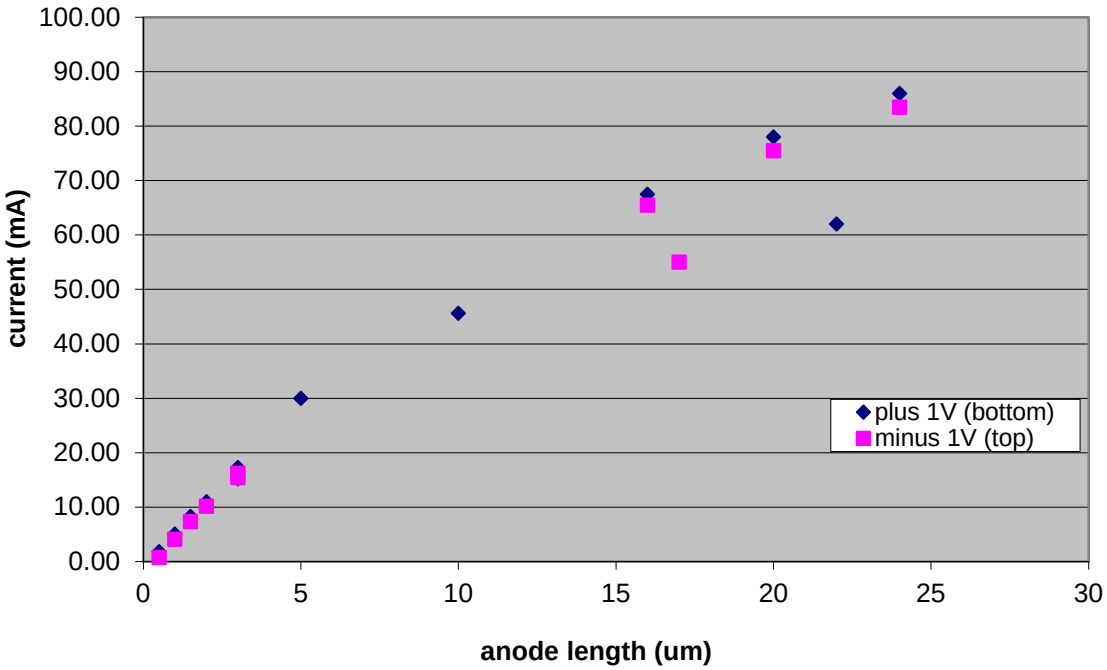

Figure 1-42 – Comparison of anode size and current – bottom and top are references to the two diodes in each pair when viewed as in Figure 1-41and the potential of +/- distinguishes the direction of the current and therefore the diode being tested.

Reverse breakdown voltage was also measured and compared between the two wafers that were processed in the first run by UMS. The first wafer (u1r-8) was sourced by RAL from their usual supplier, but the second wafer (u2r-20) was supplied by UMS and they deposited the oxide. It is yet to be confirmed what the causes of this difference are.

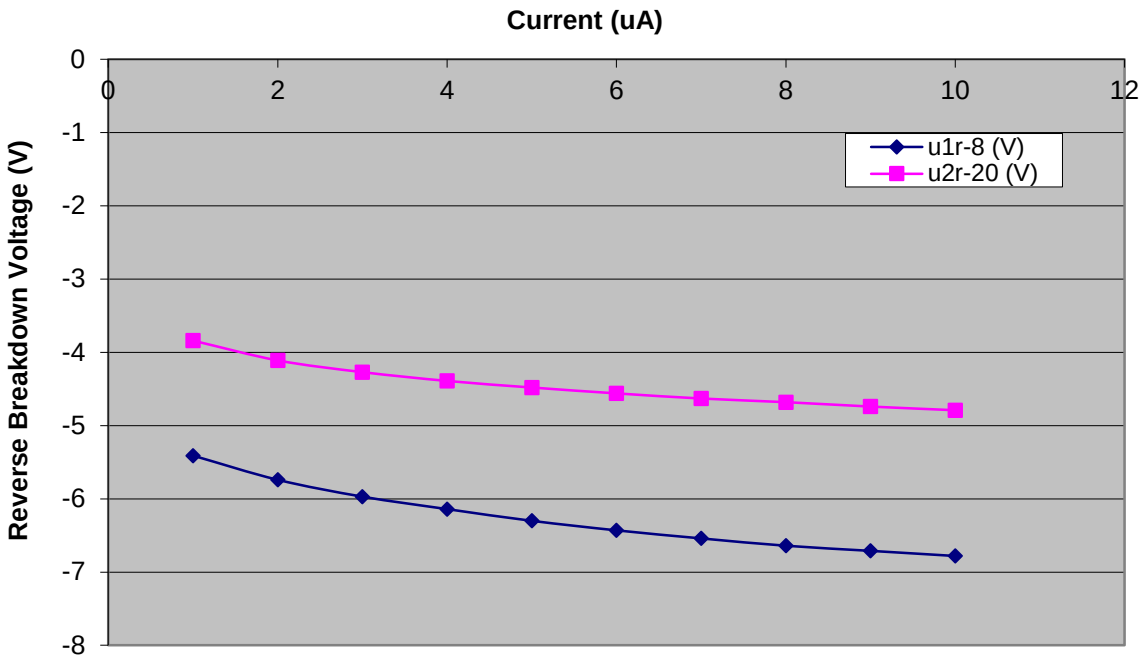

Figure 1-43 – Reverse breakdown voltage comparison

1.5 The Future

As hinted at earlier, the automatic anode alignment needs further refinement in order to increase the device yield. This can be achieved by further refinement of the alignment algorithm, some of which has been done by looking at the effect of the changes on linescans from previous exposures, but an exposure using the refined algorithm has not yet been completed, as the focus of the work in year two shifted towards the circuit design aspects. This in addition to changes to the alignment marks on the pattern, and even the shape of the pattern itself should lead to improvements in the device yield.

The main activity in the second year was the design and then fabrication of the first mixer. Which follows in the next chapters. The design work built on the HFSS and ADS experience reported in this chapter to design and optimise both the diode and the mixer block before they are produced. The first product of this process is a 660GHz subharmonic mixer.

Chapter 2 – Inductance Studies in Mixer Diodes

Diode Parameters

The overall aim of these simulations is to design a Schottky diode that performs better at high frequencies (>400GHz) in a mixing circuit than the existing design (Figure 2-4).

The first stage in this process is to try and understand the existing design better by extracting the parasitic loss parameters from the diode model so they can be controlled or changed to improve the performance of the diode.

This is done by taking a full 3d model of the diode and solving it in Ansoft's HFSS software. This produces 4 port s-parameter data for the diode which can be exported in the standard .s4p format. At this stage, the non-linearity of the diode is not considered, we are only looking at the transmission through the structure of the diode when it is placed in a simple channel.

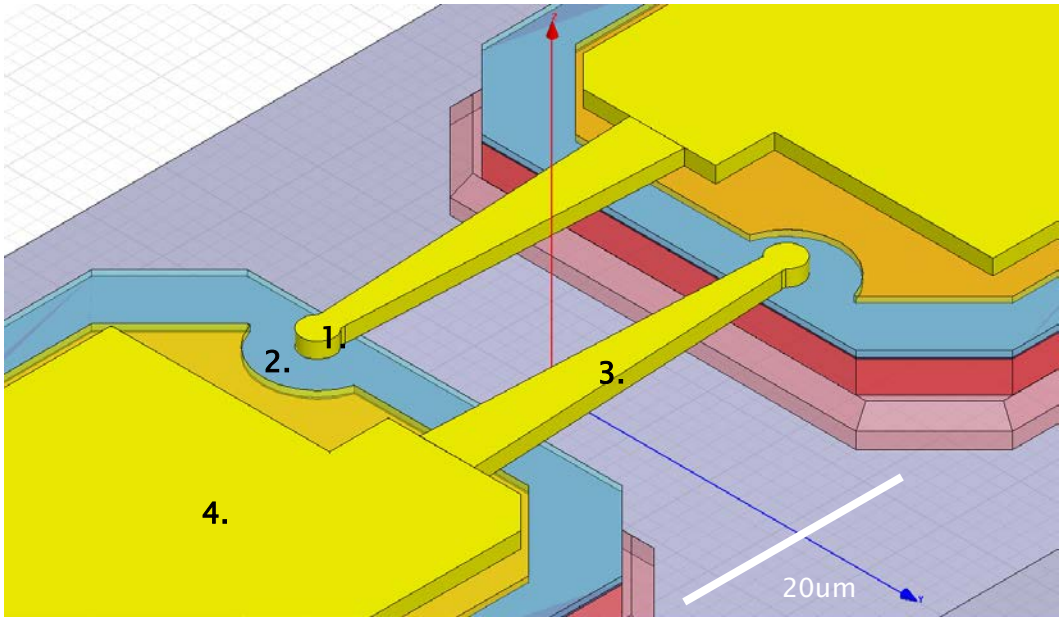

Figure 2-1 – An image of the 3D model in HFSS of the original RAL diode

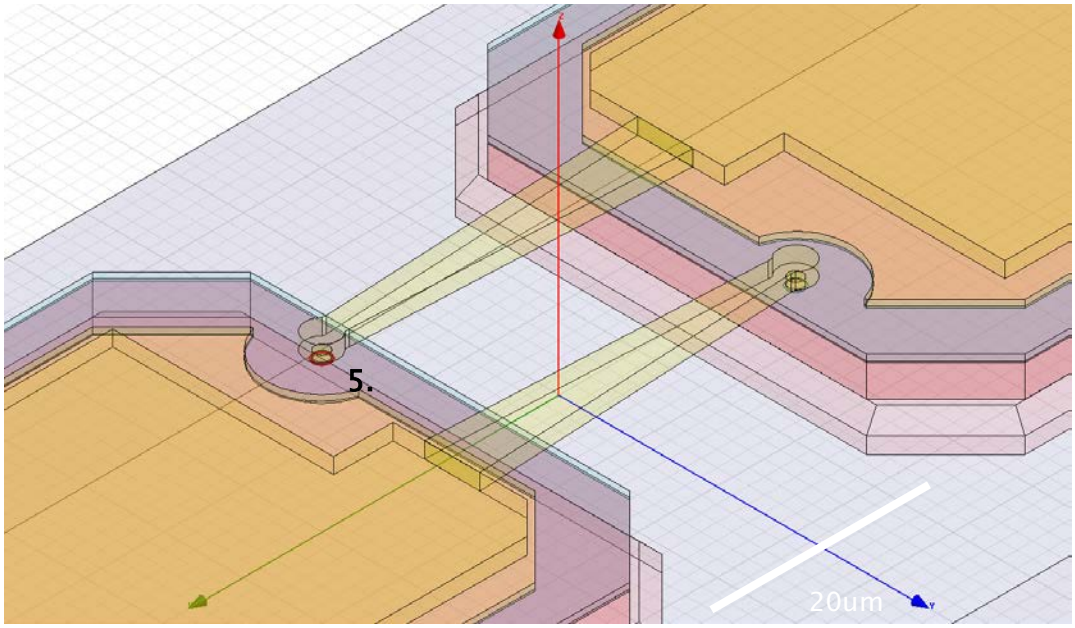

Figure 2-2 - An image of a wireframe model of the RAL diode showing the port at the anode as a red ring under the end of the finger.

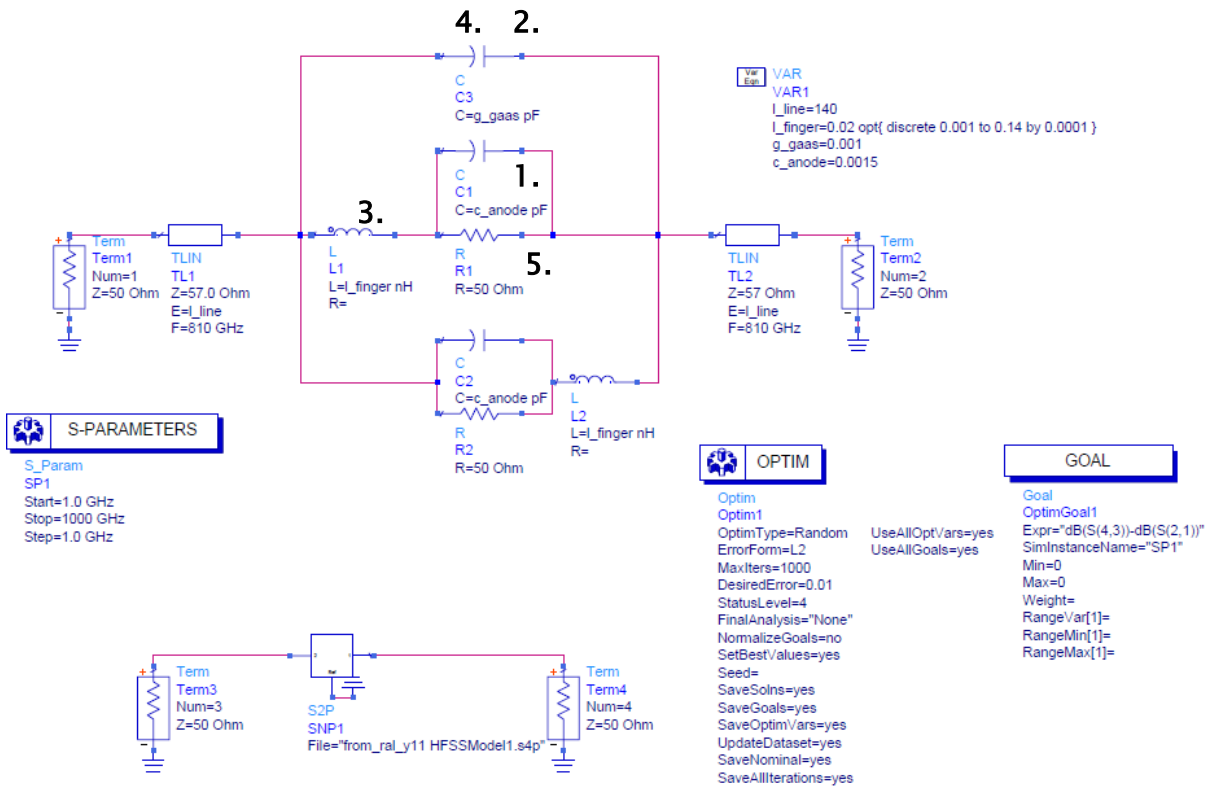

Figure 2-3 - ADS model for extracting diode parameters

The simple circuit shown at the bottom of the ADS schematic in Figure 2-3 is the exported data from the HFSS 3d model and the circuit at the top is described below.

The numbered circuit at the top is a lumped element model of the diode which is used to extract the parameters of the diode. 1 is the calculated junction capacitance of the anode which is caused by the depletion layer created when the Schottky contact is formed. 3 is the inductance of finger. 2 (and 4) is the sum of the parasitic capacitances in the device including between the end of the finger and the ohmic pad and between the two fingers and between the two pads. 5 is a 50 ohm impedance to represent the port at the anode in the 3D HFSS models as the ADS simulation only uses two ports.

In the preferred simulation technique the performance is compared by looking at the single sideband conversion loss of the mixer. This is calculated using the following equation:

$$\text{Conversion Loss (dB)} = 10\log\left(\frac{P_{IF}}{P_{RF}}\right) \quad (1)$$

Where P_{IF} is the power at the intermediate frequency, calculated from the simulated current and voltage at the IF port and P_{RF} is the known power that is put into the circuit at the RF.

There are many ways of representing the parasitics in the diode cell using lumped element models which can be as simple or as complex as you like. One aspect of the parasitics that has been neglected in previous studies is the inductance of the diode finger.

This inductance in the finger can be calculated in several ways. Perhaps the simplest way is to approximate it to a length of round wire. For high frequencies the inductance of a wire is given by this equation [39]:

$$L_{AC} = 2L\left(\ln\left(\frac{2L}{r}\right) - 1.00\right) \quad (2)$$

Where L_{AC} is the inductance in nH, L is the length of the wire in cm and r is the radius of the wire in cm. This gives an inductance of 0.03nH for an approximation of the finger in a standard RAL diode to an isolated round wire far from a ground plane or earth. The inductance can be decreased by making the finger shorter or by increasing the cross section area.

Changing the current design

The cross section area can be increased by either using a thicker layer of deposited gold to make up the finger, or by changing the design and shape of the finger.

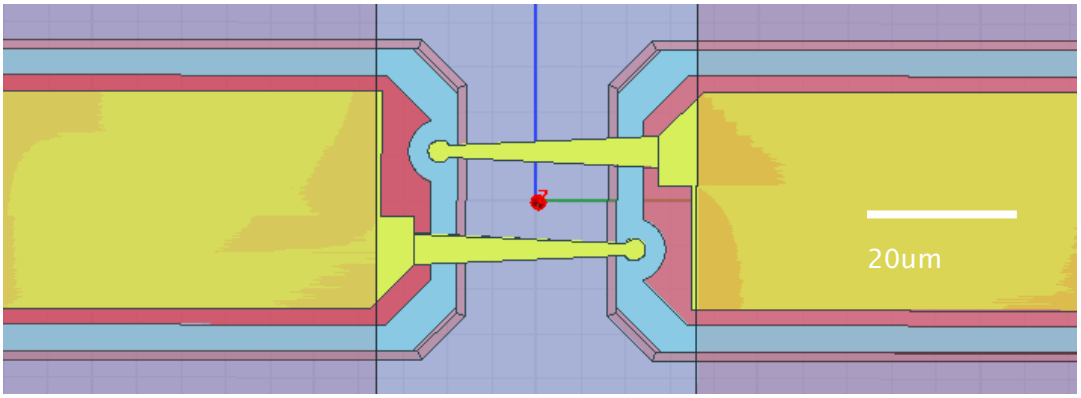

Figure 2-4 – Existing RAL diode model in HFSS

The performance of this change in design was simulated using a variety of techniques.

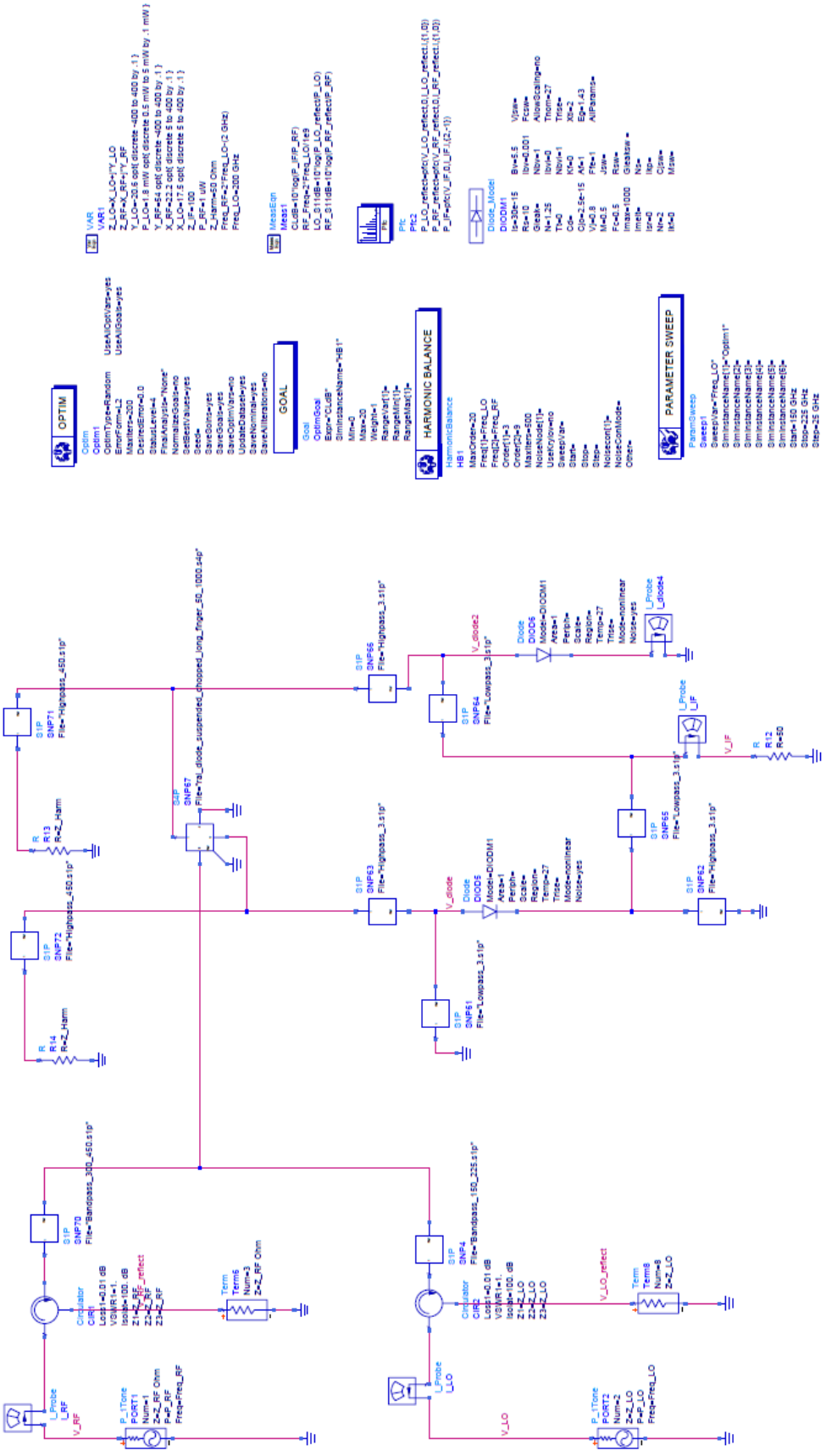

Figure 2-5 – ADS circuit used to optimise performance at a variety of frequencies

This ADS circuit shows the initial set up used. The S parameters were calculated for a diode suspended in a channel by HFSS and then exported. This circuit shows the RF and LO on the left and the diode cell and IF in the bottom right with a variety of ideal filters and circulators separating them, which may not be realizable in real-life but help to condition the initial simulation. A more detailed description of the circuit can be found in the Mixer design section. The circuit is set up to optimise the conversion loss by changing the real and imaginary components of the RF and LO impedances at each frequency every 25GHz from 300 to 750GHz (RF frequency). This should give an indication of the performance of the diode in mixers of ever increasing frequency as it is optimised at each step. Due to the constraints of the circuit the setup is duplicated at different frequency ranges of 300-450GHz RF, 400-550GHz and 500-750GHz. This means that the filters can be set up so that the RF, LO and IF signals are always isolated from each other. If the whole frequency range was done at once then LO signals could go straight to ground through the RF circuit.

To provide another comparison, a version of the RAL diode with the usual x separation of the diodes doubled was used. This would provide a model with an approximation of inductance from Equation (2) of over 0.1nH (compared to 0.03nH for the standard RAL diode).

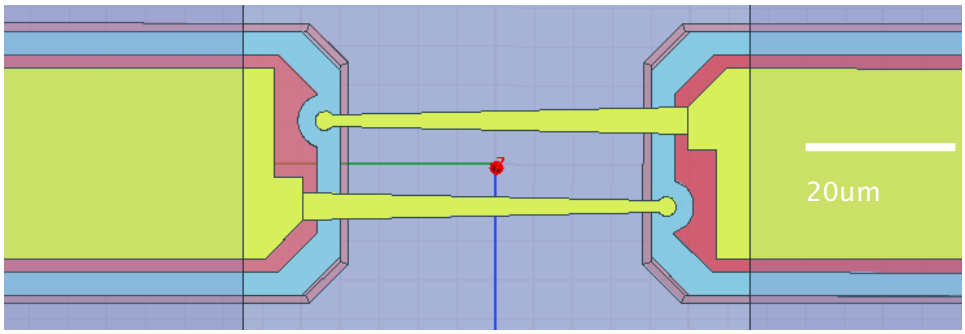

Figure 2-6 – RAL diode with 40µm fingers

The results of the ADS circuit shown in Figure 2-5 for all 3 diode models above is shown in Figure 2-7.

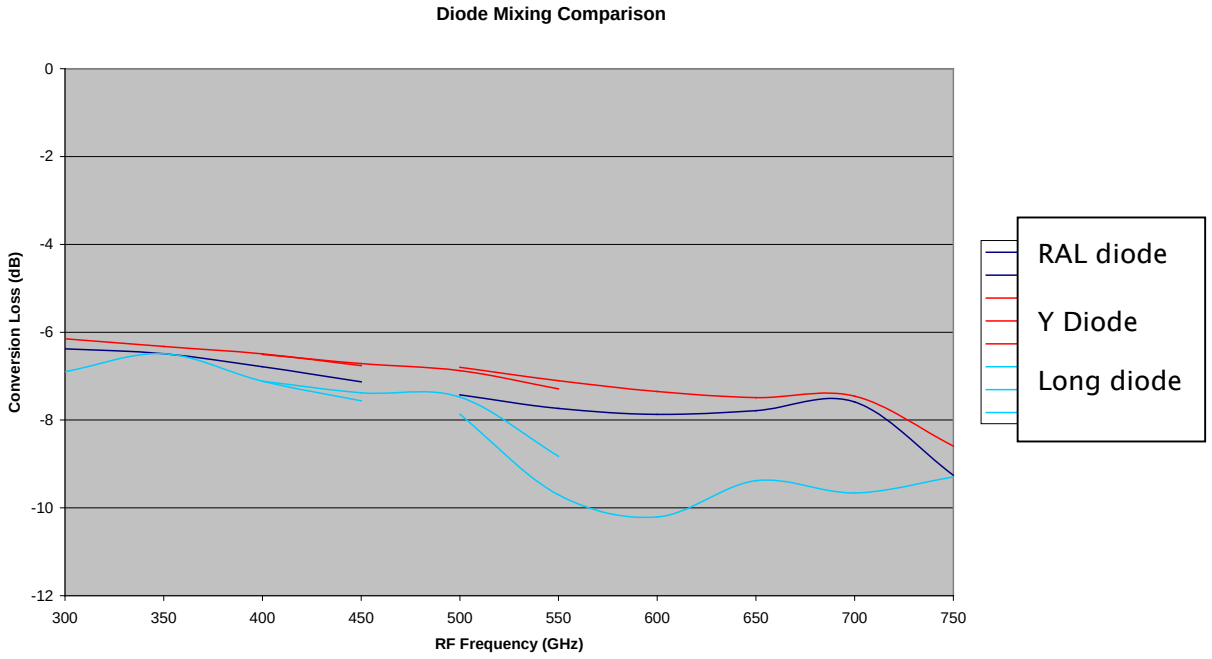

Figure 2-7 – Diode mixing Comparison, RAL diode is as shown in Figure 2-4, Long diode as shown in Figure 2-6 and Y diode as shown on right in Figure 2-23

According to this set up, the Y diode does indeed provide an increase in performance of up to 1dB over the existing diode. The existing diode's performance drops off in experimental results above 400GHz, but this is not really shown here by the dark blue line. In this respect, the Y diode (red line) is very similar but overall a little better. This is probably due to the fact that the impedances are being optimised at each frequency step.

A different approach was needed to look at the performance changes in the diode in more depth. A similar ADS circuit was used, but this time only over a single frequency range (550-750GHz). This circuit was also set up so that the impedances were only optimised for a single frequency (664GHz) which was chosen due to current project needs for a mixer at this frequency. Using a single frequency for the optimisation process also dramatically reduced the simulation time on the computer. From this optimisation of the

impedances at 664GHz the impedances are then locked and the input frequency range is scanned from 550-750GHz at the RF. The resultant conversion loss graph shows the bandwidth performance of the diode assuming the impedance values are fixed as they would be in a real mixer device. The peak conversion loss and the 3dB bandwidths can then easily be compared across diode designs to ascertain their performance.

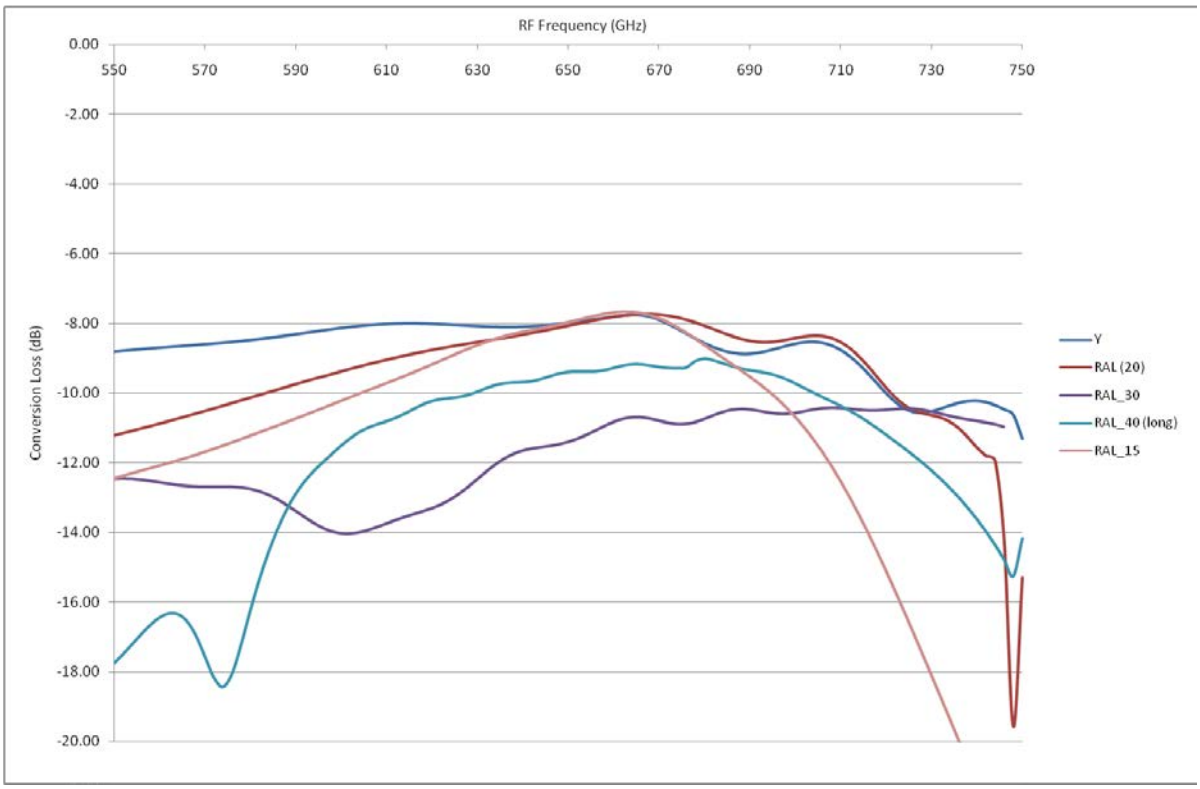

Figure 2-8 - Bandwidth performance of mixer diodes in circuit optimised at 664GHz, RAL_number indicates the length of the air bridge finger in microns.

This graph shows that the peak conversion loss (usually at the optimisation frequency of 664GHz) does not change much when the design of the diode changes between the original RAL model (RAL (20)) and the Y design. As expected it also shows that the performance drops off when the length of the fingers is extended. The bandwidth does change a lot, but cannot be compared directly by using the 3dB bandwidth figure as the performance does not drop 3dB on each side in the frequency range used. The bandwidth drops when the fingers are shortened or lengthened. To use another frequency range

would involve similar problems to those described above with regards to the band pass filters used to keep the RF, LO and IF signals separate.

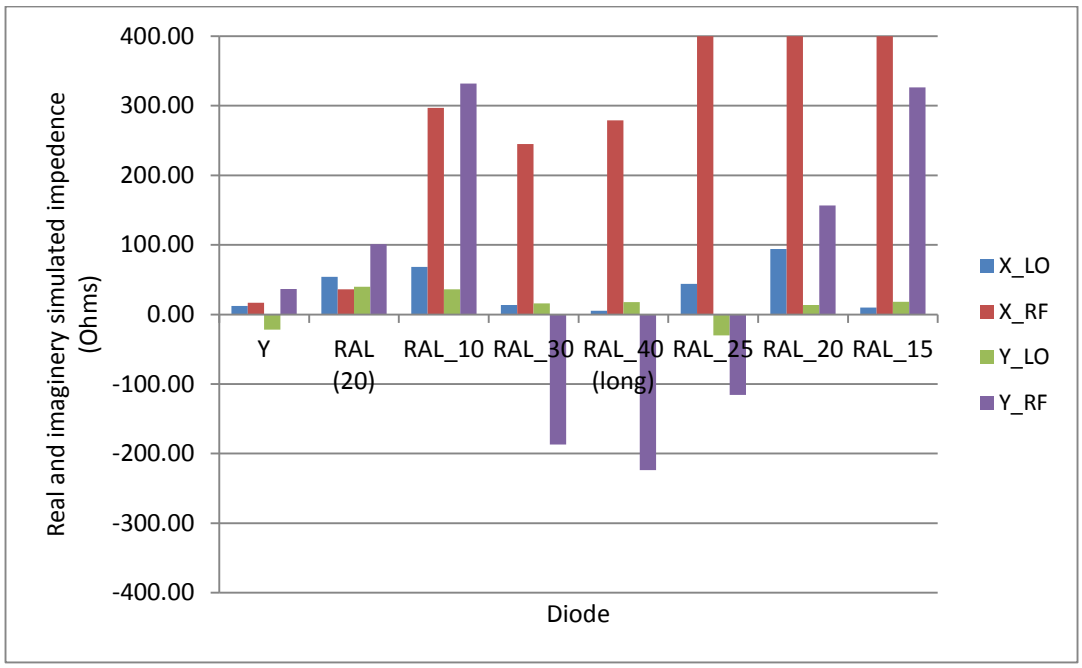

Figure 2-9 - Real (X_LO and X_RF) and imaginery (Y_LO and Y_RF) simulated impedances as optimised in ADS at 664GHz for various diode designs

Figure 2-9 shows that the impedances for most of the diode designs except the original Y and RAL designs are a bit unusual and tending towards the maximum values that were allowed during the optimisation process. This has also resulted in fairly high error function values which can be seen in Figure 2-10 which leads to the belief that something in the simulation is not going as smoothly as it should be.

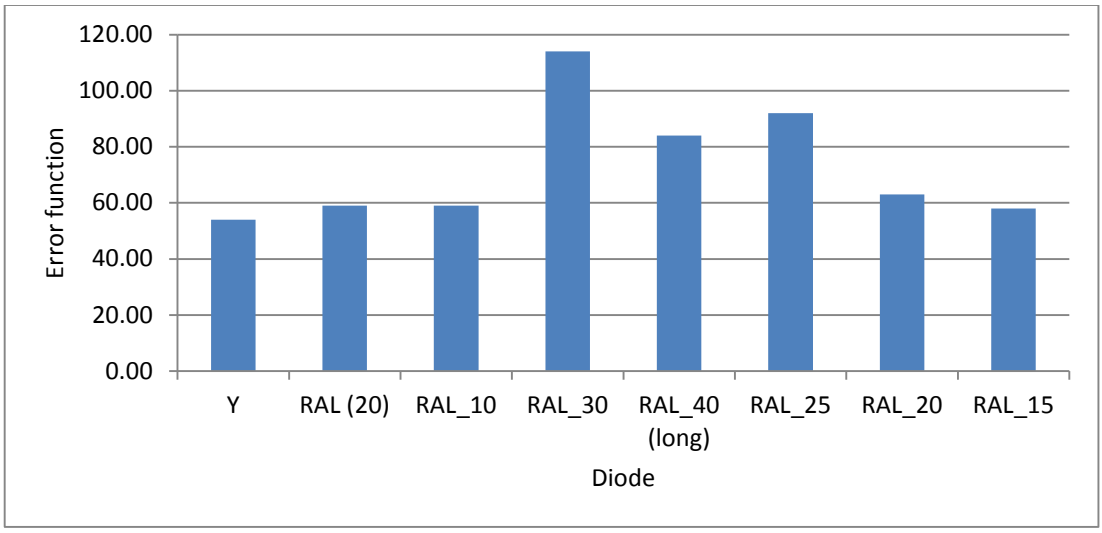

Figure 2-10 – Final Error Function for ADS simulations of various diode designs

These high impedance values and error rates were suspected to be related to the de-embedding method used in the 3D simulations in HFSS. Initially the models were de-embedded so that the distance between the de-embedding points at either end of the model was constant whilst the length of the diode fingers was changed and it is this method that produced the results above. De-embedding to the same point in the design and varying the distance between the two de-embedding points as the lengths of the fingers change should be better.

The error function shown in Figure 2-10 is based on the optimisation goals in Figure 2-5 and is a least squares formulation averaged over the frequencies of the simulation.

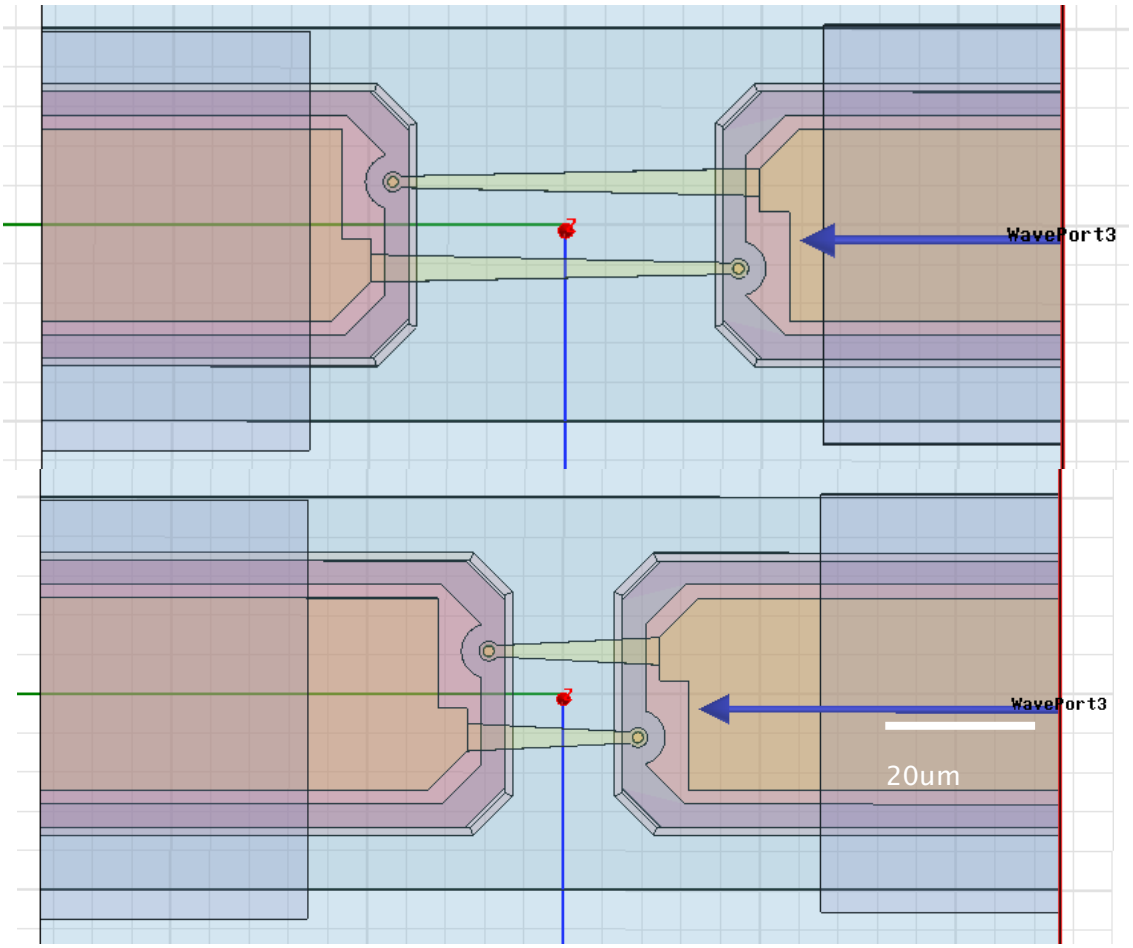

Figure 2-11 – Diode model showing new de-embedding point just behind edge of contact pad regardless of finger length.

This new de-embedding method produced a similar comparison between the diodes and the finger lengths, but with much more sensible optimised impedances and lower error functions.

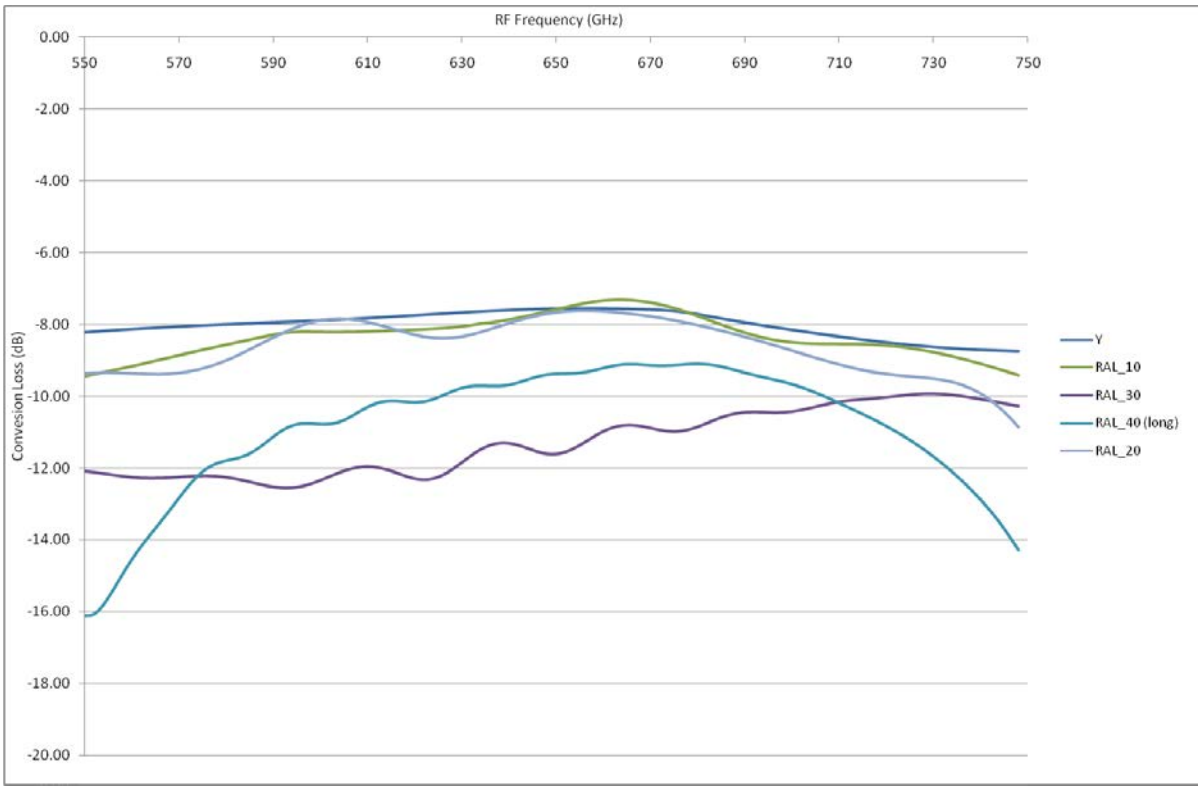

Figure 2-12 - Performance of different diode designs with new de-embedding method

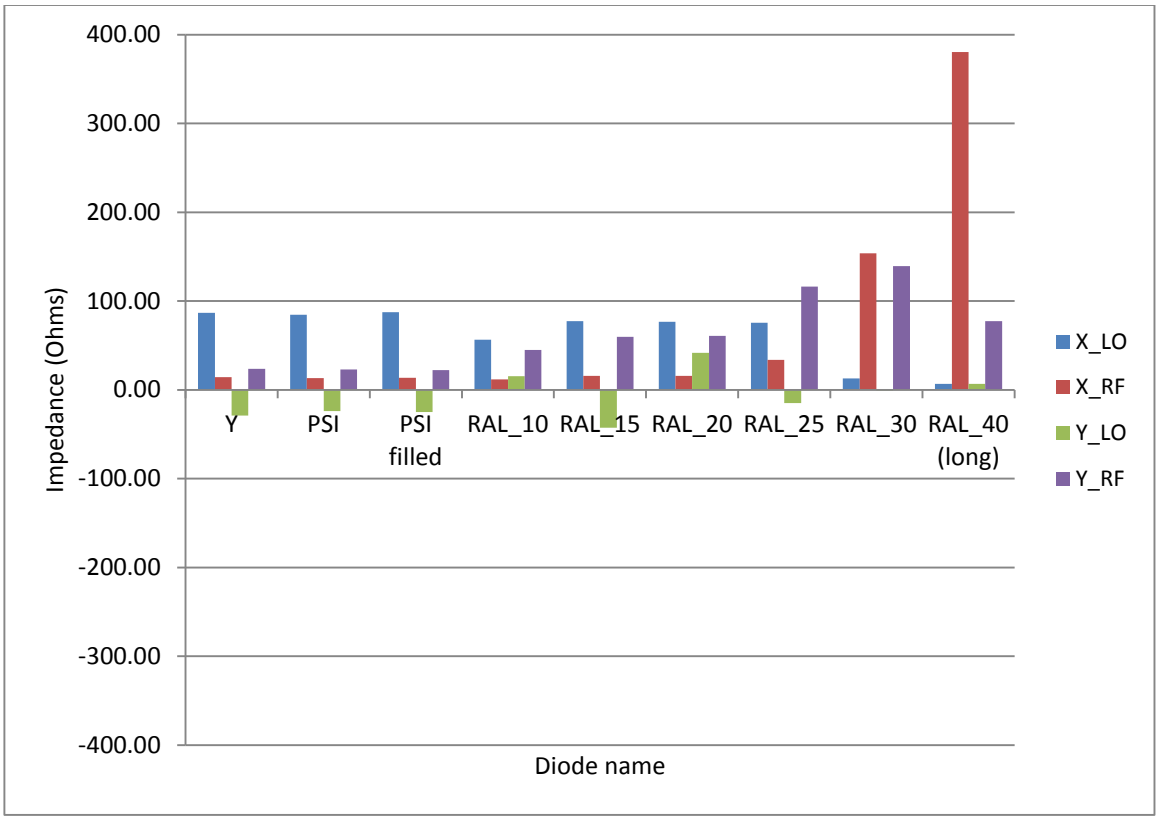

Figure 2-13 – Impedance values for diode designs with second de-embedding method (y axis which shows the range of allowed values has been kept the same as the first one for comparison)

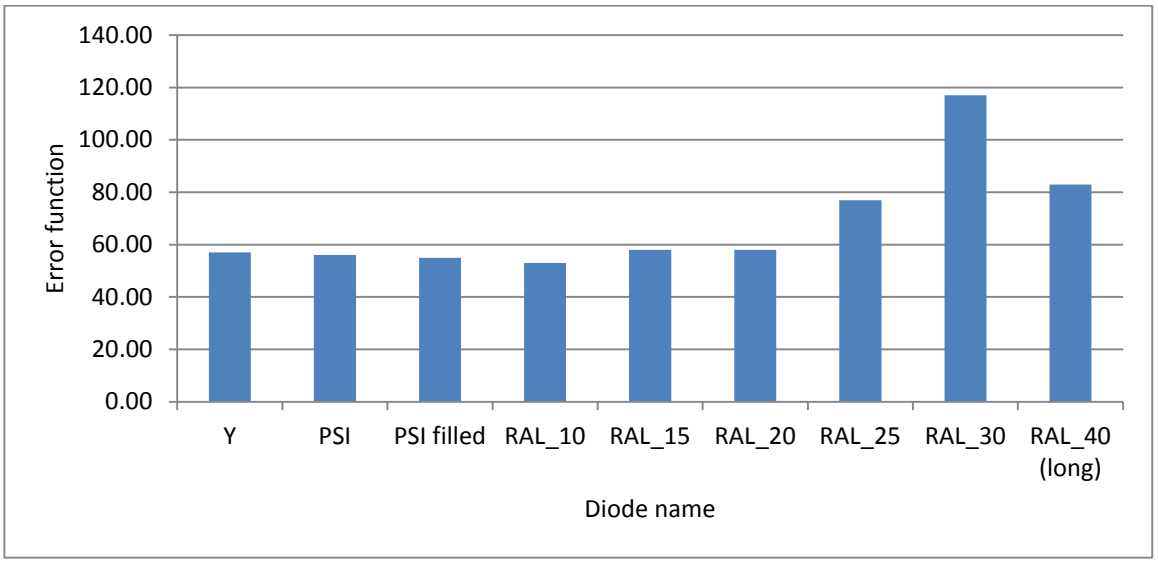

Figure 2-14 – Final Error functions for second de-embedding method

These changes haven't really made the comparison between diode designs any more useful, but they have increased the reliability of the comparison as the impedance values

are much more sensible. This can easily be seen by comparing the impedance graphs in Figure 2-9 and Figure 2-13.

The simulations detailed so far have provided comparisons between different diode designs, but they are fairly arbitrary in terms of how the change in design affects the electrical performance of the devices.

Electrical Performance

In order to increase understanding of these effects, a lumped element model of the diode was put into the ADS circuit in place of the imported s parameters as per Figure 2-3. This enabled the lumped inductance to be directly changed to see if this change related in any way to the change in the length of the finger.

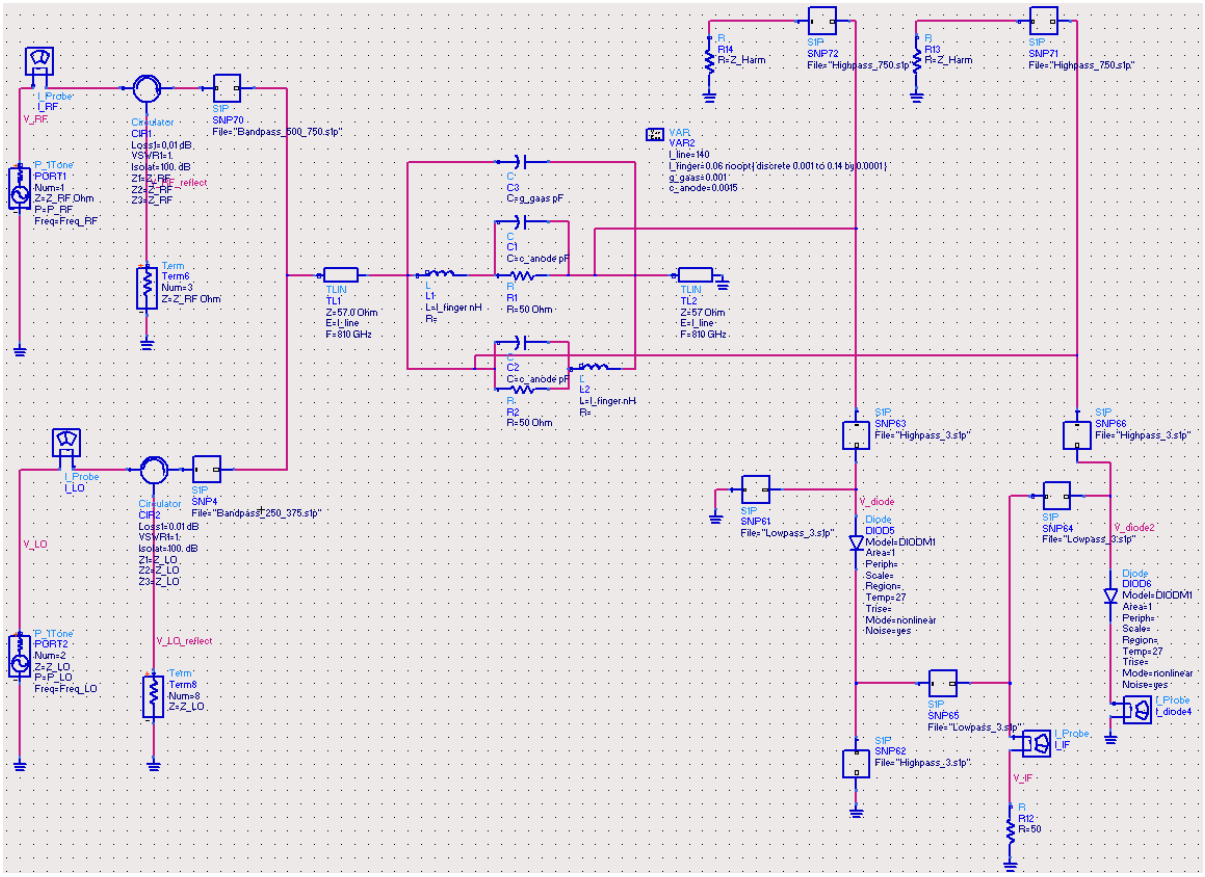

Figure 2-15 - Lumped element model in ADS circuit

Figure 2-15 shows a similar circuit to Figure 2-5, but the S-parameters extracted from the HFSS simulations have been replaced by a lumped element circuit. This enables the inductance element to be directly changed to look at the expected changes in performance of the mixer circuit. If the changes to the performance are similar to those seen when the length of the finger in the HFSS model was varied then we will be fairly confident that it is the change in inductance that is bringing the improved performance.

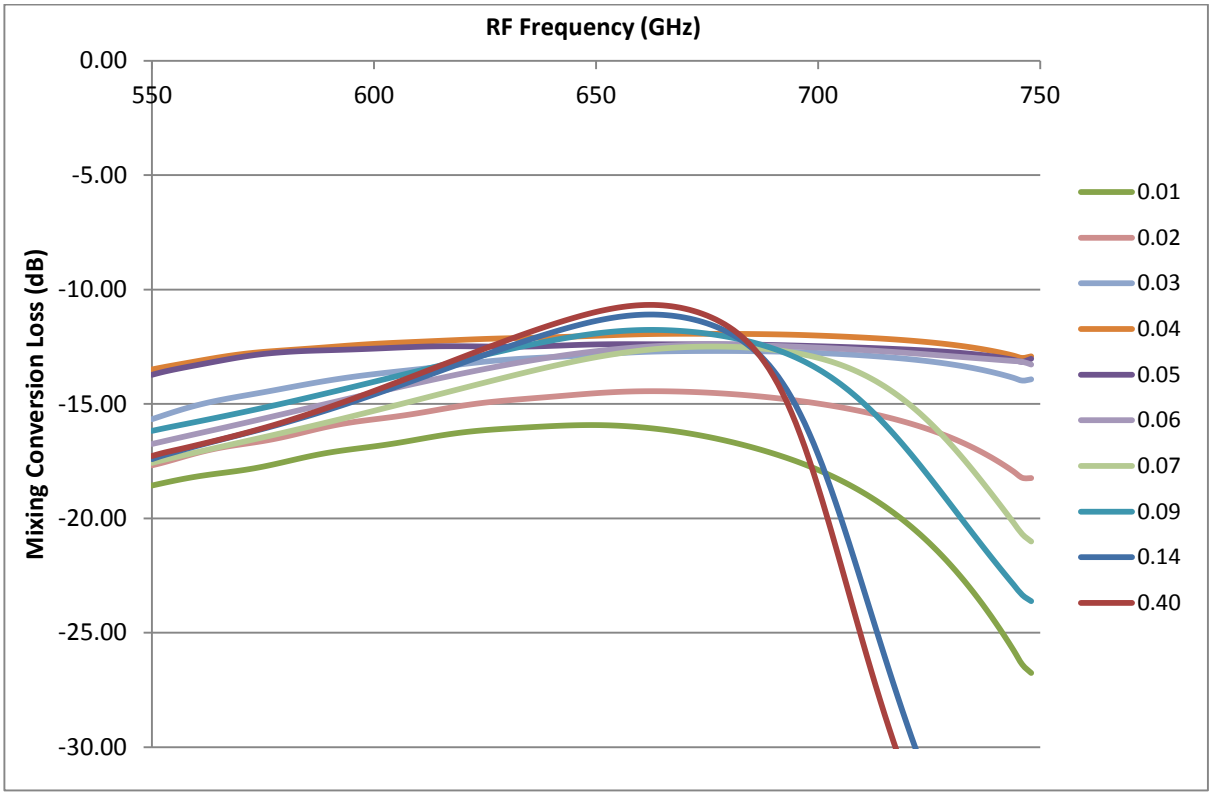

Figure 2-16 – Effect of changing the finger inductance in the lumped element model (legend shows inductance in nH)

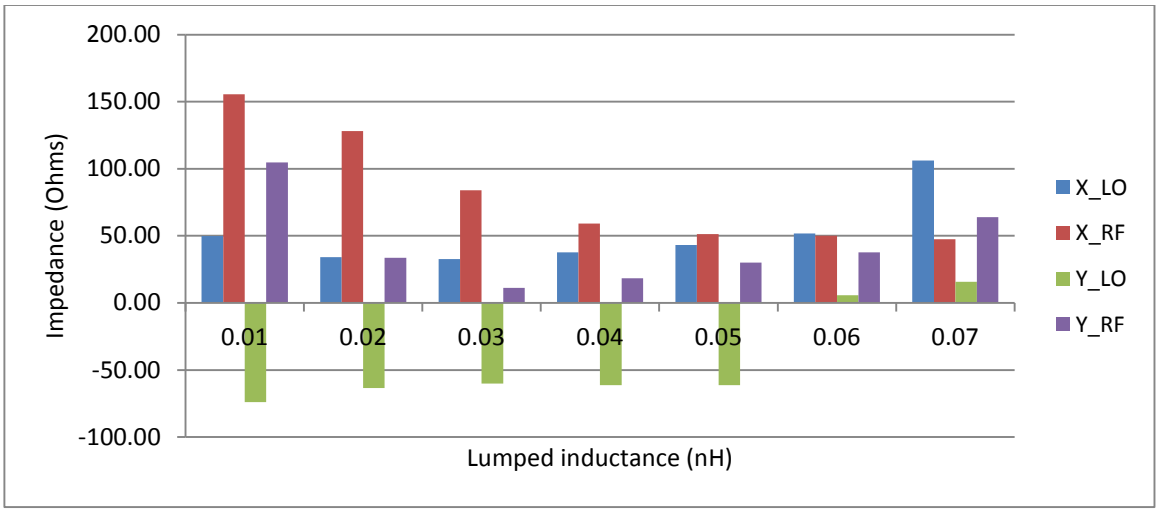

Figure 2-17 – Impedance values changing as a result of changing lumped inductance (nH).

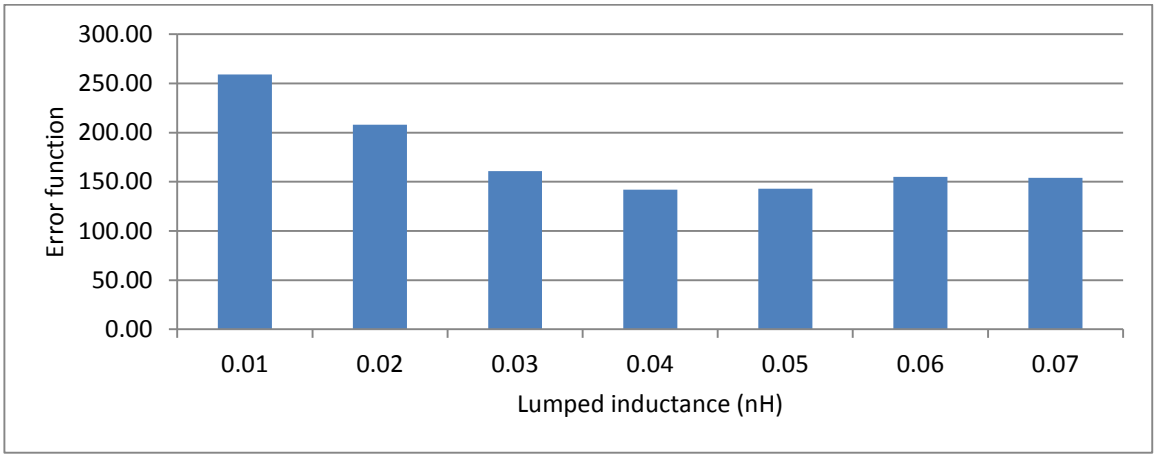

Figure 2-18 – Final error function of changing inductance simulations.

The effect of changing the inductance shown in Figure 2-16 shows that there is a peak at 0.04nH of finger inductance that provide the best conversion loss and bandwidth. Some higher values (>0.09nH) have a slightly better peak conversion loss at 664GHz, but fall off more dramatically as the frequency increases. This almost coincides with the value calculated using the equation in Equation (2). For the standard RAL diode which was 0.03nH. The difference can be attributed to the geometry of the finger compared to the ideal case of a round wire which was used in the calculation. The proximity of ground planes and other elements can also affect the inductance in the 3d model.

In order to look at this inductance matching further, a simple 3d model was constructed containing a simple 1x1x20um strip of gold in a vacuum. The S parameters of this structure were then exported and a simple circuit was set up in ADS to try and match the exported S parameters. The result of this was an inductance of 0.0075nH which is a factor of 4-5 difference from the values previously gained, this difference can probably be attributed to similar effects and geometry differences as mentioned in the previous paragraph. The capacitors seen in the circuit were necessary to get a good match.

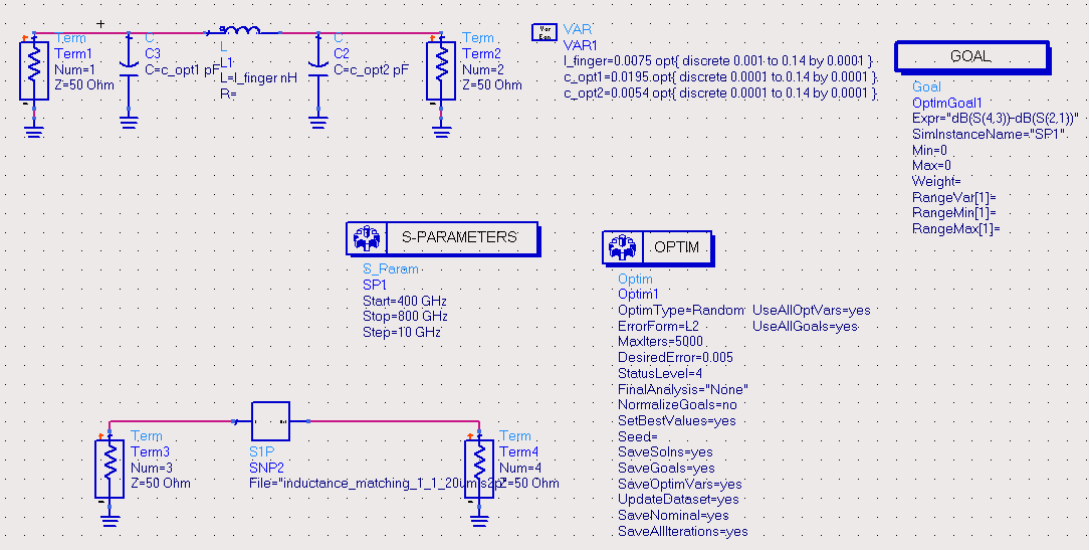

Figure 2-19 - ADS circuit for inductance matching.

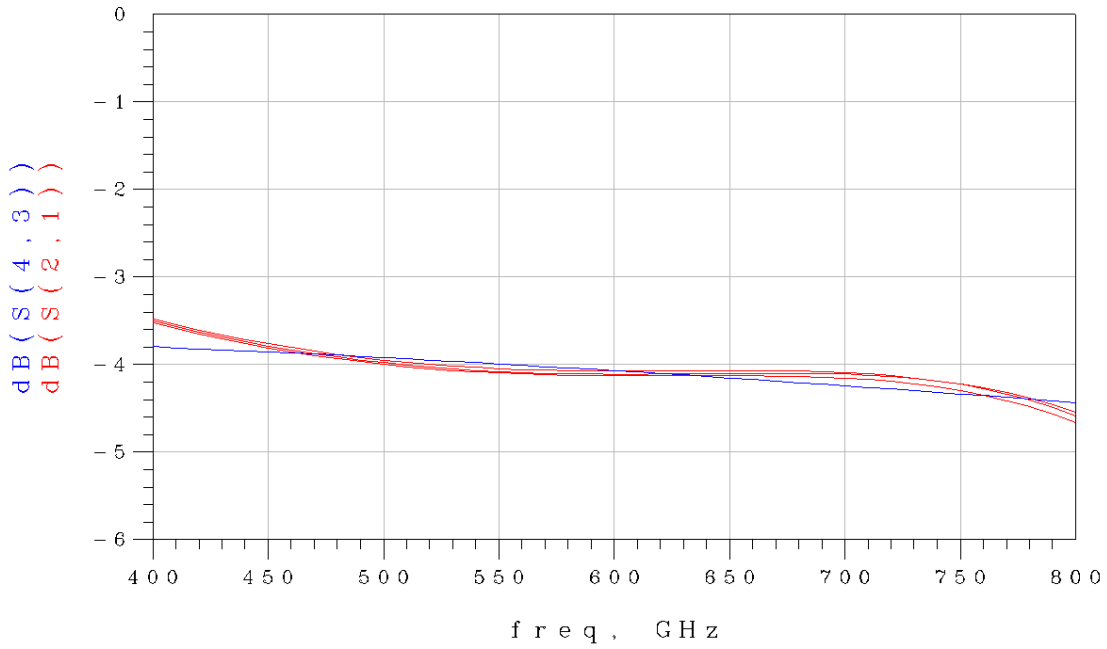

Figure 2-20 – S parameter matching of the simple 3d model (blue) and the ADS inductance circuit (red).

Refining the diode fingers

Changing the width of the diode fingers was also studied as the radius is another key component in the inductance equation (2).

Changing the width of the finger in the simulations had a small stepped effect on the performance of the diode in a mixer circuit, but not as great an effect as changing the length of the diode finger.

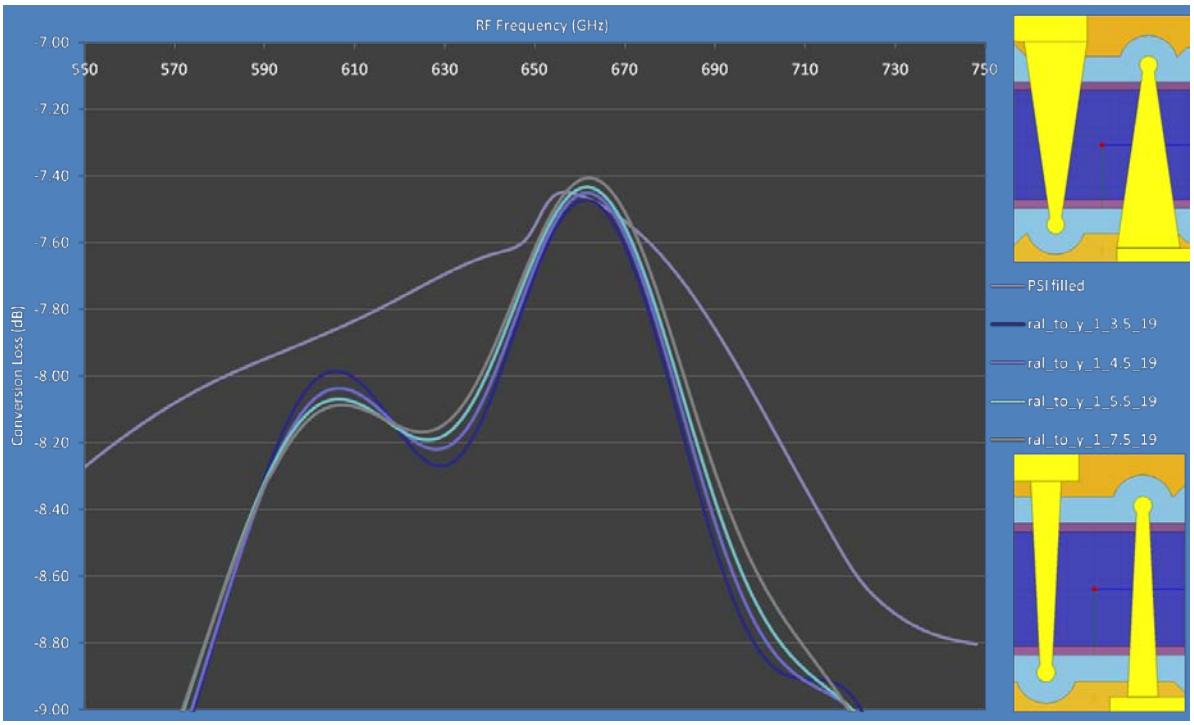

Figure 2-21 – The effect of changing the width of the diode fingers with 19um long fingers

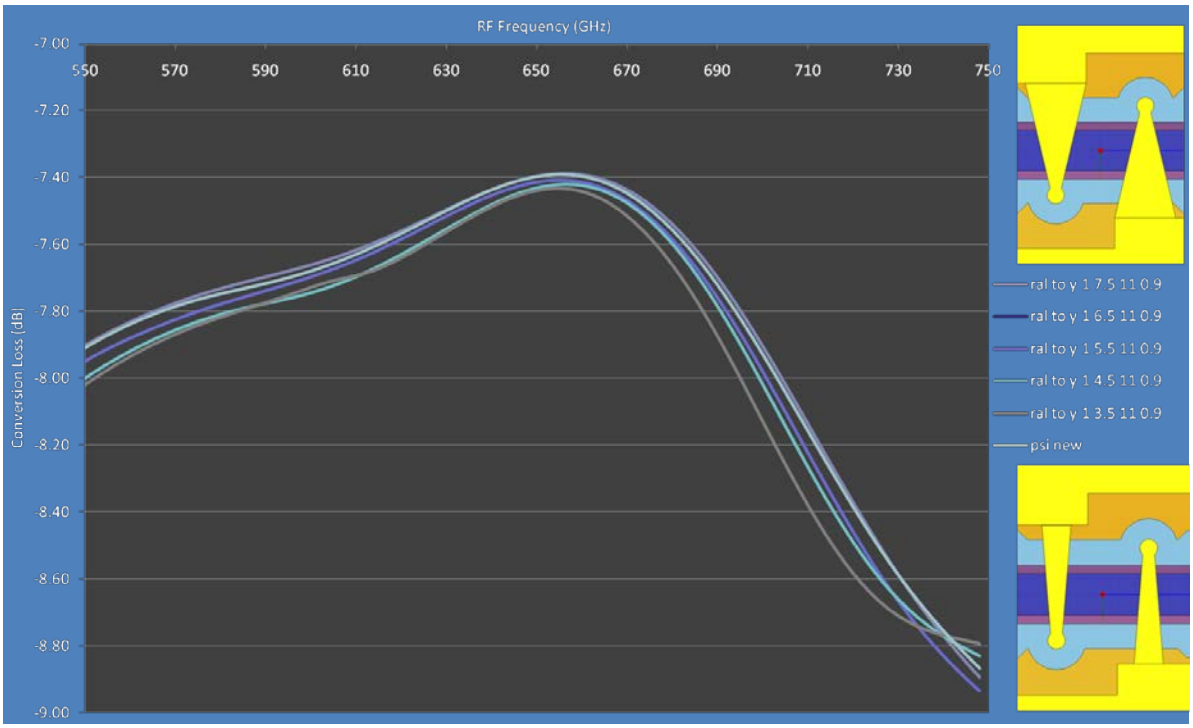

Figure 2-22 – The effect of changing the width of the diode fingers with 11um long fingers

The result of all these simulations shows gradual improvement of the performance of the diode in a mixer as the finger length is shortened and the width of the finger is increased, which is what might be expected intuitively. Changes have to be made to this design however in order that it can actually be fabricated. The first change is to change the shape of the diode slightly to try and reduce the parasitic capacitance by making the finger thinner at the anode end. At the other end the finger is kept as wide as possible (Figure 2-23). This gives a very similar overall shape.

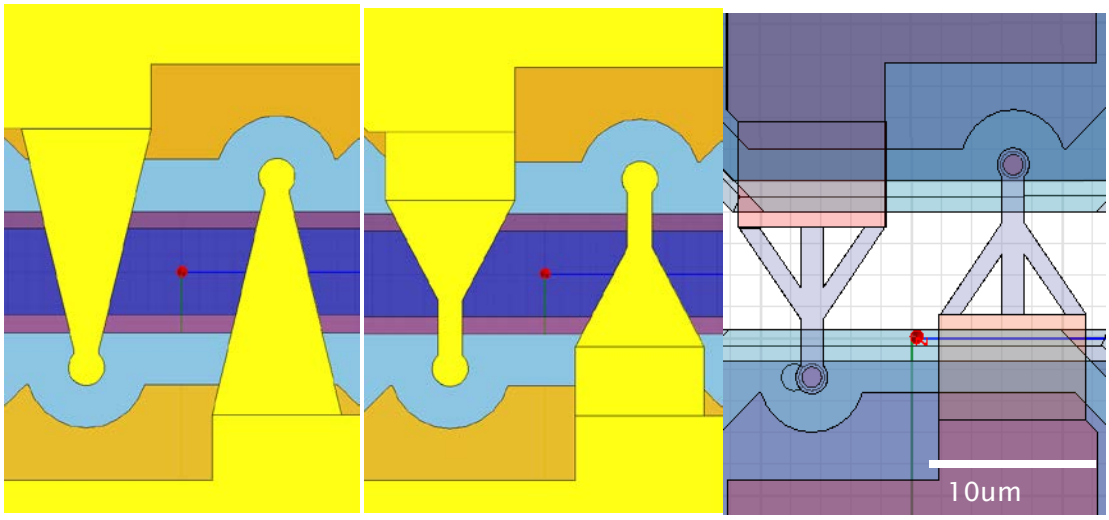

Figure 2-23 - Evolution of ideal diode design to one that can actually be produced.

Final Design

This design has almost identical performance to the Y design including matching impedances which can be seen in Figure 2-13. There is however still a processing problem with this design. In order to create the air bridge, the material underneath the finger needs to be etched away and this was not possible with such a wide feature being suspended. This meant that holes had to be created in the fingers to create something more similar to the Y design. This resulted in the “psi” diode due to its similarity to the Greek letter. This further processing need has also had no effect on the performance or matching of the diode as seen in Figure 2-27 the results are almost identical for the diode with and without the holes required for processing.

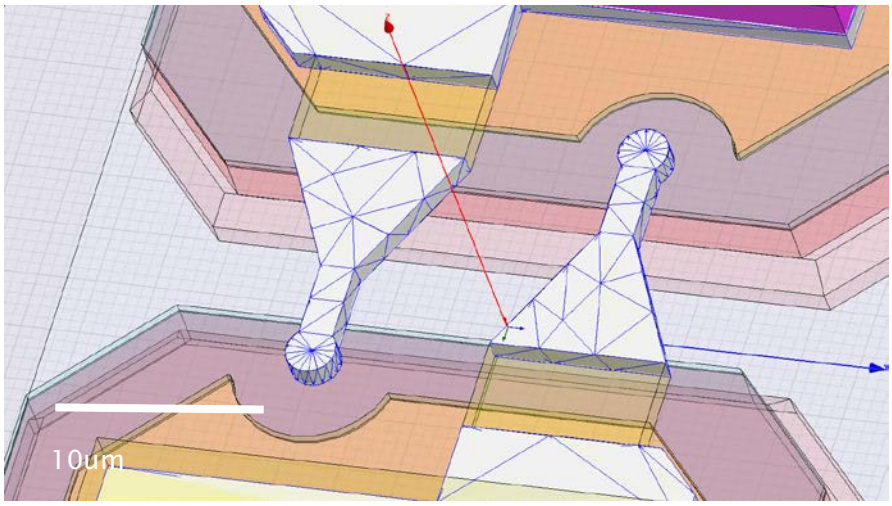

Figure 2-24 – Diode fingers showing simulation cells

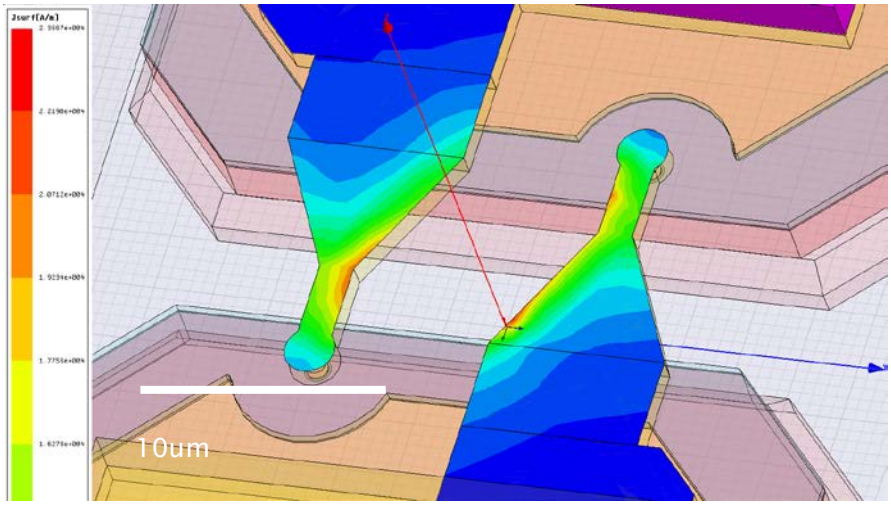

Figure 2-25 – Diode fingers showing surface current density

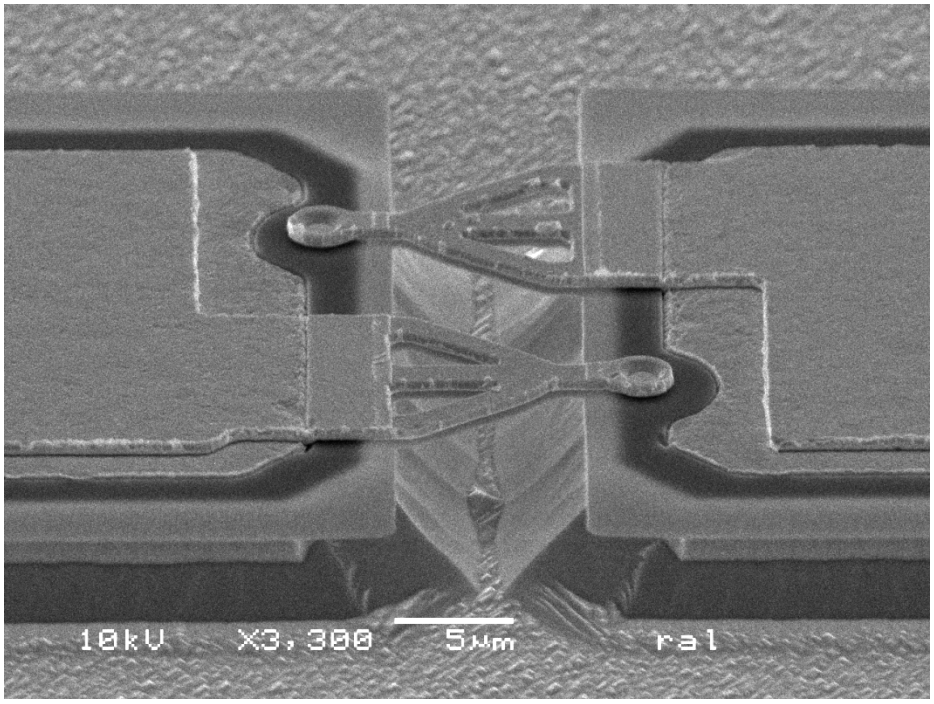

Figure 2-26 – SEM image of fabricated "Psi" Diode

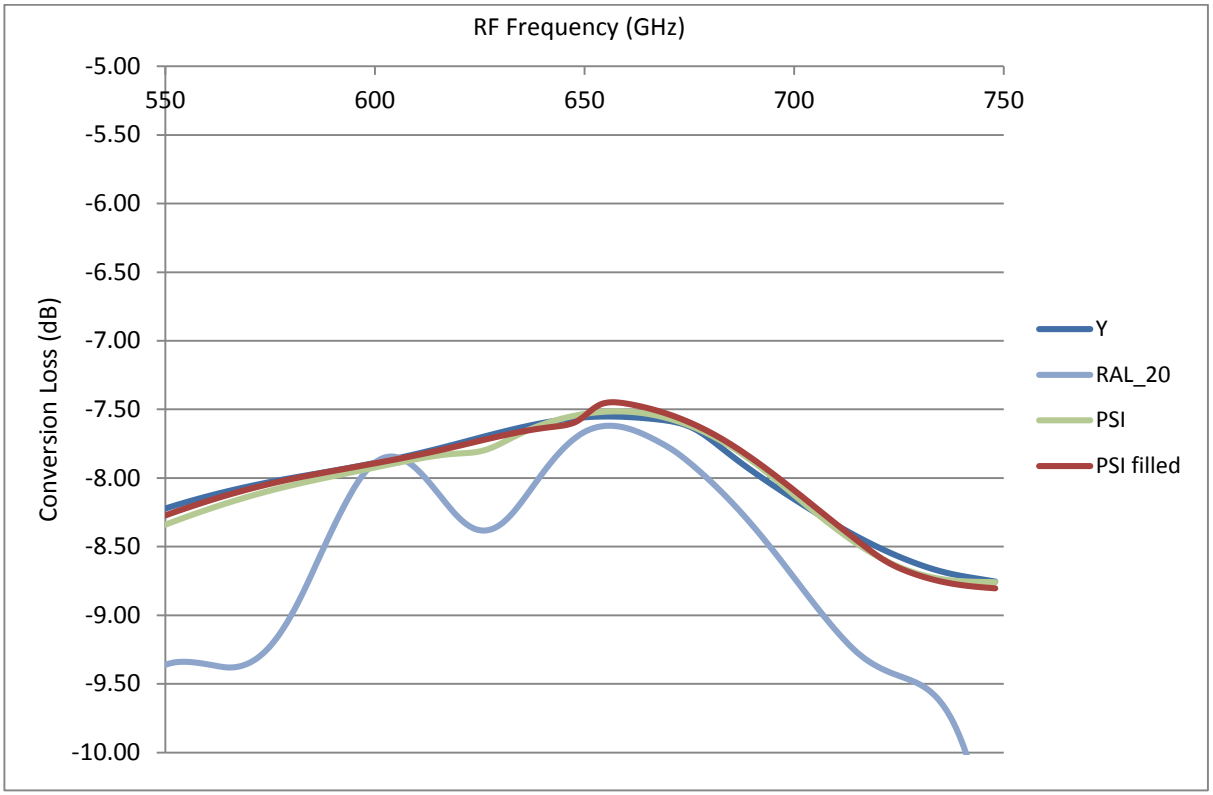

Figure 2-27 – Performance of latest diode designs in a simulated mixer

Further production batches of the diode design have shown that in some diodes where the holes were not created properly the under etching still occurred without any problems so it appears that the holes are not actually required for processing as initially posited.

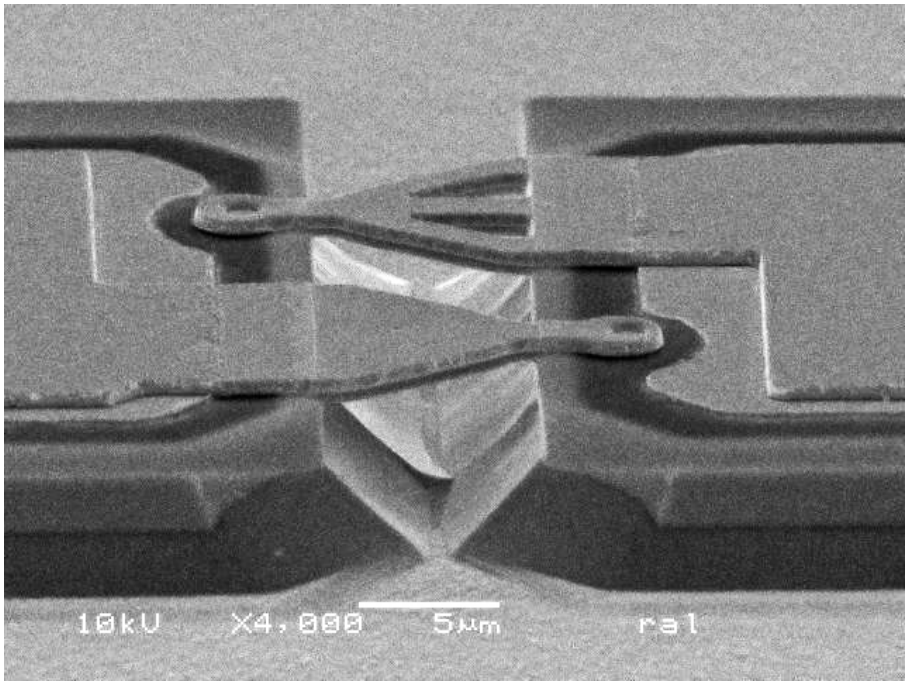

Figure 2-28 – SEM image of fabricated diode with no holes in one finger

Conclusion

The diode parameters have been extracted using simulation and experimental results then the inductance has been focussed on and the diode design changed in order to improve the performance of the diodes at high frequencies.

Chapter 3 - 664 GHz Sub-harmonic Mixer Design

The overall aim of these simulations is to design a sub-harmonically pumped Schottky diode mixer that operates at 664GHz with state of the art performance.

Mixer circuit configuration

The circuit design used is similar to that developed by Thomas et al [40] and is shown below.

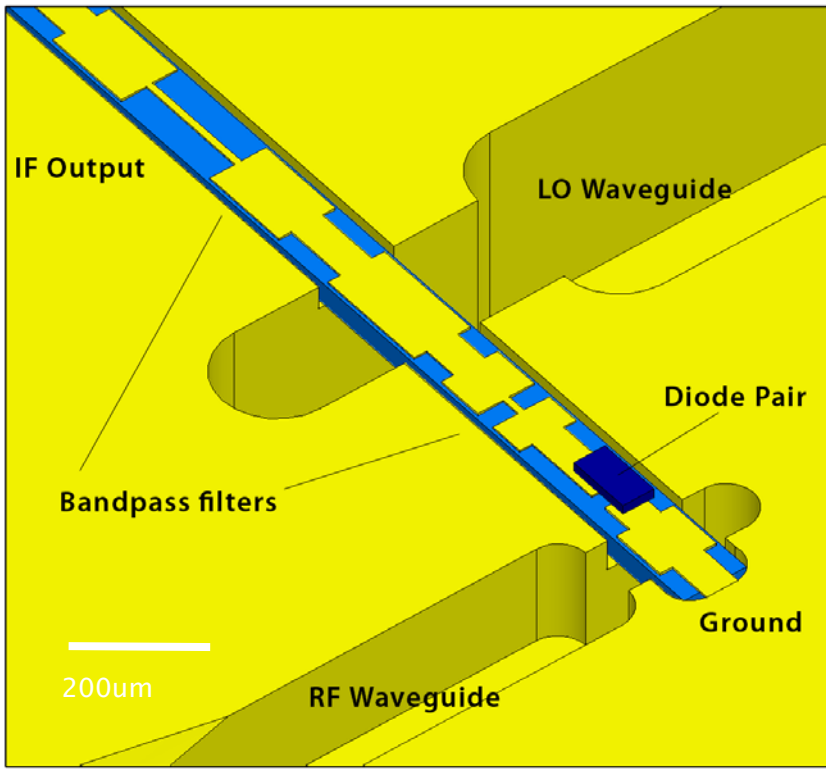

Figure 3-1 - Circuit configuration shown as bottom half of split waveguide block

The incoming signals are coupled to the circuit through a feedhorn antenna for the RF signal and a waveguide port for the LO signal via waveguide to microstrip probe transitions. These transitions incorporate a machined step and a backshort, the position of which can be tuned in order to increase the match to the filter circuit. The shape of the step was questioned due to advances in machining equipment in order to test whether or

not the overall mixer performance could be improved. Whilst the original shape showed the worst performance in simulations where only the transition was considered it did not make a noticeable difference to the overall mixer performance and due to the time involved in creating and refining new machining techniques, it was decided to stay with the traditional curved transition.

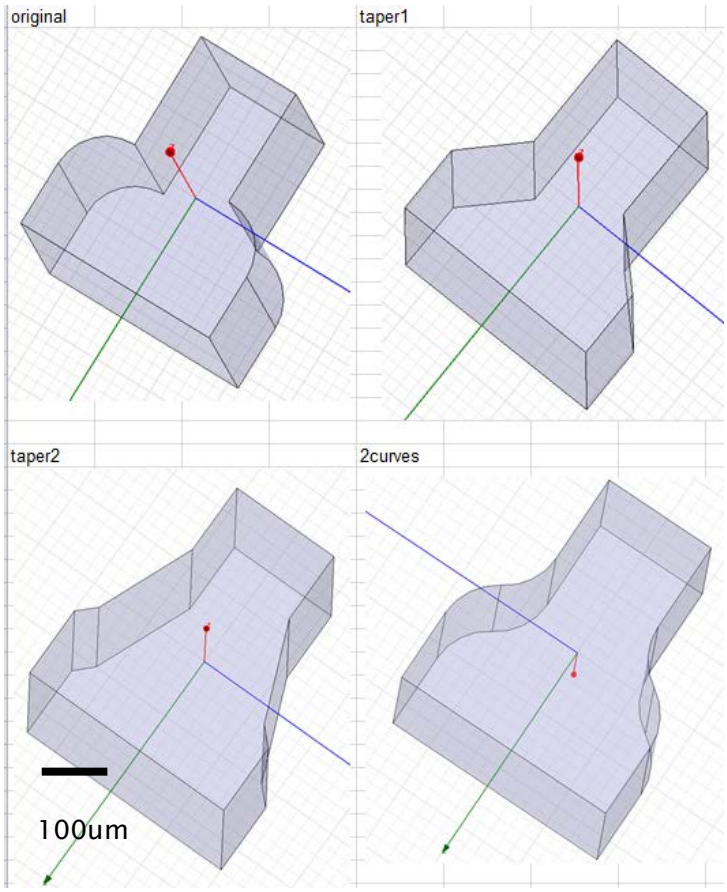

Figure 3-2 – waveguide transition shapes tested

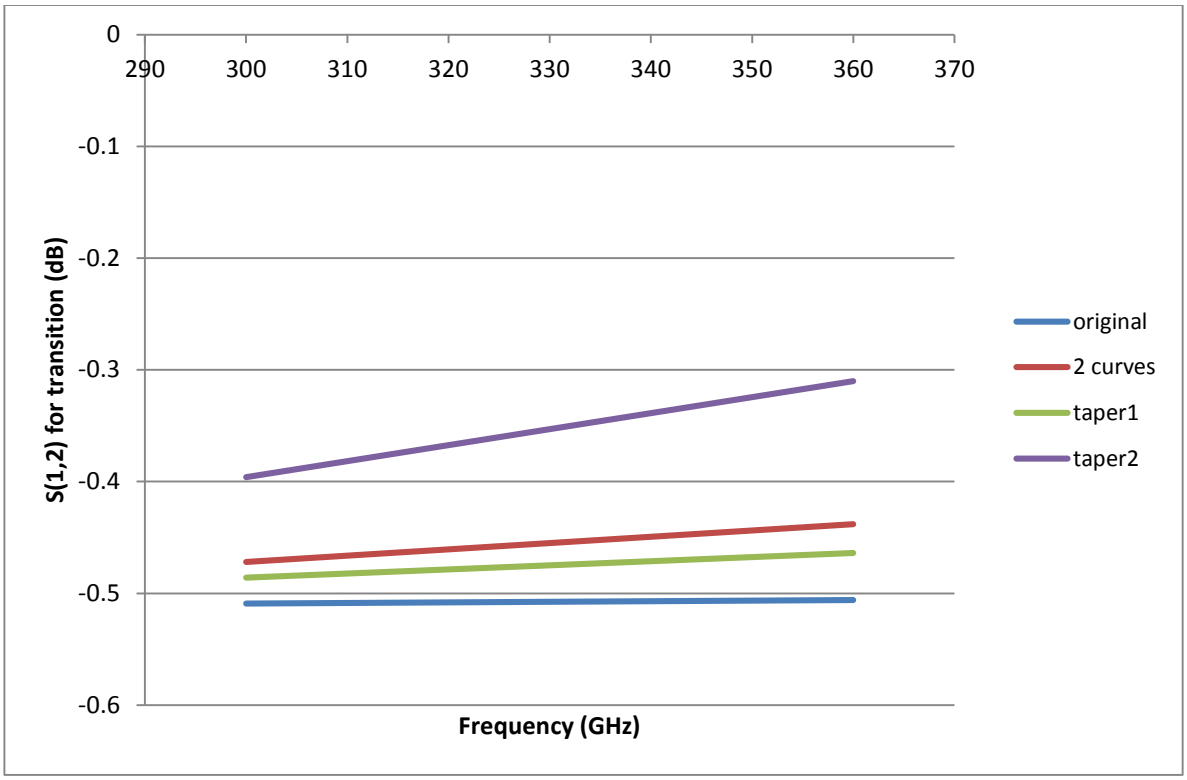

Figure 3-3 – Waveguide transition simulation performance

The RF probe is located in close proximity to the diode pair in order to couple the maximum signal and reduce losses. This is important due to the expected strength of the RF signal in field applications. Step-impedance microstrip filters are used to direct the LO and RF energy through the circuit. These filters are straightforward to optimise and manufacture compared to other filter options. Both filters are low-pass filters. The filter closest to the diodes is designed to reflect any RF power that passes the diodes from the probe back to them whilst letting the LO signal pass through to the diodes from the LO to microstrip transition. The second filter is designed to reflect the LO signal away from the IF port and towards the diodes. The IF signal is able to pass through both filters to the IF port from the diodes. There is also no possibility of the IF signal leaking into the waveguides via the probe transitions as the size of the waveguides means that the cut off frequency for transmission is far higher than the IF signal. The circuit ground is created at the opposite side of the RF probe from the diodes by trapping a beamlead between the two halves of the waveguide block.

The block is manufactured in two halves for ease of machining access and mounting the circuit in the block. The split plane is parallel to the filter circuit as this reduces any waveguide losses caused by a break in the conductivity of the inner waveguide surface.

The LO and RF waveguides are facing each other so that the signals are dealt with at opposite sides of the 2cm cube for easy experimental setup. The IF port is located at the opposite end of the circuit from the ground on a third face of the cube. The waveguide sizes were chosen to match with a 332GHz doubler currently in design to act as an LO for the mixer and to match with waveguide sizing convention with metricised versions of the EIA waveguide WR series.

Some work was done to look at the high frequency waveguide losses as due to the standard 2cm block used there is almost 10mm of LO waveguide in the configuration used and if the block was re-drawn to be used with an external feedhorn (like a corrugated feedhorn) for better performance then there would be almost 10mm of RF waveguide too.

Blocks were designed and manufactured to measure this loss at 3cm and 6cm lengths which included surfaces within the design that would be worked with the same tool as the waveguide channel to measure the surface roughness of the bottom and sides of the waveguide.

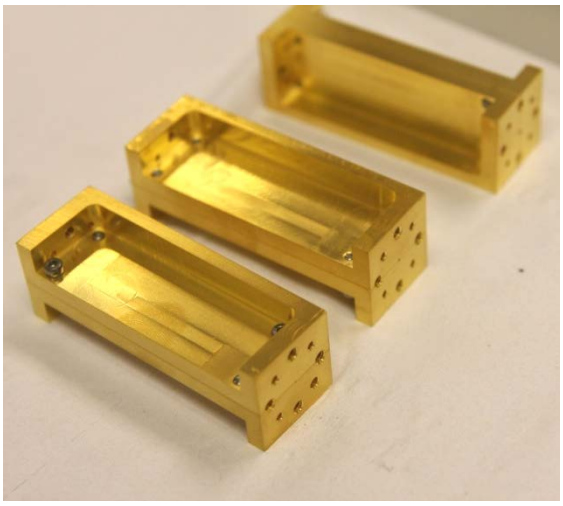

Figure 3-4 – Waveguide test blocks (6cm long)

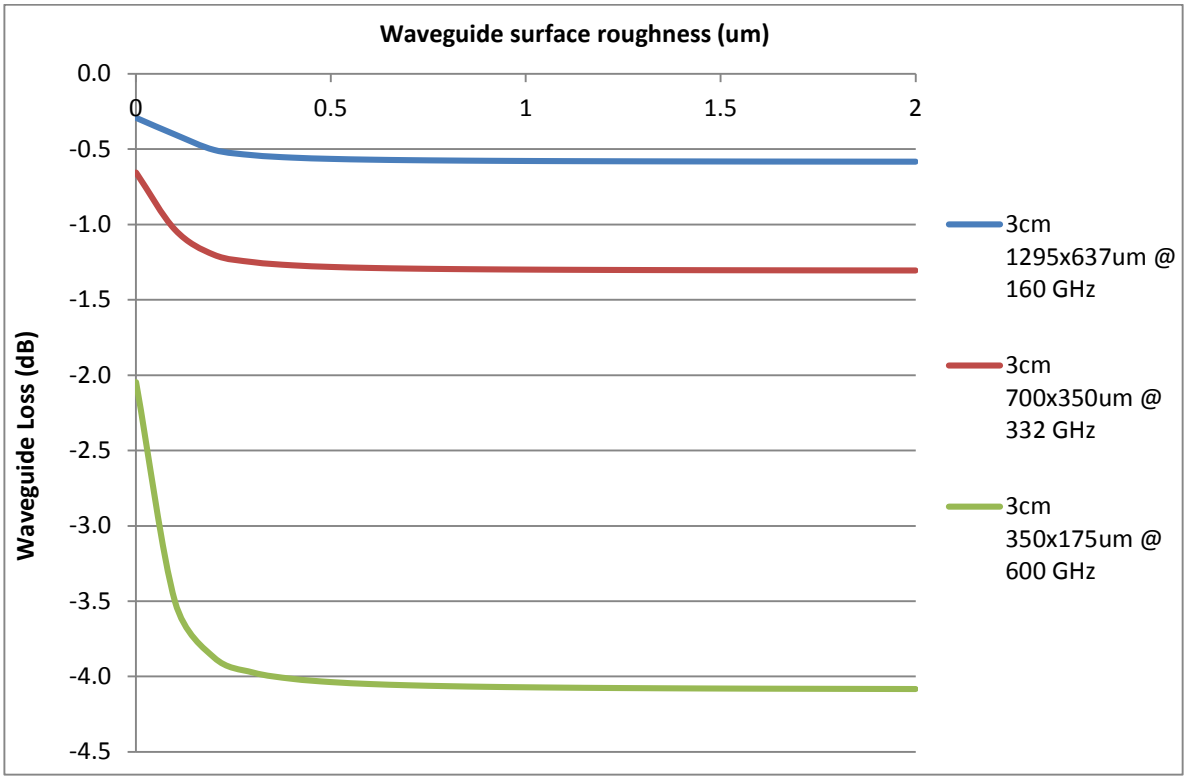

Figure 3-5 – Simulated waveguide loss at varying frequencies and surface roughnesses

Due to time constraints and the difficulty in measuring losses accurately at high frequencies these have not yet been characterised. A team from VDI [41] have since published some work on this subject when testing VNA extender systems and they have

shown that simulation is within a factor of 1-1.5 of experimental results. There is only data published in the RF frequency of interest to this thesis though.

Methodology for Circuit design

The first step in the design process is to simulate a model of the diode in an ideal circuit in order to determine the embedding impedances of the diode. For this simulation a standard diode model is used but it is customised with known parameters that have been gained from calculations and characterisation of existing diodes.

The embedding impedances are calculated by a software optimisation technique that works out what impedances are required in order to give the best conversion loss of the mixer circuit.

Changing the diameter of the anode on the diode changes the capacitance associated with the diode. This in turn affects the associated embedding impedances of the diode. This can be useful as bringing the impedance of the diode closer to 50 ohms will make it easier to match the input signal to the diode and the output from the diode.

Diode Configuration

The diode pair for the sub-harmonic mixer will be in an anti-parallel configuration as shown in Figure 3-5. This is because we have chosen not to add complexity to the circuit through the addition of a DC bias.

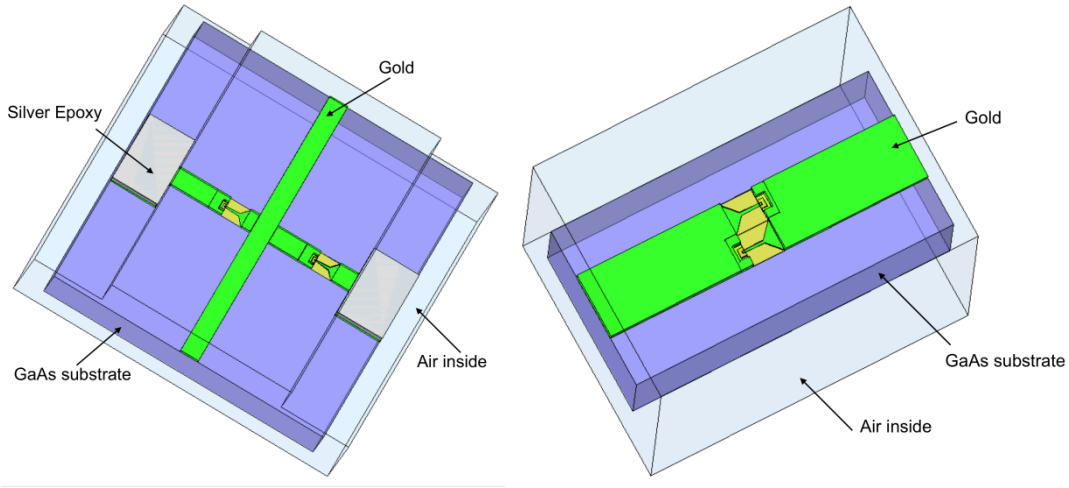

Figure 3-6 – Open loop configuration (left) and anti-parallel diode configuration

Methodology for Circuit design

The simulation methodology for the mixer design is described below, some examples from the sub-harmonic mixer design later are given as examples to illustrate some of the stages. Each stage of the process for the mixer design is described in detail and here is an overall process flow:

- Determine ideal diode impedances.
- Define circuit topology.
- Optimise diode cell.
- Calculate S parameters and transmission line properties of circuit elements.
- Perform S parameter matching to optimise constituent lengths.
- Perform harmonic balance analysis of final circuit. Backshort lengths are re-optimised in these final nonlinear simulations.

Ideal Diode Impedances

An anti-parallel pair of diodes and some ideal matching elements is the first circuit to be analysed. This is done in ADS using the harmonic balance calculations. This is a two-tone nonlinear analysis that enables the voltages across the diodes to be measured as well as the current through them which can be related to all the mixing products generated by the diode pair. This analysis enables the impedances of the diodes at the all the frequencies $f_{m,n} = \left| m \times f_{RF} + n \times f_{LO} \right|$ (where m and n are relative integers) but in practice, this is limited to m=3 and n=9 to save on computational complexity. The LO multiplier is higher due to the much larger LO powers that are expected to be present in the system, meaning the resultant harmonics will be larger in magnitude and more should be considered in the simulation. The embedding impedances Z_RF and Z_LO presented to the pair of diodes at f_{RF} and f_{LO} are the most important. They are the input impedances looking into the diodes mounted in the circuit. Z_RF has an impact on the conversion loss and therefore the noise performance of the mixer. Z_LO has an impact on the amount of LO power needed to pump the mixer. The impedances are optimised to maximise the coupling to the diodes at f_{RF} and f_{LO} which means that a mixer with the minimum conversion loss that requires the minimum LO power can be designed.

The diode model used in this simulation circuit can be tweaked using averaged measured values of junction capacitance, ideality and series resistance taken from known batches of production diodes.

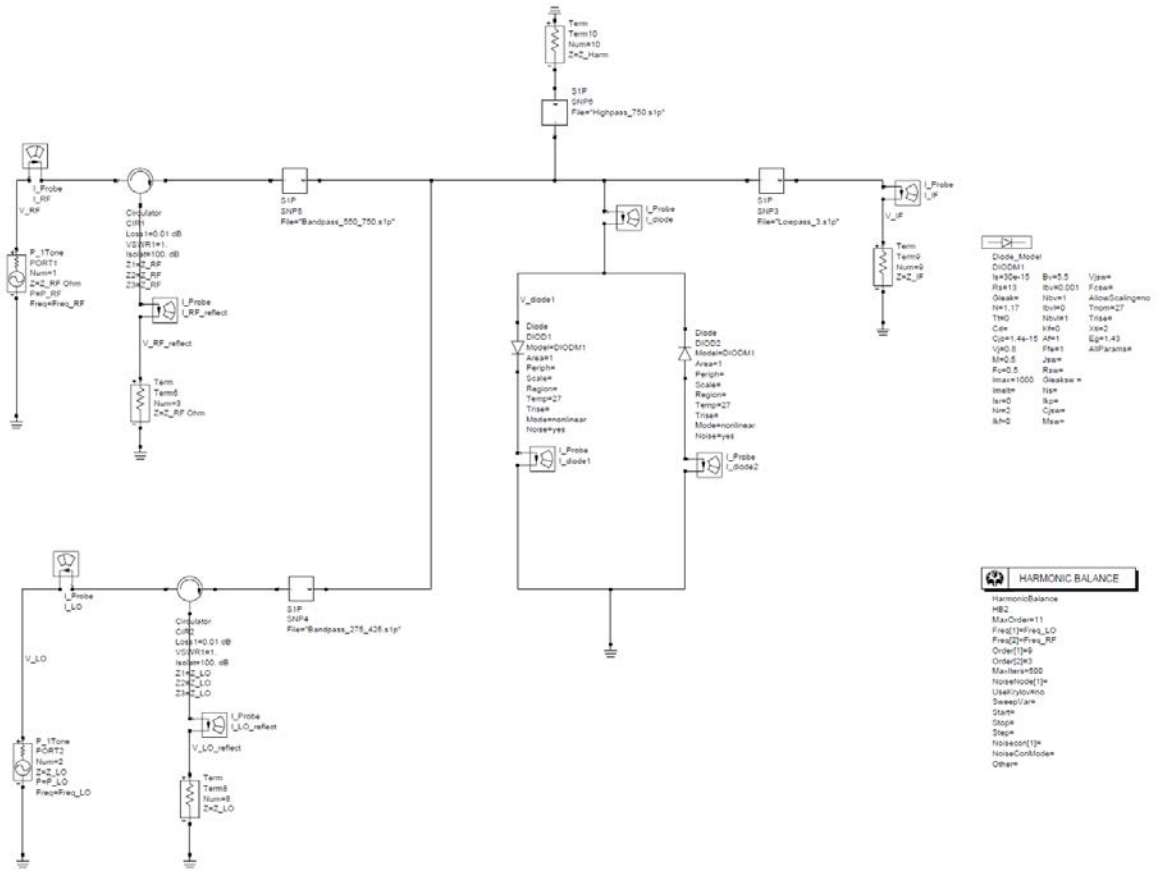

Figure 3-7 – Circuit for embedding impedance calculation

Linear Circuit Matching

The optimised values of Z_RF and Z_LO are used in the design of the matching circuit for the diodes. In order to do this a linear analysis of the transmission and reflection between the diodes and the signal sources is performed. This cannot be performed with the non-linear diode model as seen in Figure 3-6 so it is replaced with a data component representing it's calculated impedances over the RF and LO simulation frequency ranges.

Using the linear analysis the transmission and reflection coefficients between the diodes and the RF and LO source can be calculated. For an ideal mixer the maximum value of $S_{diode-LO}$ or $S_{diode-RF}$ is $\sqrt{0.5} \approx 0.707$.

Diode and Circuit Configuration

An optimised diode configuration (see diode chapter for more detail) is modelled at this point using the finite-element method in HFSS. This involves solving an accurate 3D model of the diodes which include wave ports at the anodes and at either end of the diode structure. The other independent parts of the mixer are also drawn and analysed using 3D models from which the S parameters are extracted and imported into an overall circuit in ADS. Other electrical parameters are also calculated in HFSS and used to refine items in the ADS model such as standard microstrip circuit components. This approach enables the lengths of the different sections of the LO and RF filters as well as the waveguide backshorts to be optimised using the target of 0.707 as the perfect transmission goal.

The circuit configuration is then taken from the optimised model and put into a harmonic balance model where further refinements to the configuration take place, usually on the backshort and microstrip to waveguide transition lengths.

Suspended microstrip filters

Differing widths of suspended microstrip lines present different impedances, if this difference is large then they can present a discontinuity at their interface that causes the signal to be rejected. If several interfaces like this are constructed in series then this filtering is stronger.

Due to the frequency dependant nature of the electrical characteristics of the microstip lines, separate simulations are performed for the LO and RF frequencies in order that the optimisation is accurate.

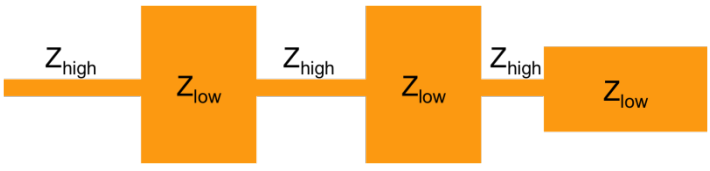

Figure 3-8 – simple filter schematic

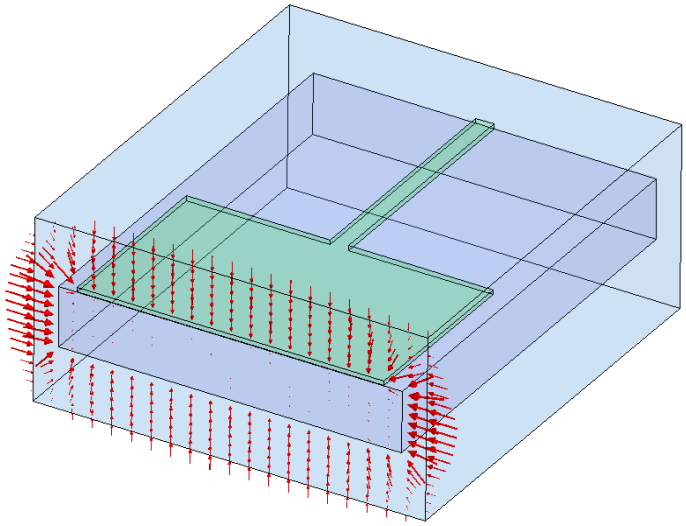

Figure 3-9 – Electromagnetic field at the low impedance port shown on a high impedance to low impedance microstrip transition as used for export of 2-port S parameters to ADS for length optimisation.

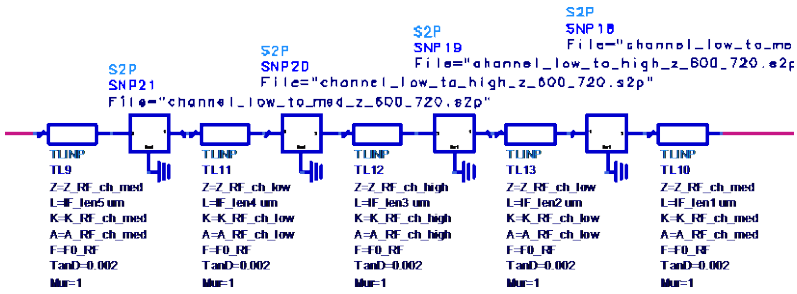

Figure 3-10 – Example of an entire RF filter in ADS using standard transmission lines and the imported S parameter files from HFSS

Changing the diameter of the anode on the diode changes the capacitance associated with the diode. This in turn affects the associated embedding impedances of the diode. This can be useful as bringing the impedance of the diode closer to 50 ohms will make it easier to match the input signal to the diode and the output from the diode.

Circuit Design for 664GHz Mixer

The first step as per the methodology was to optimise the S-Parameters which represent the coupling between the LO and RF inputs and the diode pair.

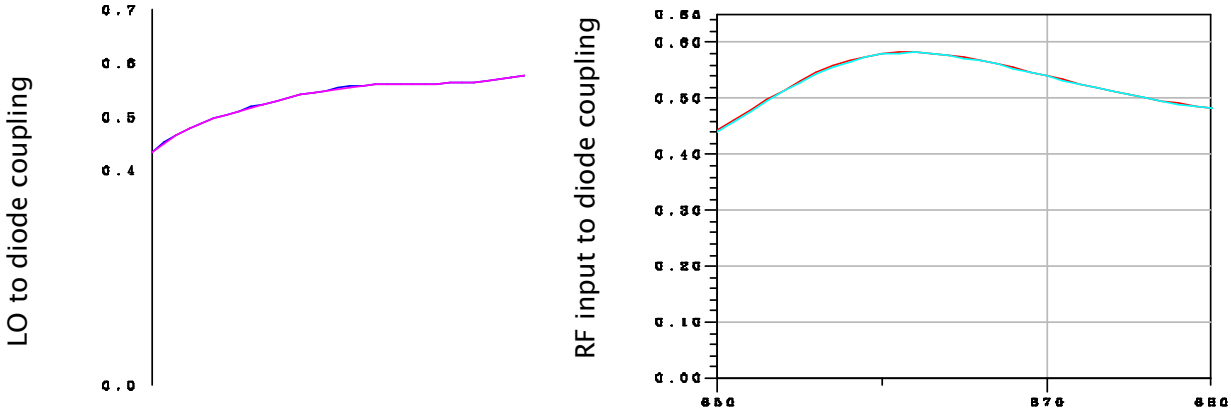

Figure 3-11 – S-Parameter coupling between the inputs LO (left) and RF (right) and the diodes.

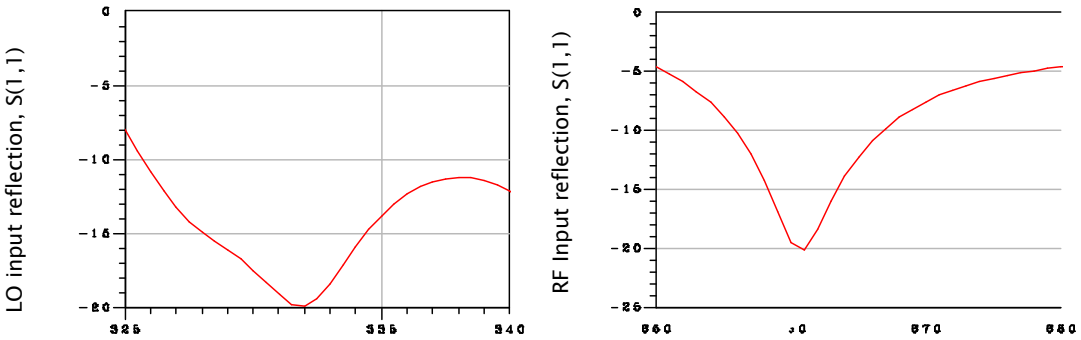

Figure 3-12 – Reflection at the LO (left) and RF (right) ports show fairly good coupling.

Non-linear optimisation of the backshort lengths followed and the overall performance was optimised giving the final performance as shown in the figure below which gives a conversion loss of better than 10dB for the range between 650 and 690 GHz given enough LO power. The optimisation goals for the non-linear circuit were (equally weighted) Conversion Loss with a target of 0, and reflection of the LO and RF signals with a target of between -30 and -40dB.

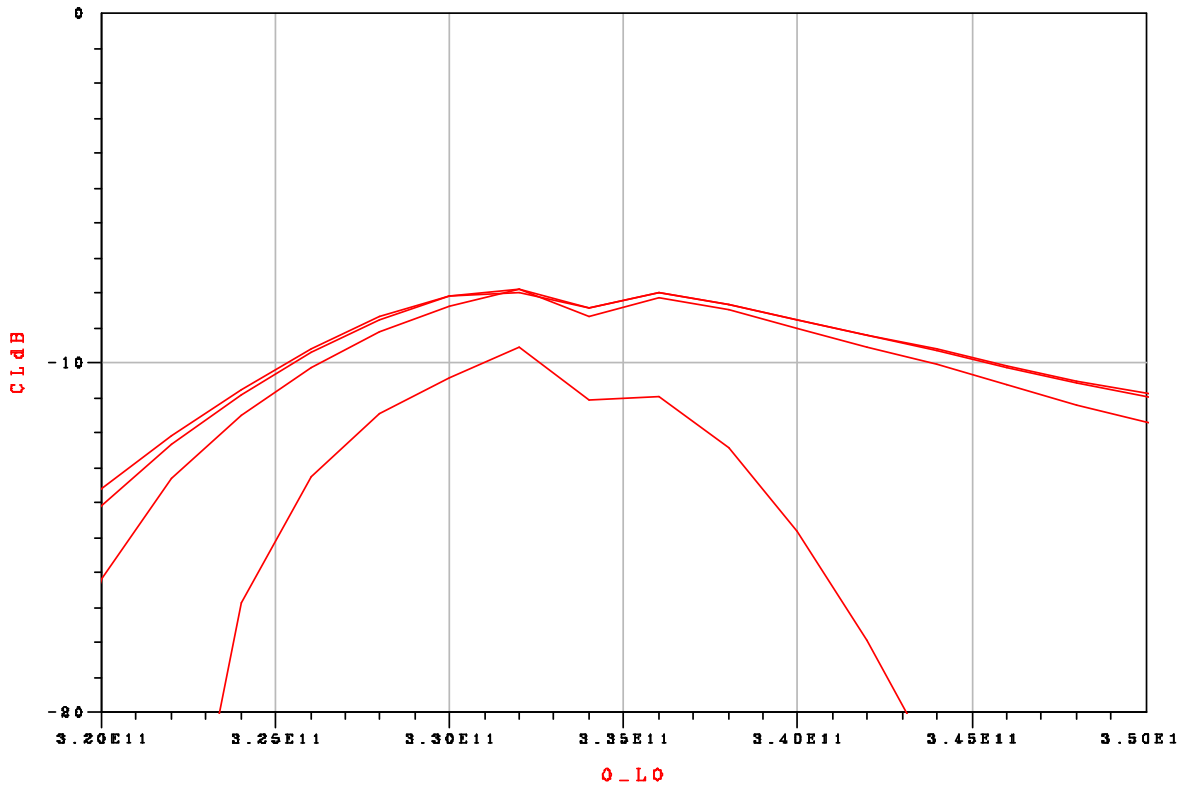

Figure 3-13 – Mixing performance of the final design at varying LO powers (2, 3, 4, 1mW from top) across the LO band of interest.

The figures above and below show that the design should function well given an LO power of >1.5mW going into the waveguide to microstrip transition.

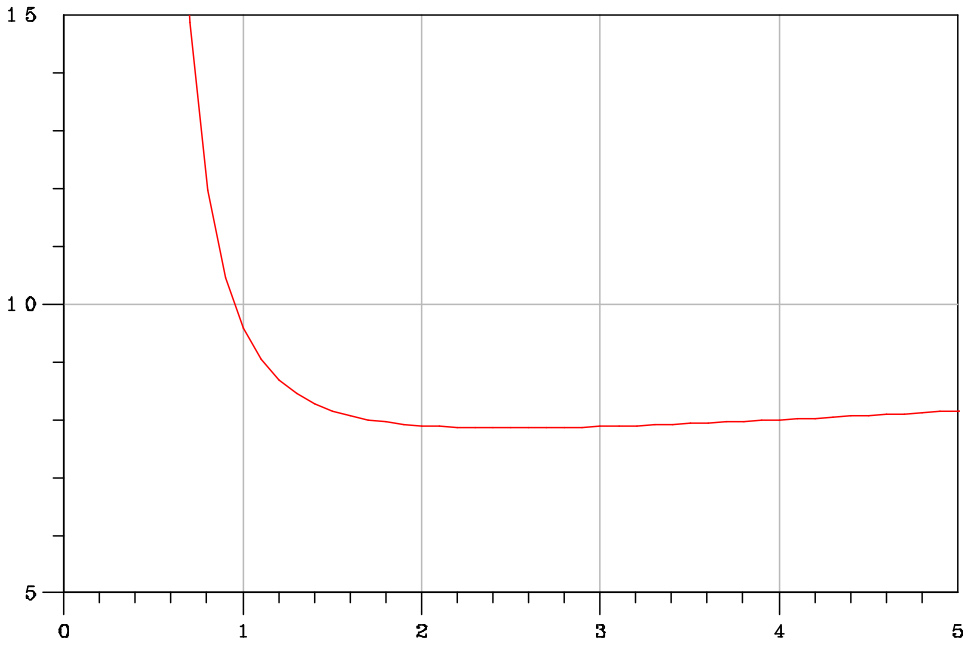

Figure 3-14 – Conversion loss at 664GHz vs LO Power

The figure below shows the final configuration of the mixer block and the filter strip in it.

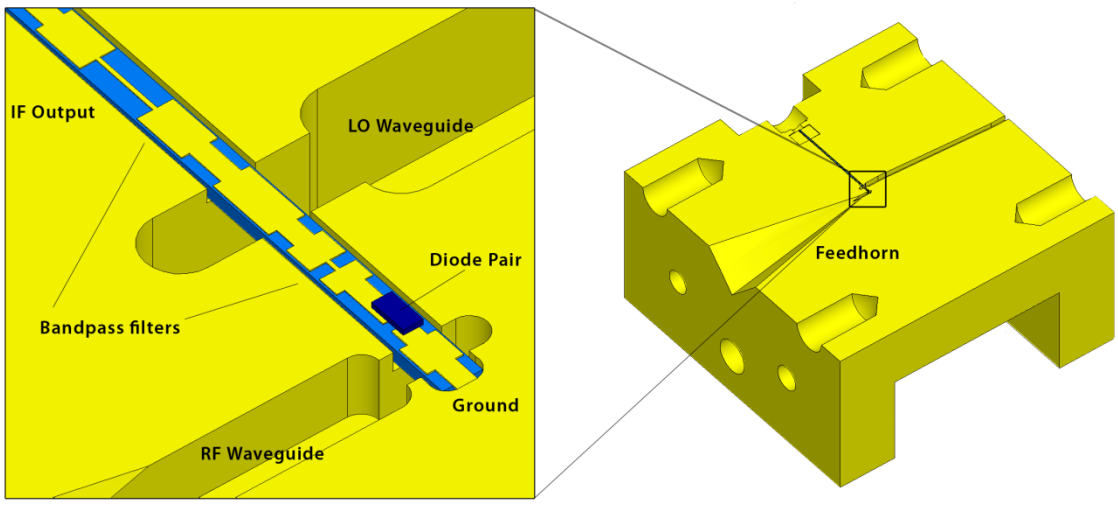

Figure 3-15 – Overall block design including circuit and diode pair

Block manufacture

Figure 3-16 – Standard 2x2x1cm half mixer block blanks

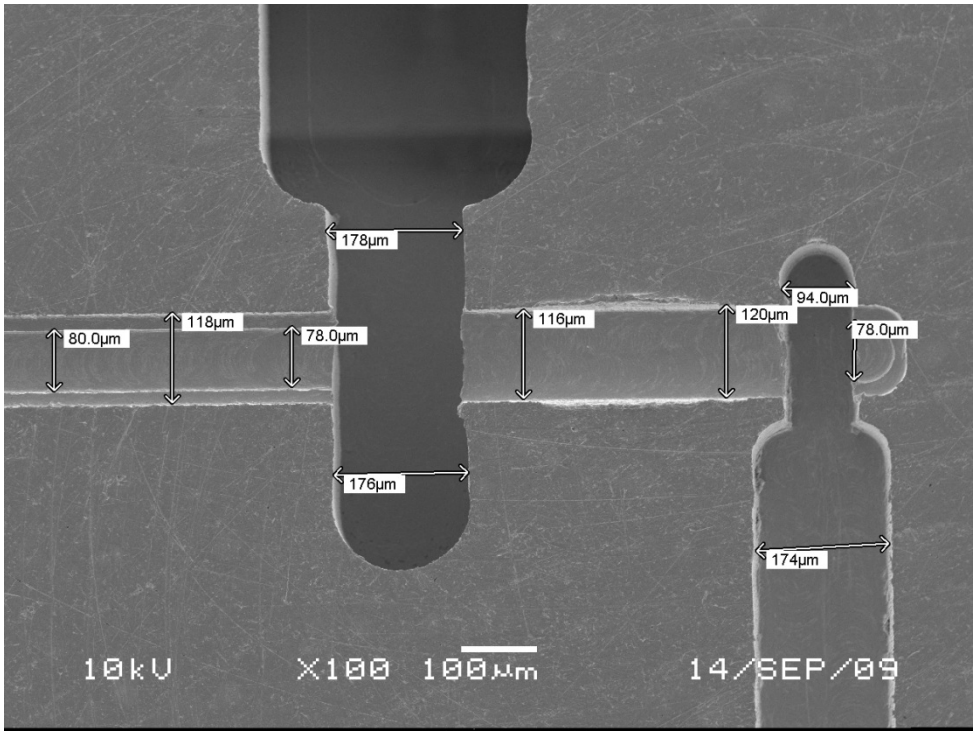

Figure 3-17 – SEM micrograph of channels after machining

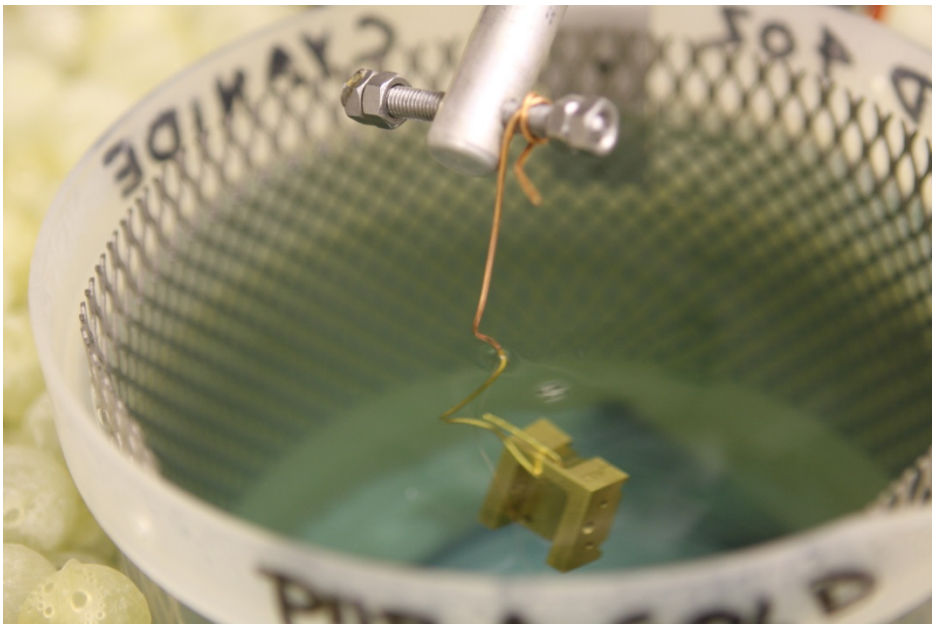

Figure 3-18 – Finished mixer block half undergoing gold plating in solution

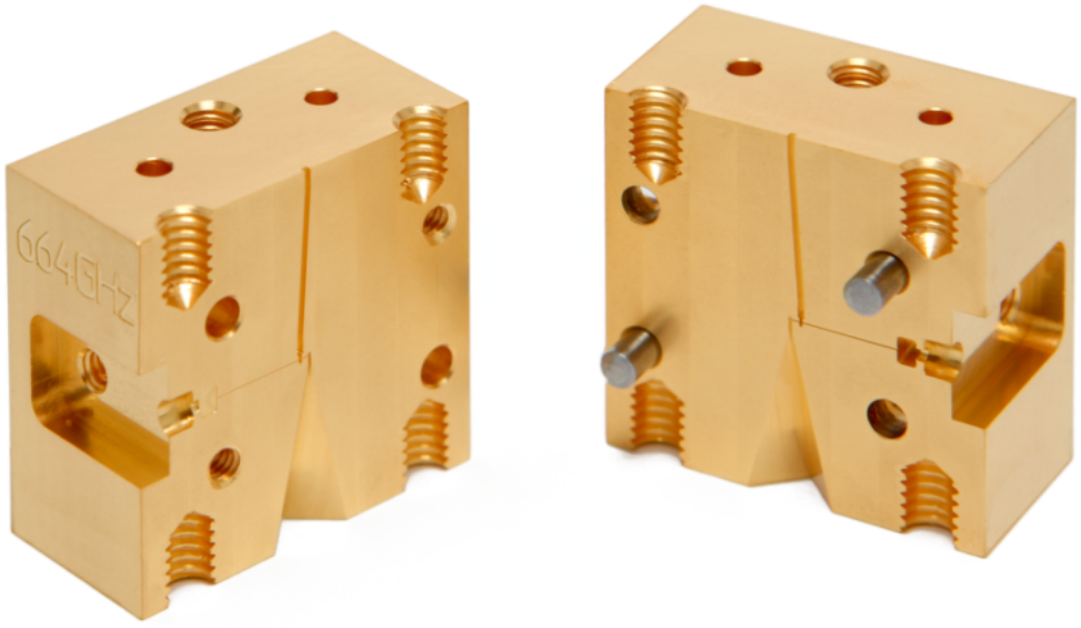

Figure 3-19 – Finished mixer block halfs

Filter Manufacture

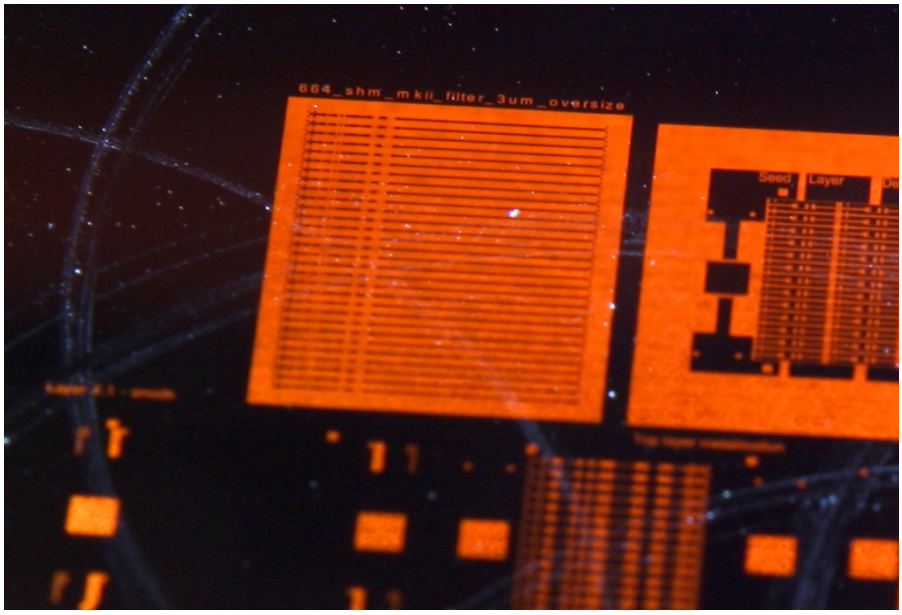

Figure 3-20 – Filter circuit mask close up

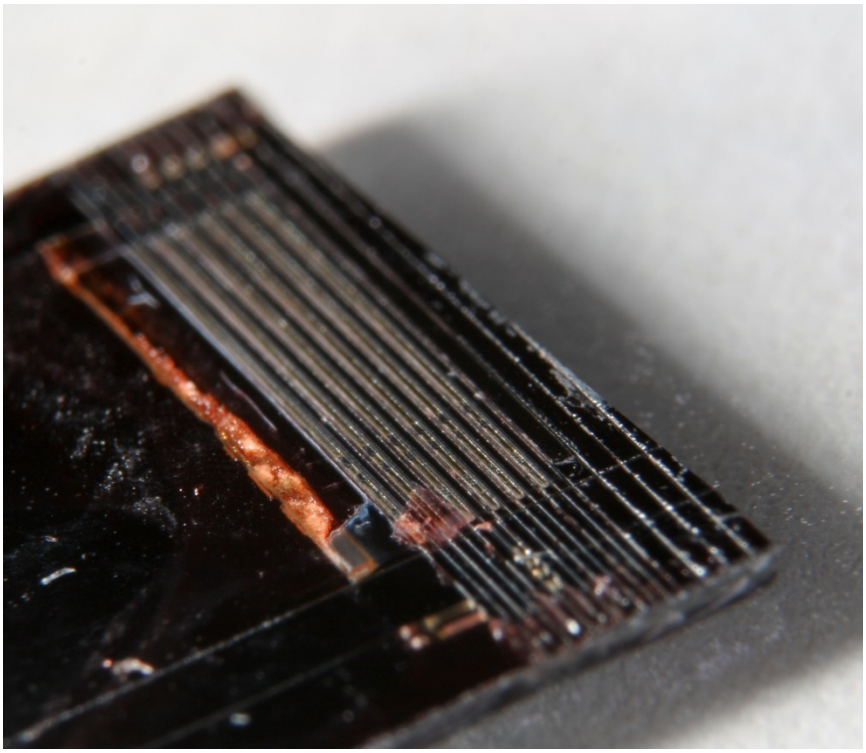

Figure 3-21 – Manufactured filter circuits on Quartz covered in protective layer of resist

Circuit Assembly Process

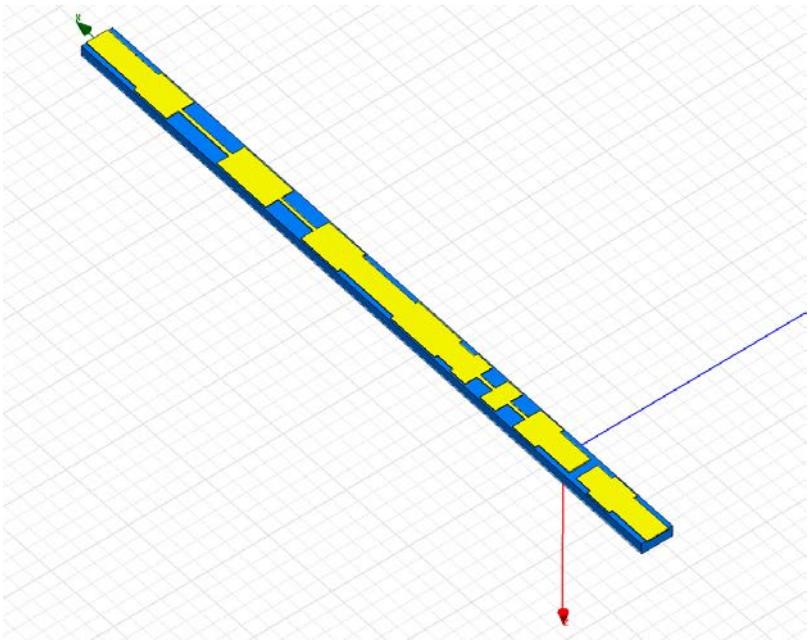

Figure 3-22 – First the circuit is selected and placed under a microscope where it is checked

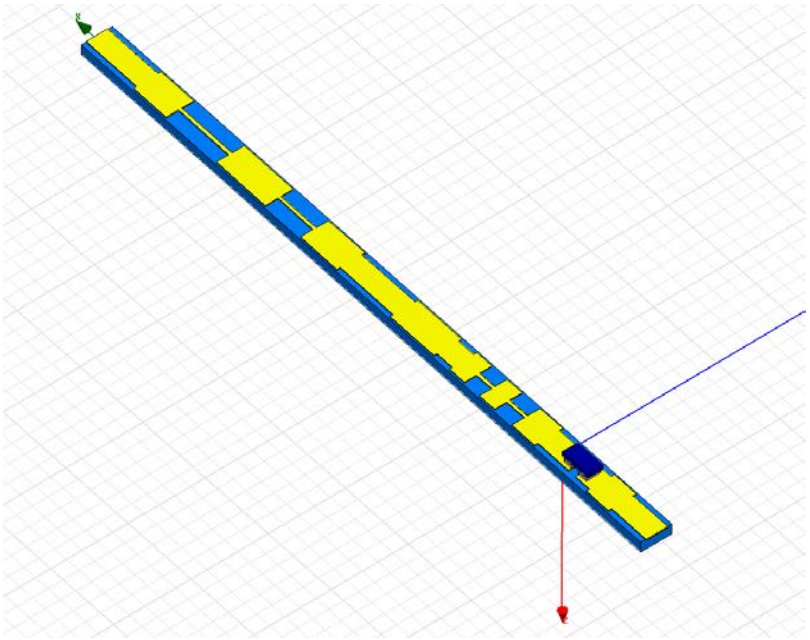

Figure 3-23 – Then a diode is tested electrically, selected, soldered onto the circuit and tested again to ensure it's DC characteristics have not been affected by the process

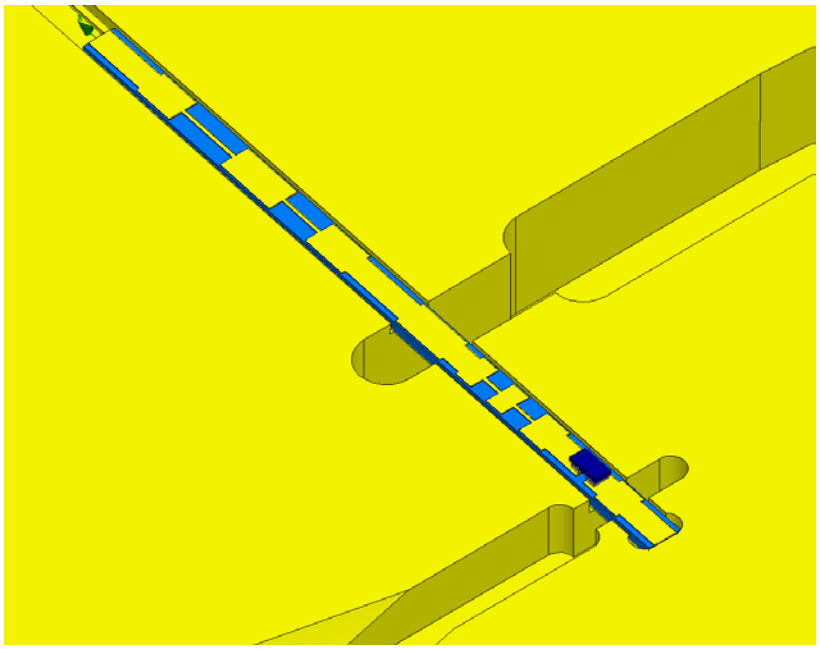

Figure 3-24 – Finally the completed circuit is glued into the mixer block

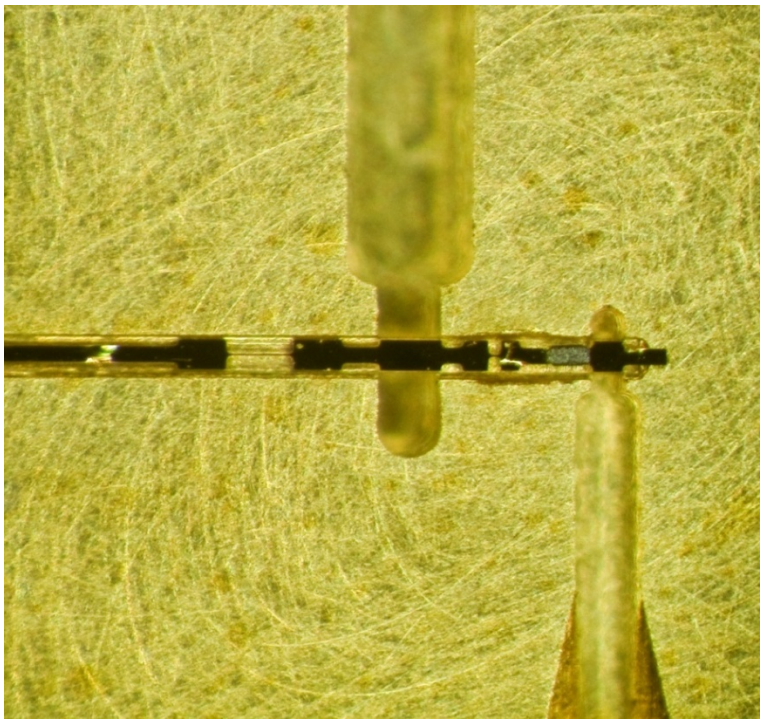

Figure 3-25 – Micrograph of assembled mixer circuit showing diodes mounted on circuit in lower half of block

Chapter 4 - 664GHz Sub-harmonic mixer evaluation, re-design and modification

The original mixer design was tested at with 6mW then 11mW of LO power at 332GHz but no mixing was observed.

On further investigation into the original simulations it was discovered that there were some inconsistencies.

Waveguide Port Impedances

The first of these was the differences in the methods used by the two main software packages used in the way that they calculate rectangular hollow waveguide port impedance. ADS only uses a single method for hollow waveguide and a different one for microstrip ports (like the IF port).

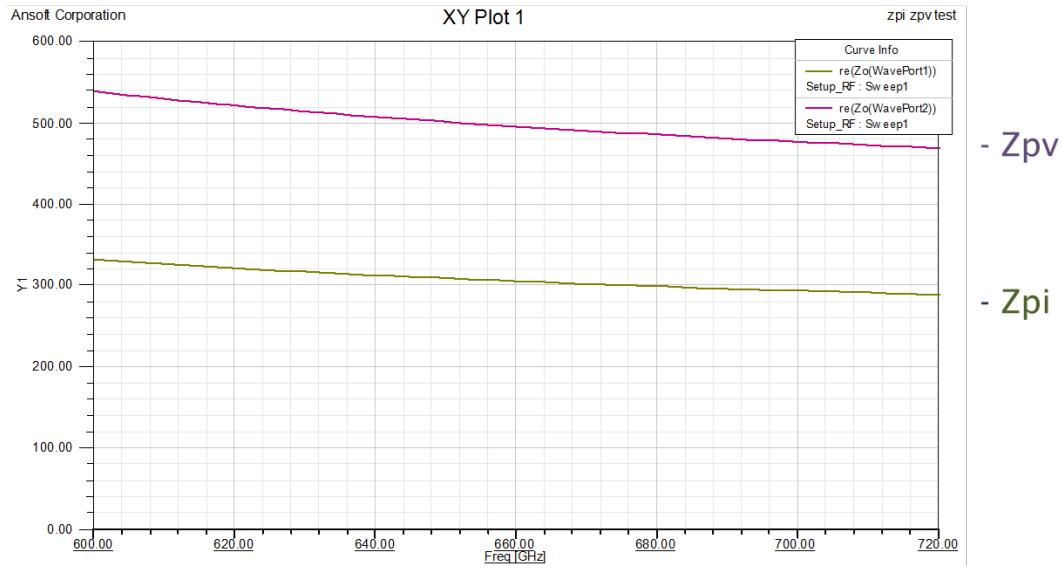

Figure 4-1 - Port impedance calculated using two different methods at either end of a simple piece of rectangular waveguide

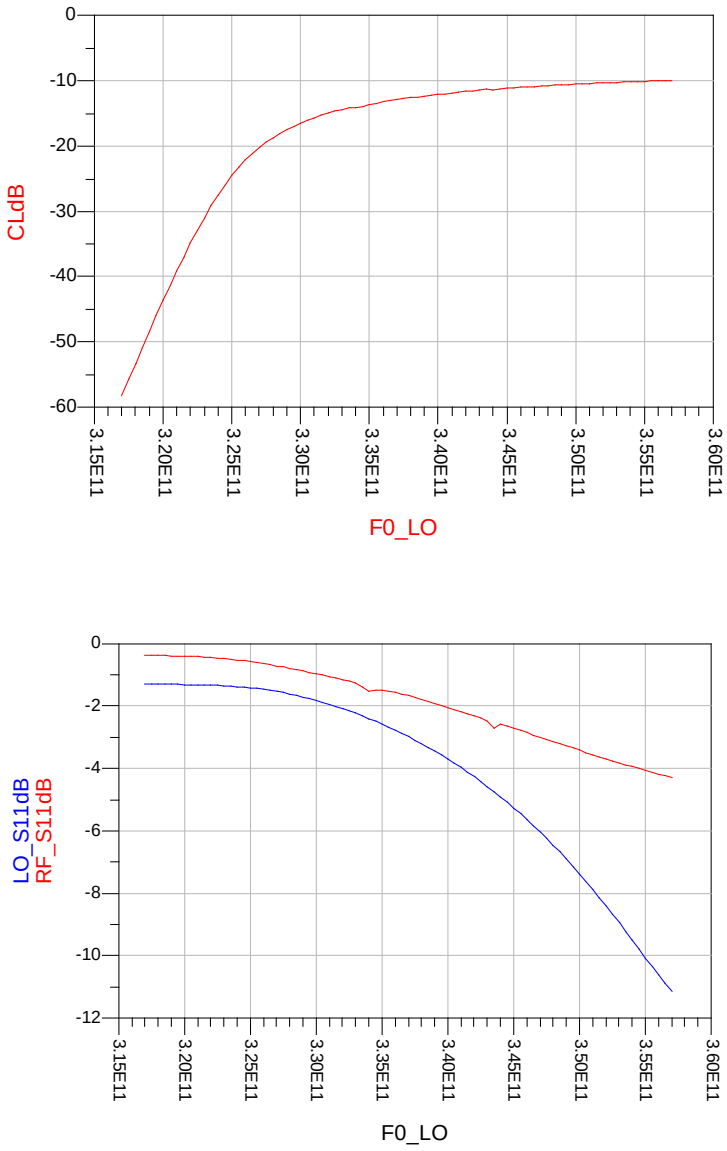

Figure 4-2 – Original simulation (Conversion Loss above and LO and RF input reflections below) after correcting port impedance methods

This large difference in the LO and RF match using the new method (fig 4.1) could explain the lack of mixing as the reflections at 664GHz are high, between 1- and -3dB. This would still mean 1-2mW would reach the diode pair though, so some mixing would still be expected. Re-optimisation of filter lengths eliminates this mismatch though and simulated performance returns to expected levels.

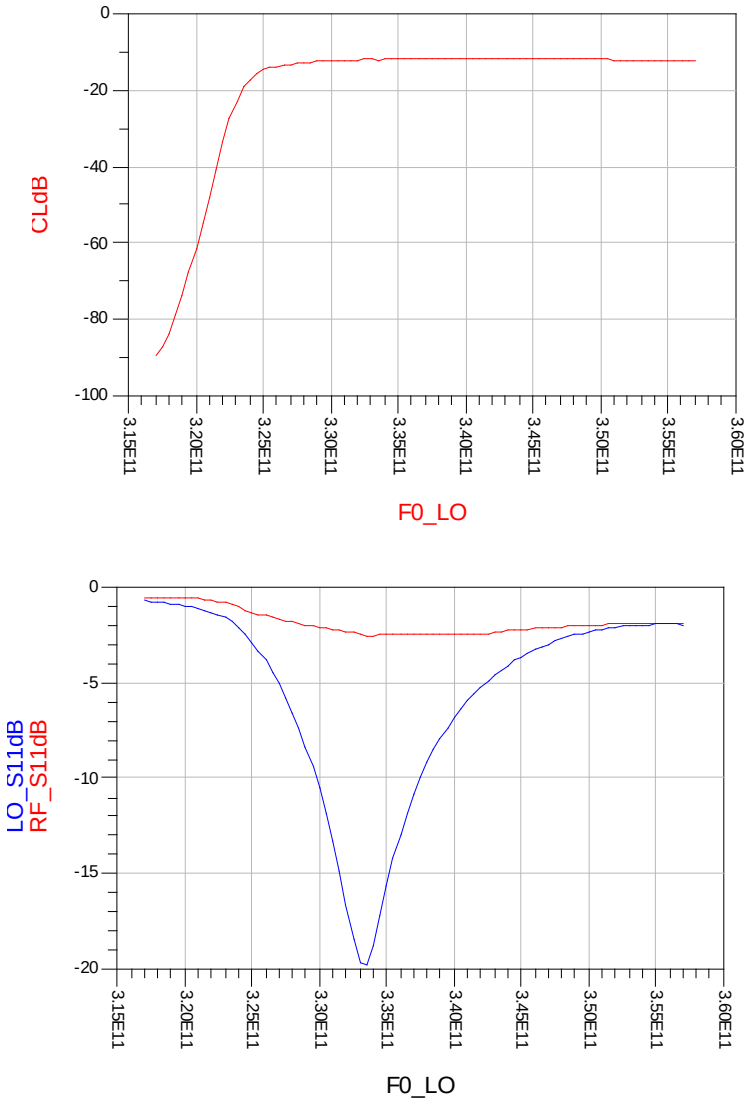

Figure 4-3 – Re-optimised simulation returns performance to expected levels

After this correction there was still a lack of correlation between the whole mixer model from HFSS and the distributed model with the extracted s parameters of each section in ADS.

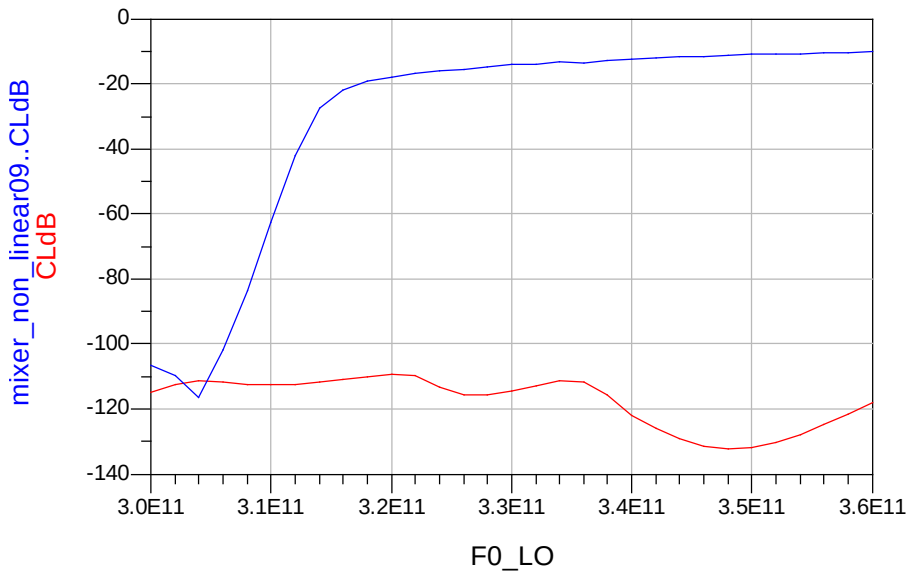

Figure 4-4 – 664GHz mixer whole model in red and distributed in blue

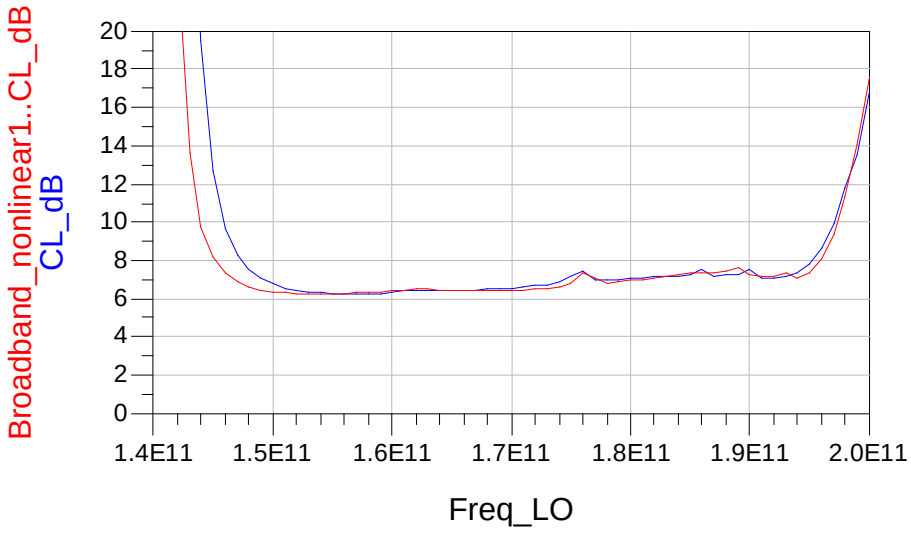

Figure 4-5-A 320GHz mixer design (by M Henry)for comparison showing whole model in red and distributed in blue.

Breaking down the model into smaller pieces

Several "semi-distributed" models were run as discussed in the next sections and the problem was narrowed down to the waveguide to microstrip transitions, but could not be eliminated.

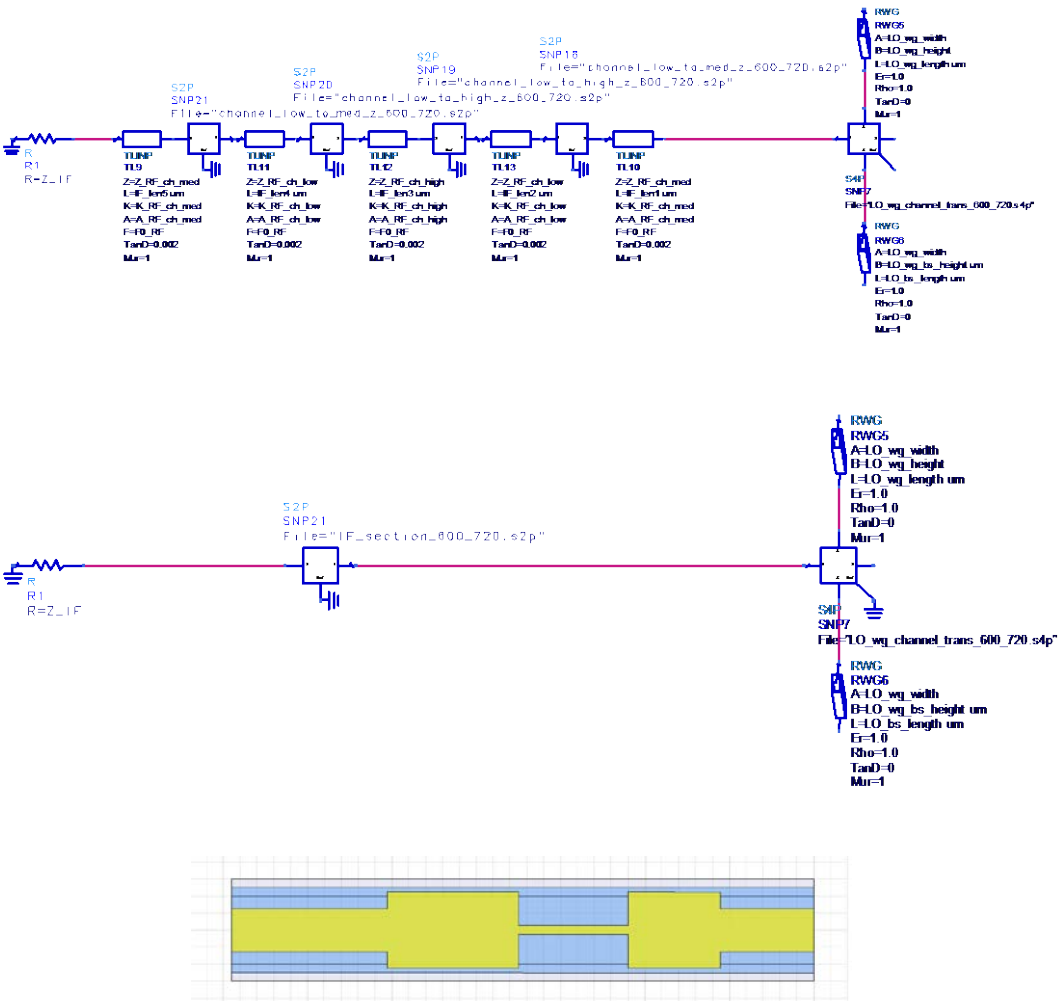

Figure 4-6 – First Stage of semi-distributed model, replacing the IF filter with the whole filter from HFSS (below)

This didn't appear to make a difference on the simulation.

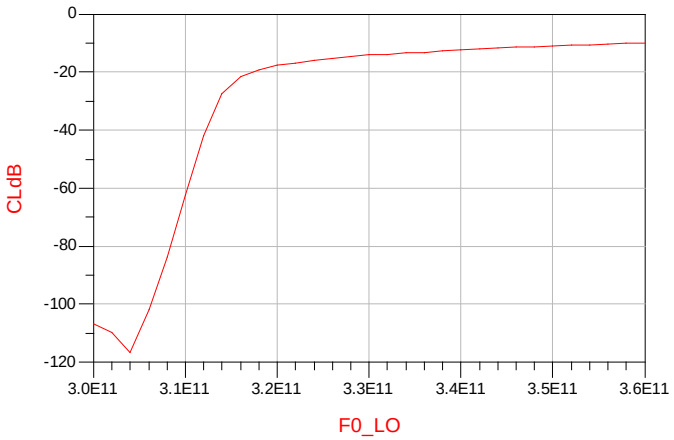

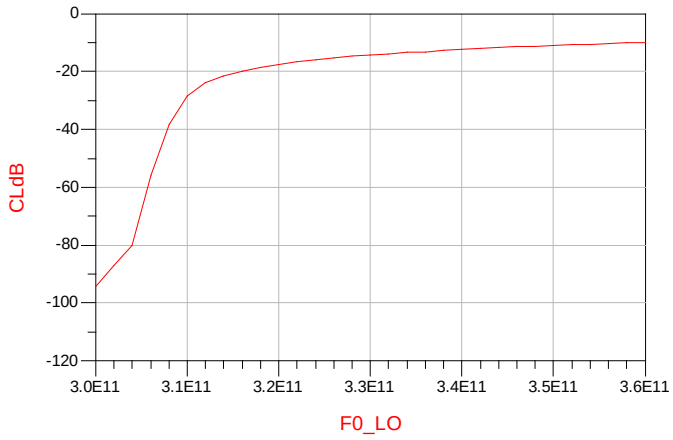

Figure 4-7 – First stage of semi-distibuted model (below) with original distributed model (above)

Next the RF low pass filter was also substituted with the whole version, but this also had no effect on the simulation.

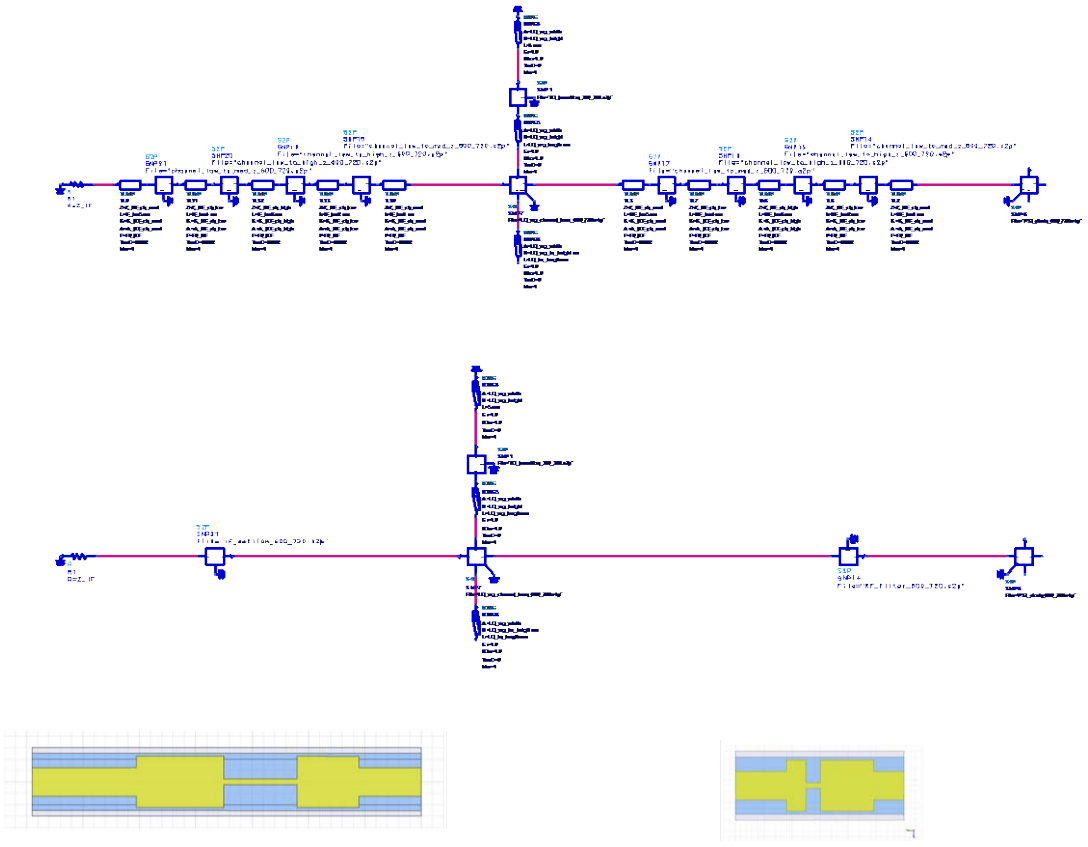

Figure 4-8 – Second stage – overview of original (above) and semi distributed model (middle) with IF and RF filters replaced (below) in order to get a feeling of the circuit changes

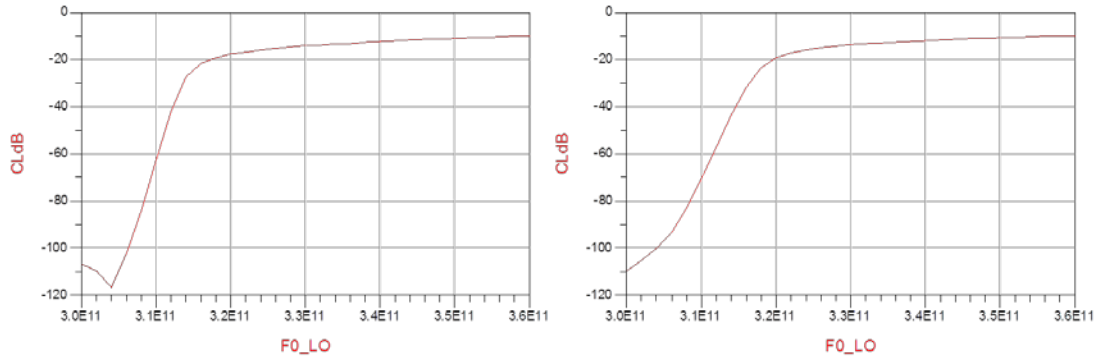

Figure 4-9 – Second stage results still similar, distributed left and semi distributed right

Replacing the RF input and ground starts to indicate a problem with differences in the models. This could be due to circuit errors in ADS or 3D drawing errors in HFSS.

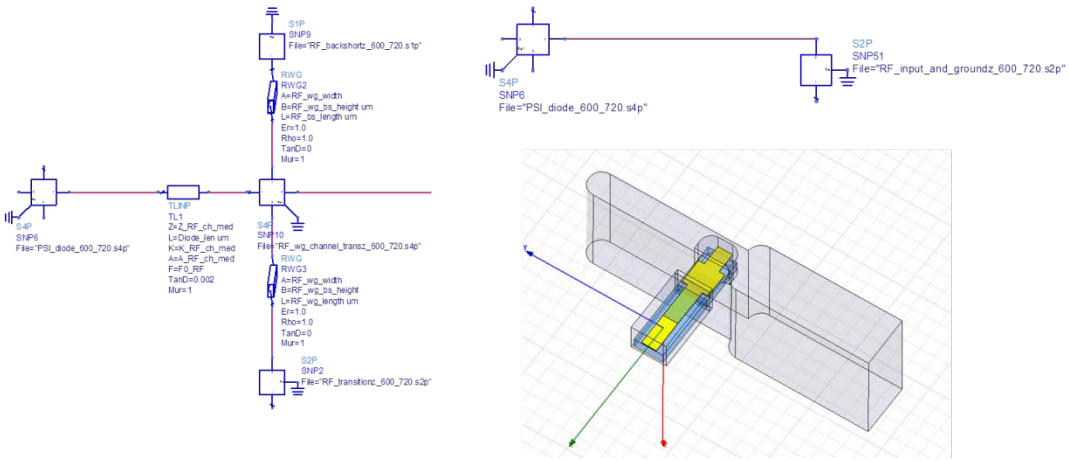

Figure 4-10 – Stage 3, replacing the RF input and ground with the full model s-parameters from HFSS

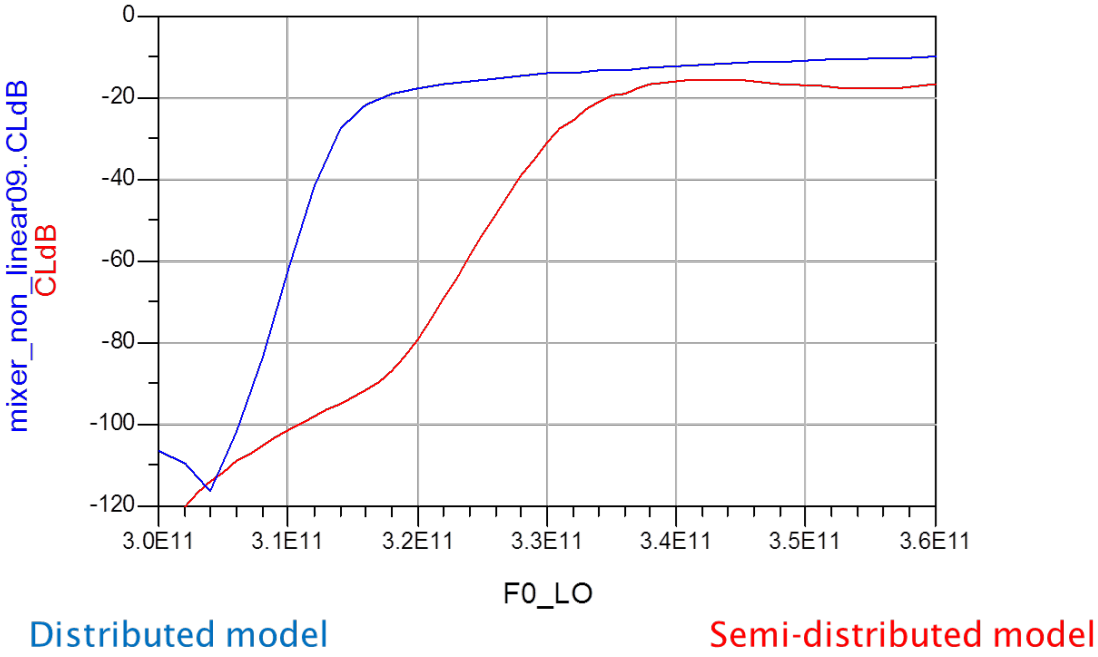

Figure 4-11 – Stage 3 semi-distributed model

Stage 4 was to replace the entire RF half of the model in ADS with it's HFSS equivalent.

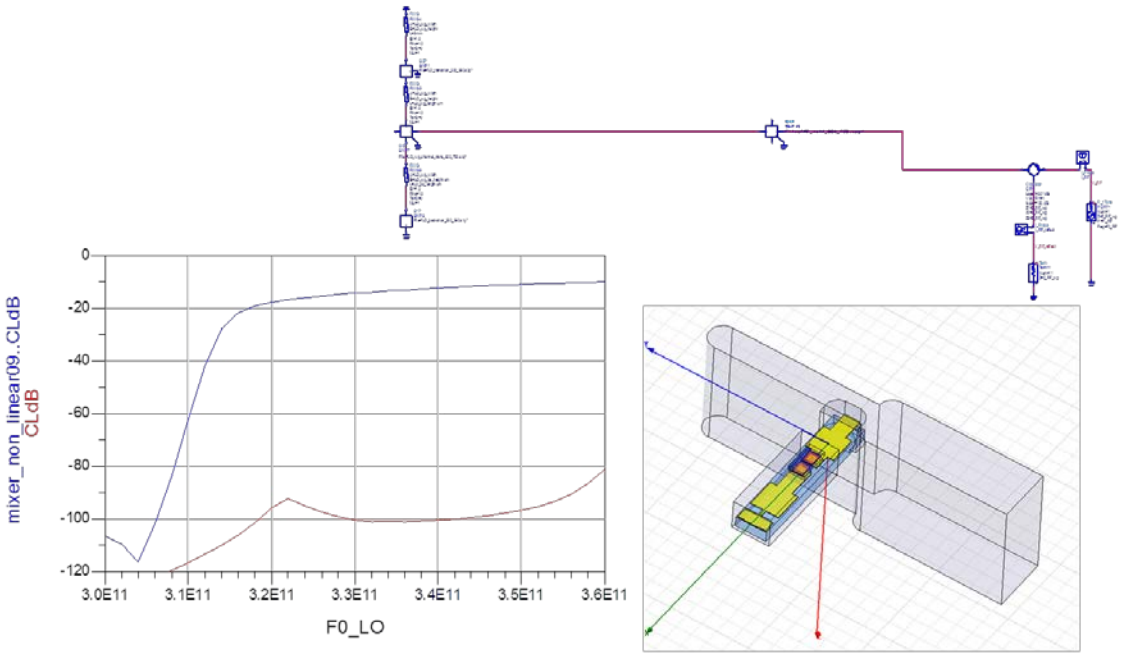

Figure 4-12 – Stage 4 semi-distributed model and results

This time there is huge differences between the two models. The final stage was to repeat with the LO half of the circuit model and this again showed large differences like the whole model comparison in Figure 4-4.

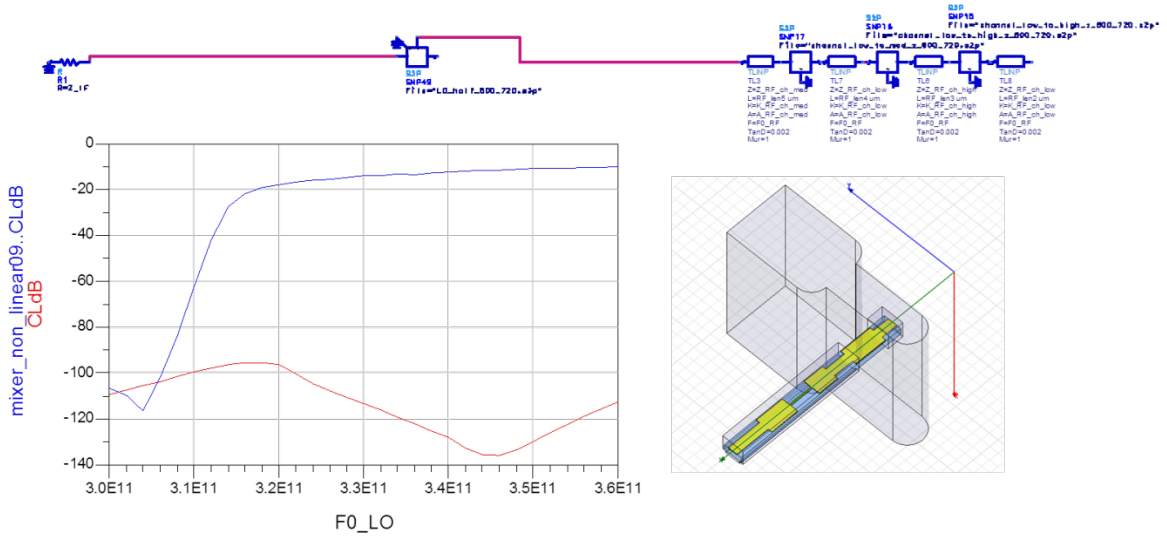

Figure 4-13 – Stage 5 of semi-distributed model

The next few tests were derived to check the method and the models to try and discover what was causing the differences in the models. The first step was to look at the port de-embedding and it was decided to switch to comparing s-parameters instead of conversion loss as this would me more sensitive to small changes than the conversion loss (as will be seen later on).

Port de-embedding tests

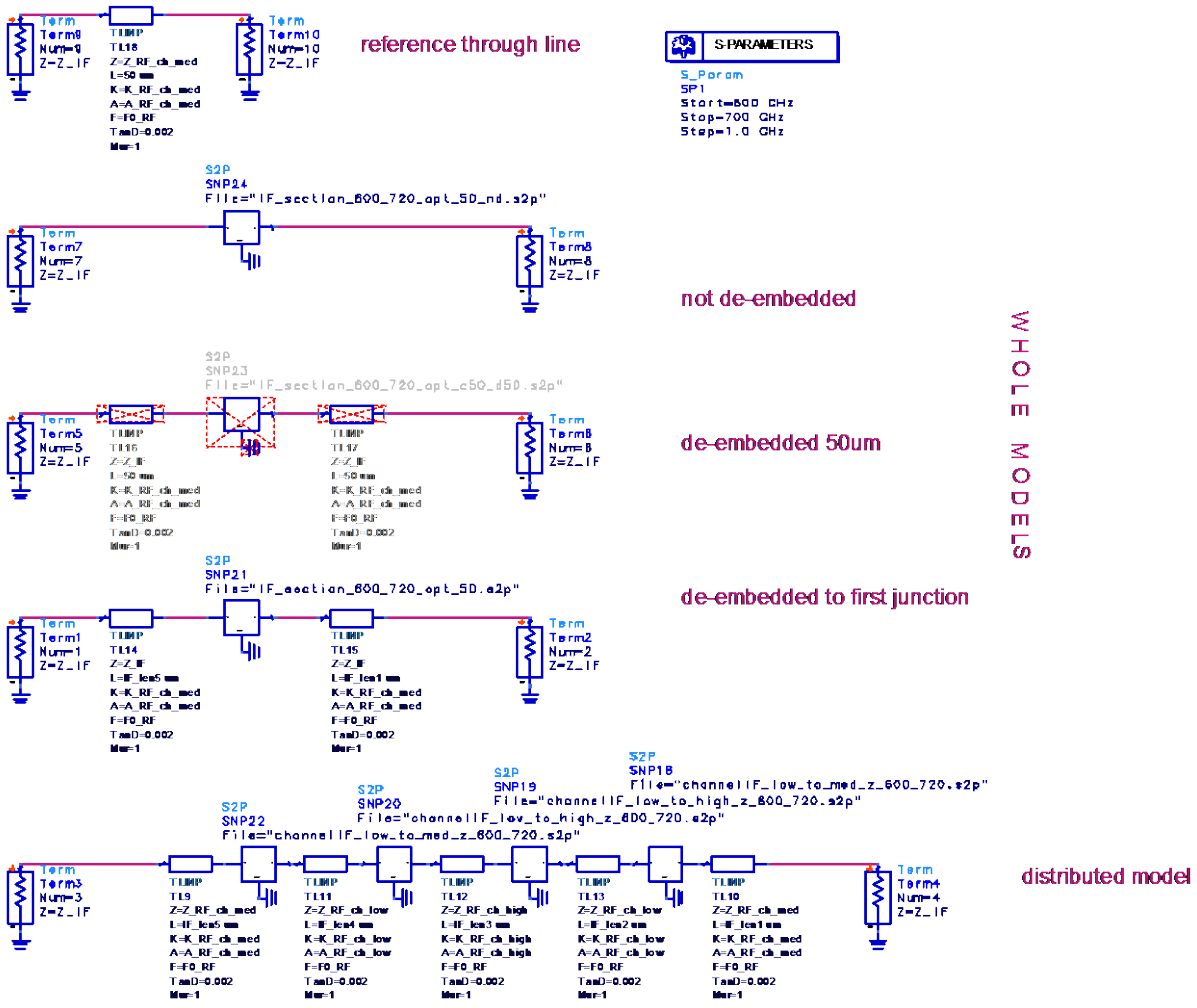

Figure 4-14 - De-embedding test circuits including a reference through line and the full distributed model

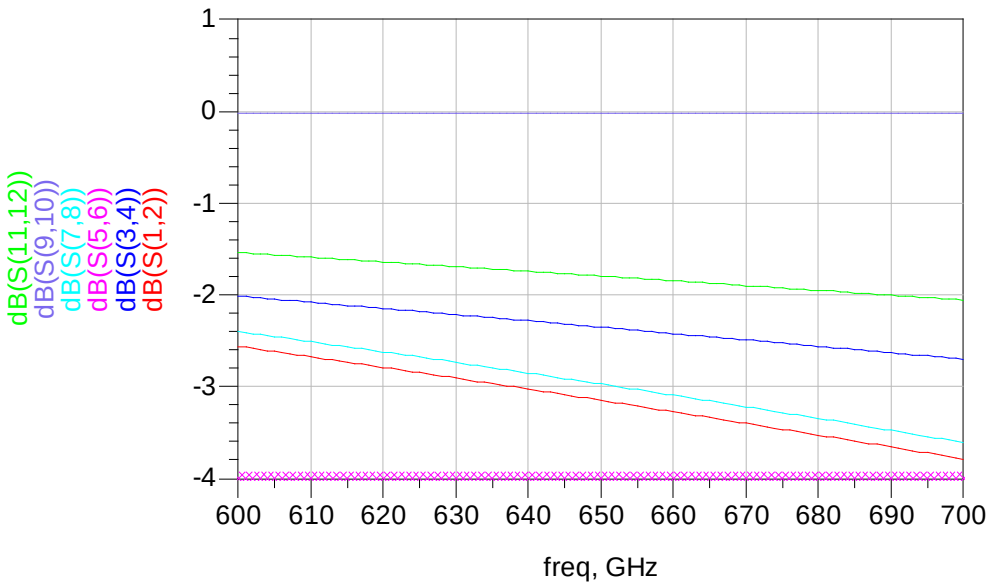

Figure 4-15 – De-embedding tests initial results

The initial results did not match as expected (above) but this was improved upon once the correct port impedances were put in place (below). This shows that the filters match as expected when the de-embedding method is changed.

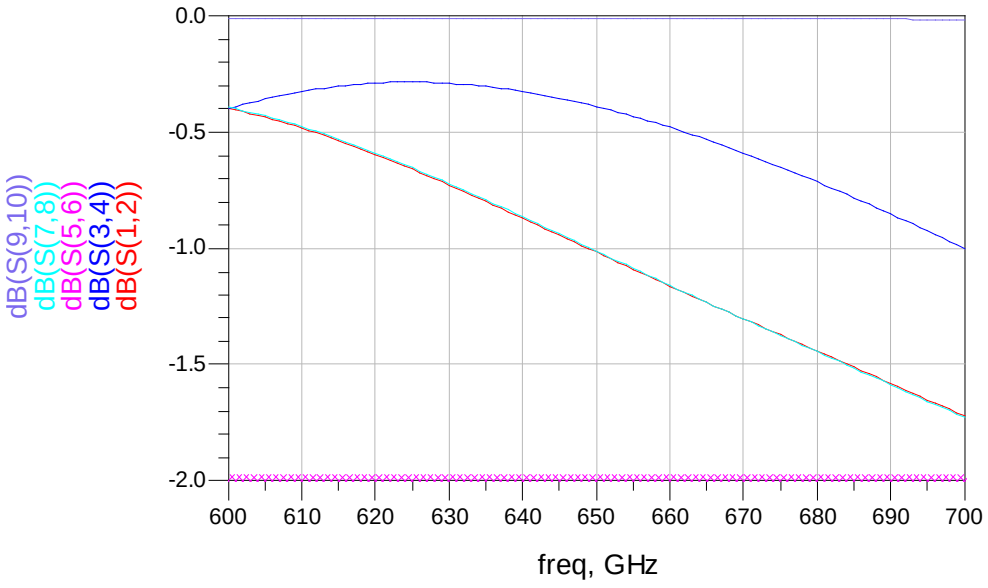

Figure 4-16 – De-embedding test results showing good matching. Dark blue line has no de-embedding and is not expected to match.

This knowledge about de-embedding methods was applied and the distributed and whole models were updated with a new, consistent de-embedding method but they still did not match up.

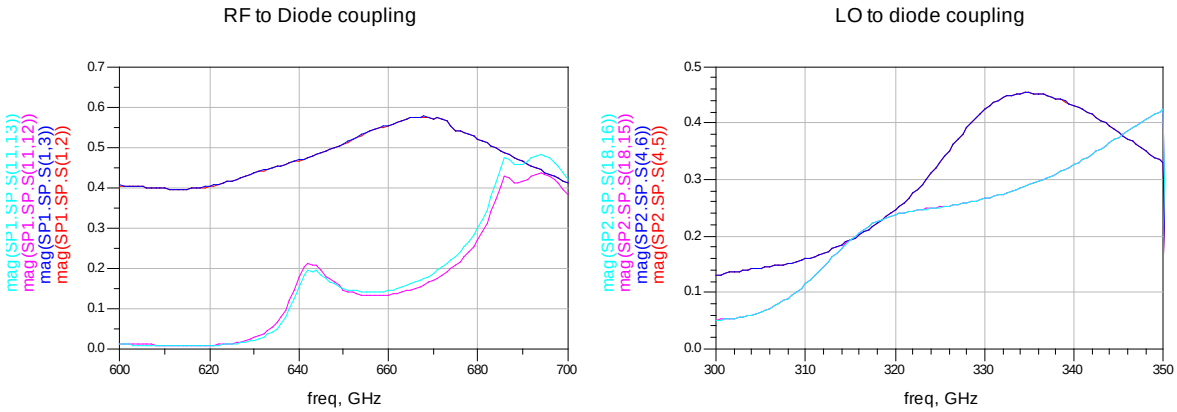

Figure 4-17 – RF and LO coupling in distributed (red and blue) and whole (cyan and pink) models

After all of these investigations the models still did not match, so the HFSS model and ADS circuits were both re-drawn from scratch. The S-parameter optimisation stage was also removed from the whole process in order to simplify it.

Re-building and Simplifying the Simulation Models

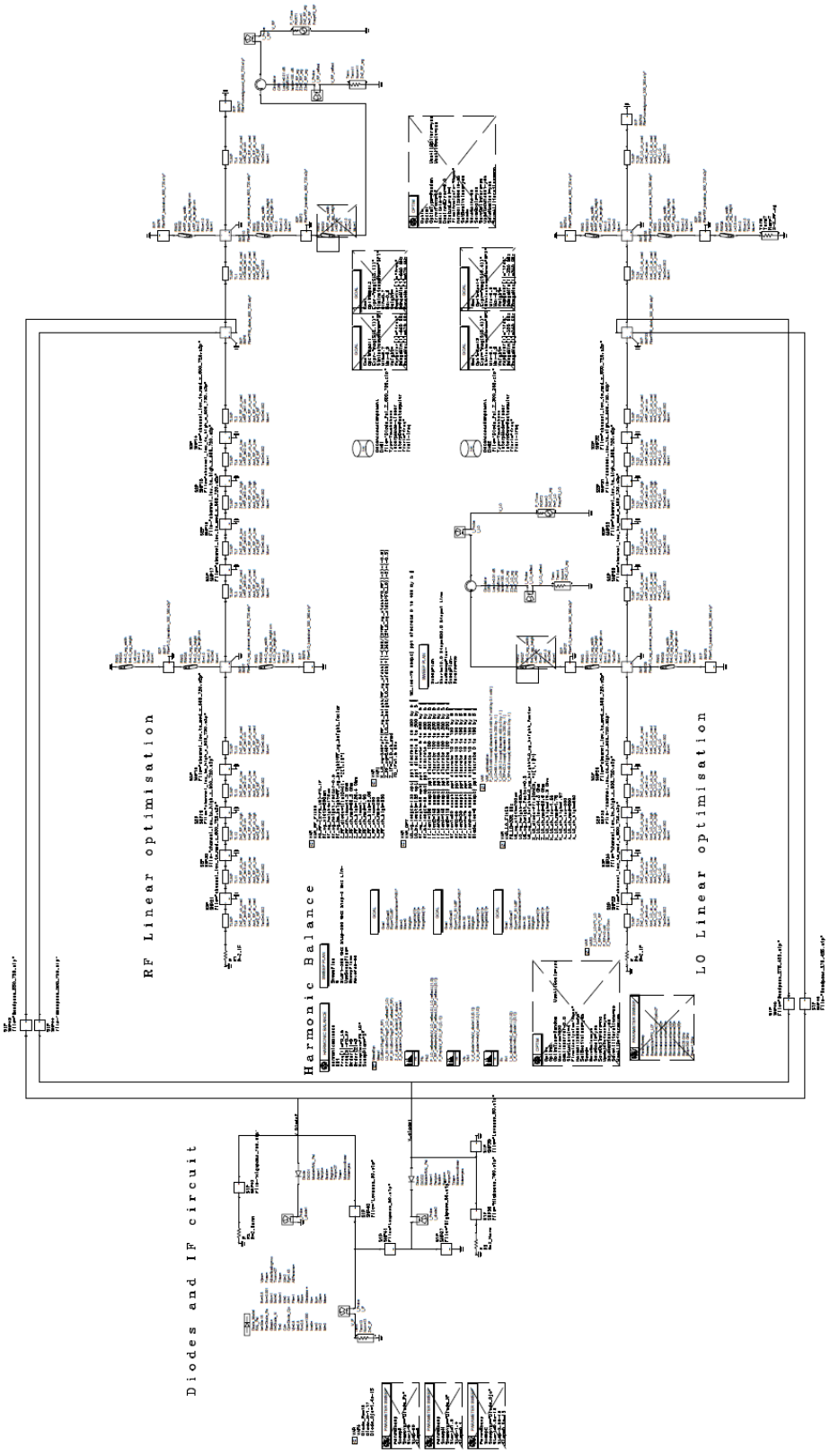

Figure 4-18 – old distributed ADS model

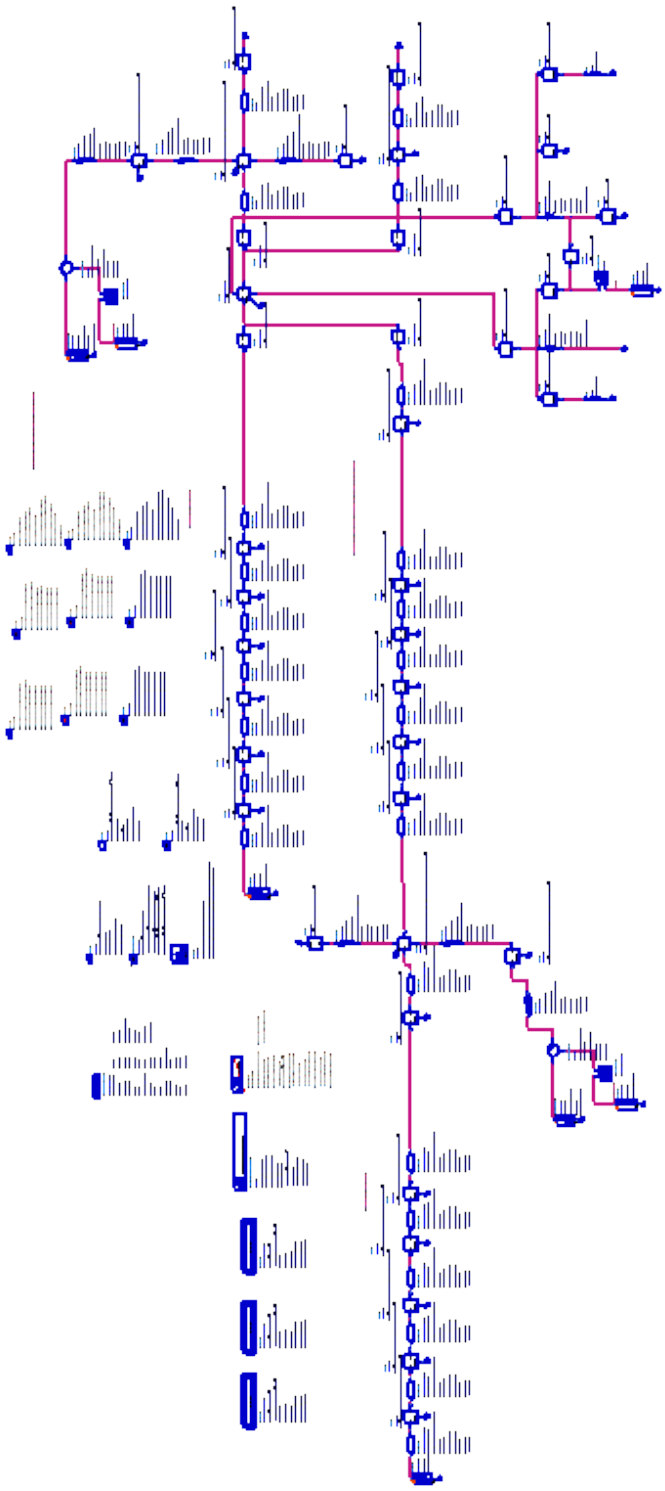

Figure 4-19 – new simpler distributed ADS model

Re-evaluating the Filter Performance

The performance of the filters was also re-examined and it was decided to change from a 3 element filter to a 5 element filter. This is due to the smaller difference in impedance in the different microstrip line widths because of the narrow quartz substrate compared to lower frequency mixers where a 3 element filter is normally adequate. It was decided that the 7 element filter was not needed as this would further increase simulation timescales and did not provide as much benefit as moving from 3 elements to 5 as can be seen below.

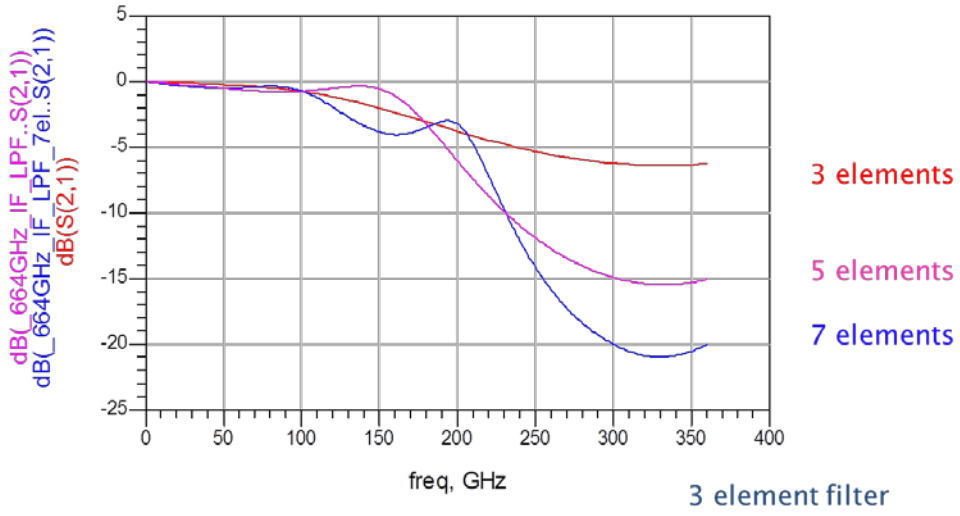

Figure 4-20 – Performance of differing IF low pass filters

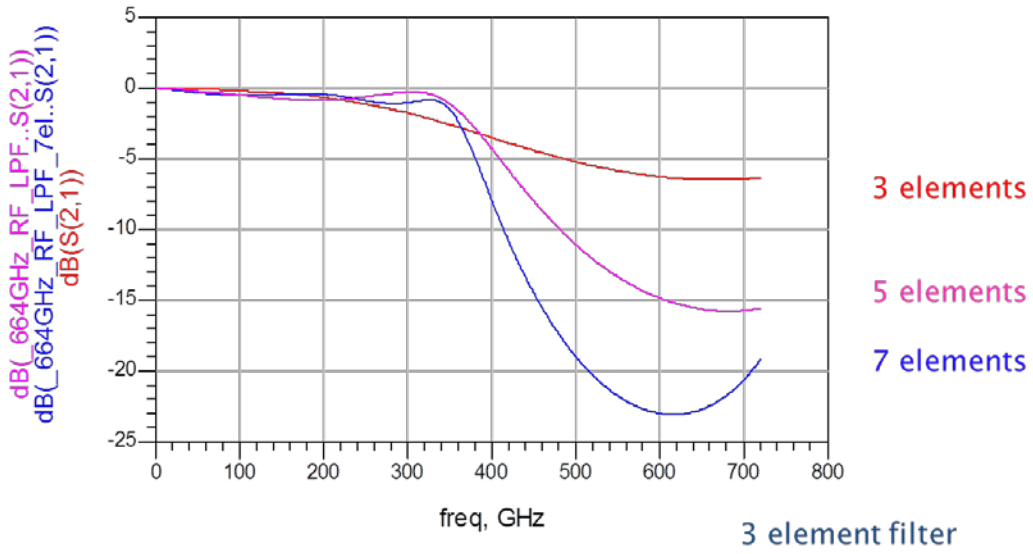

Figure 4-21 – Performance of differing RF low pass filters

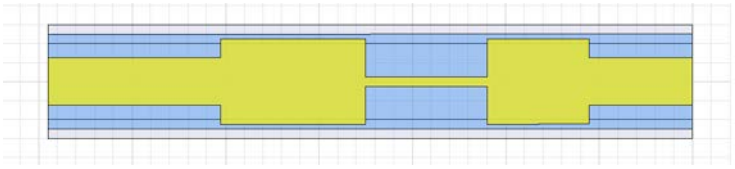

Figure 4-22 – 3 element filter between two sections of 50ohm microstrip

The filters were optimised separately before being combined in the distributed model and being further optimised.

Bringing all the Pieces Back Together

This gave a similar performance to the original distributed model, but now there was much better correlation between the whole model and the distributed model. An almost complete model was formed so that the backshort lengths could still be optimised.

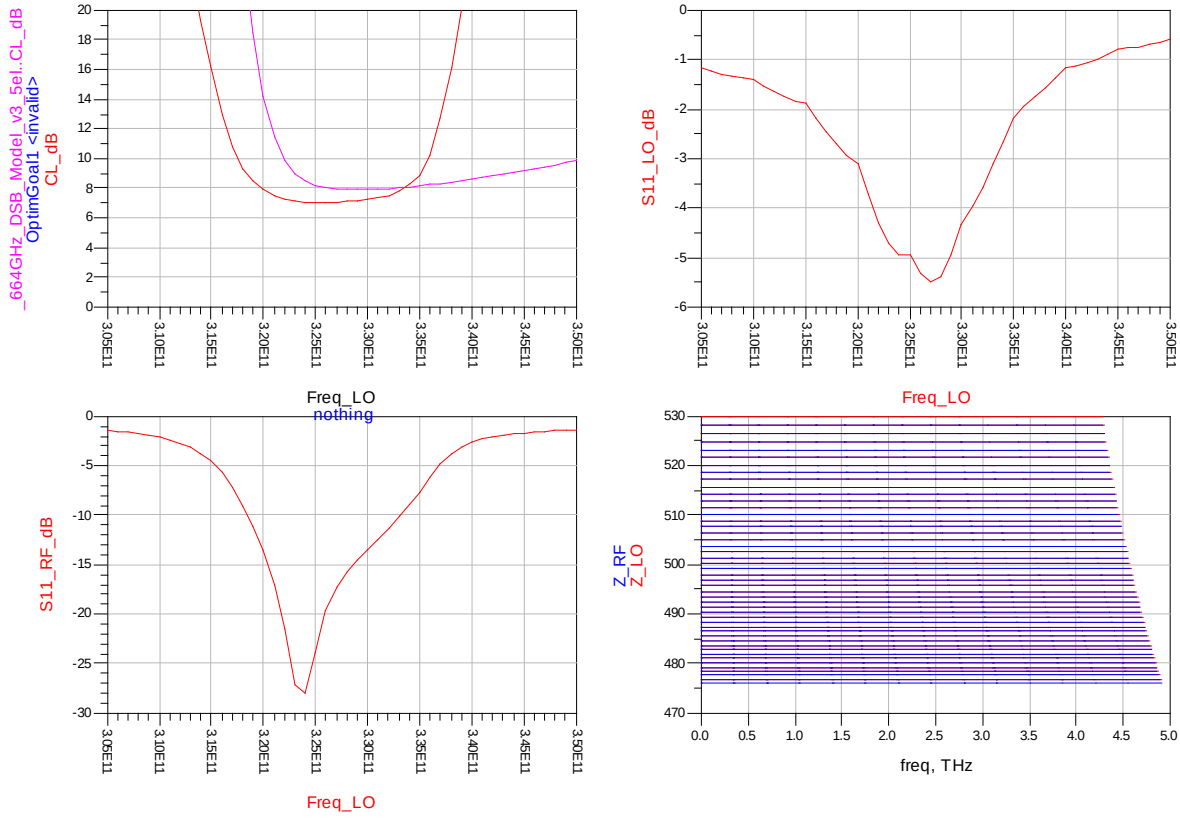

Figure 4-23 – new model performance of almost whole model (whole model in pink in top left)

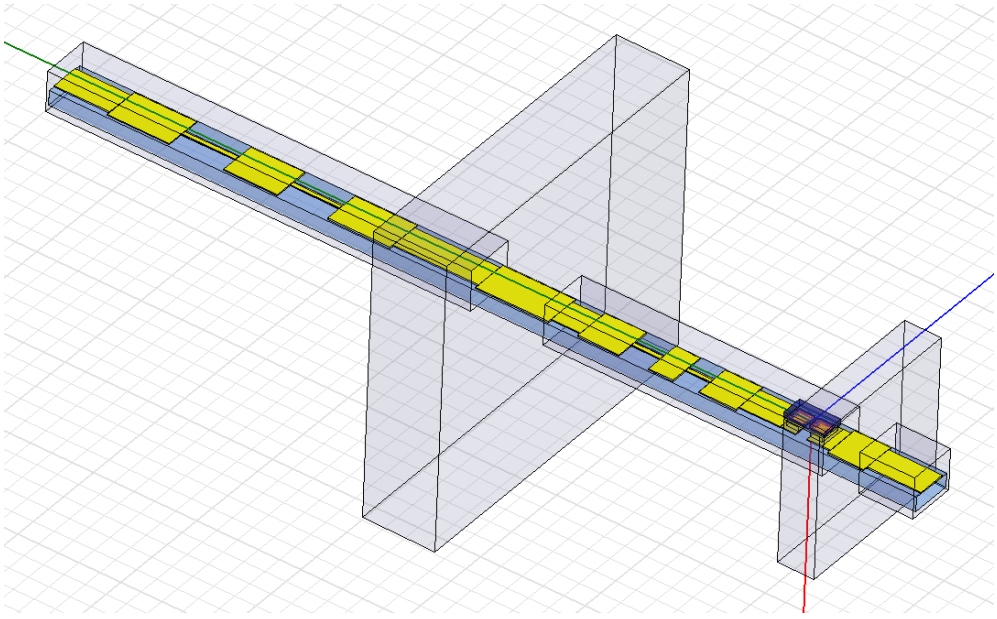

Figure 4-24 – Almost whole model

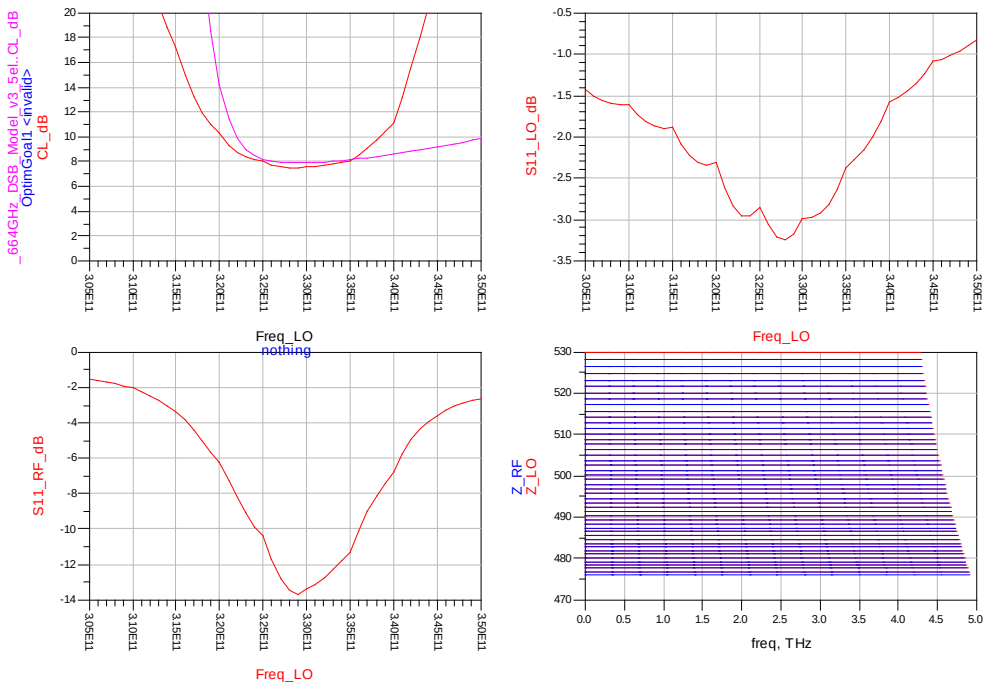

Figure 4-25 – Same simulation as above after further 200 optimisation iterations for the 325-240GHz LO range

The performance at this point is not perfect and the LO reflection in particular is poor. I went back to the distributed model and re-optimised for the whole simulation range (300-360GHz at LO). This provided a set of results which looked less than ideal, but with a good conversion loss.

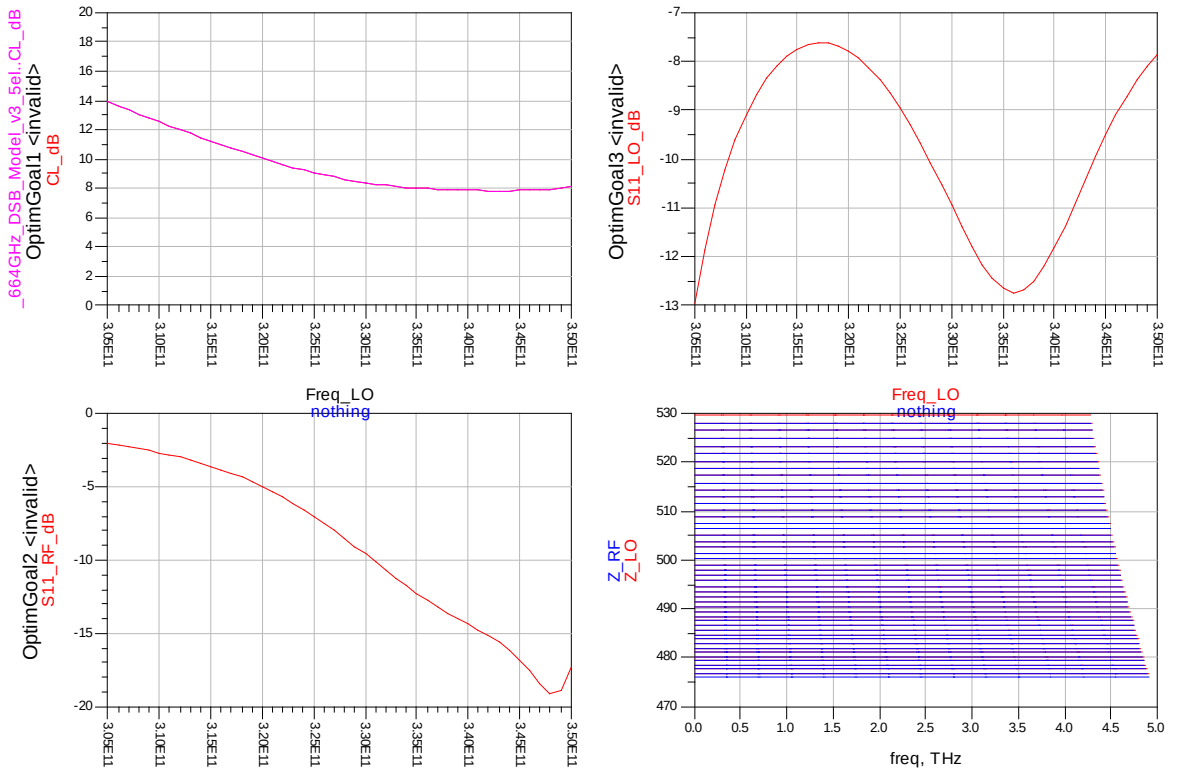

Figure 4-26 – distributed model (with the extracted s parameters of each section in ADS) optimised across full simulation range

With these results the RF and LO matching are both off centre but this should be corrected by optimising the waveguide backshort and transition lengths in the almost whole model.

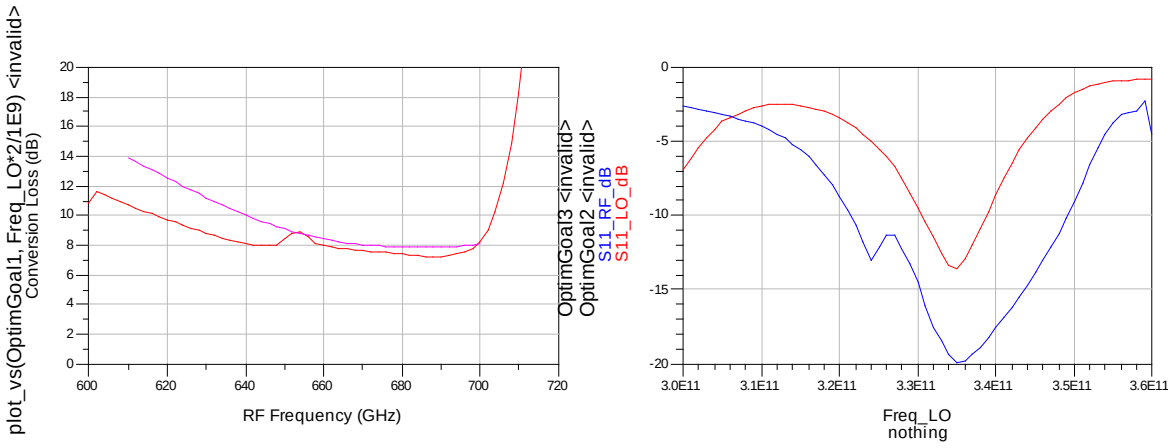

Figure 4-27 – Almost whole model optimised

For verification these lengths are applied back into the whole model and the simulation is run again to ensure it matches.

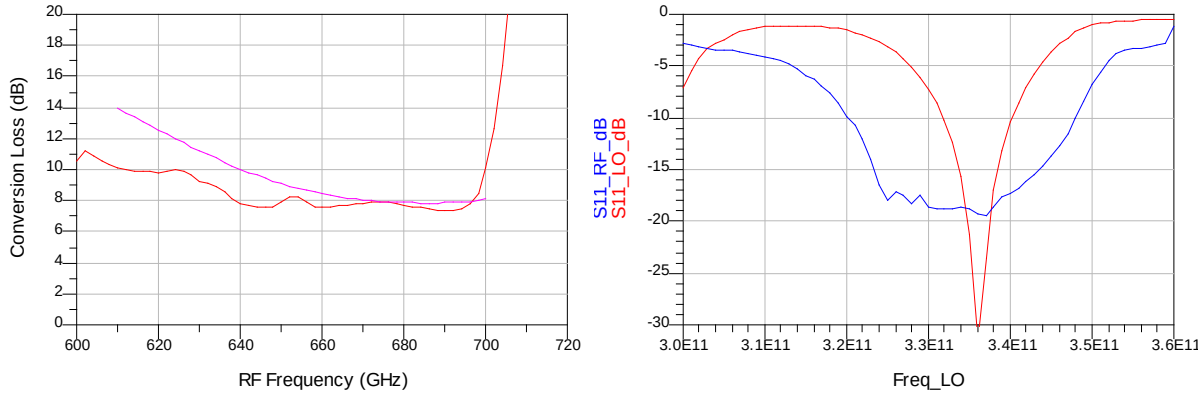

Figure 4-28 – whole model and distributed model correlation can be seen on the left. Input reflections for the whole model are shown on the right

The LO reflection is a little sharper than hoped for so the relevant parameters were optimised in the whole model in HFSS to see if any improvement could be gained, but there was little change to the LO reflection or the conversion loss. This is very computing resource intensive so the number of iterations are limited.

Optimising the Backshort lengths

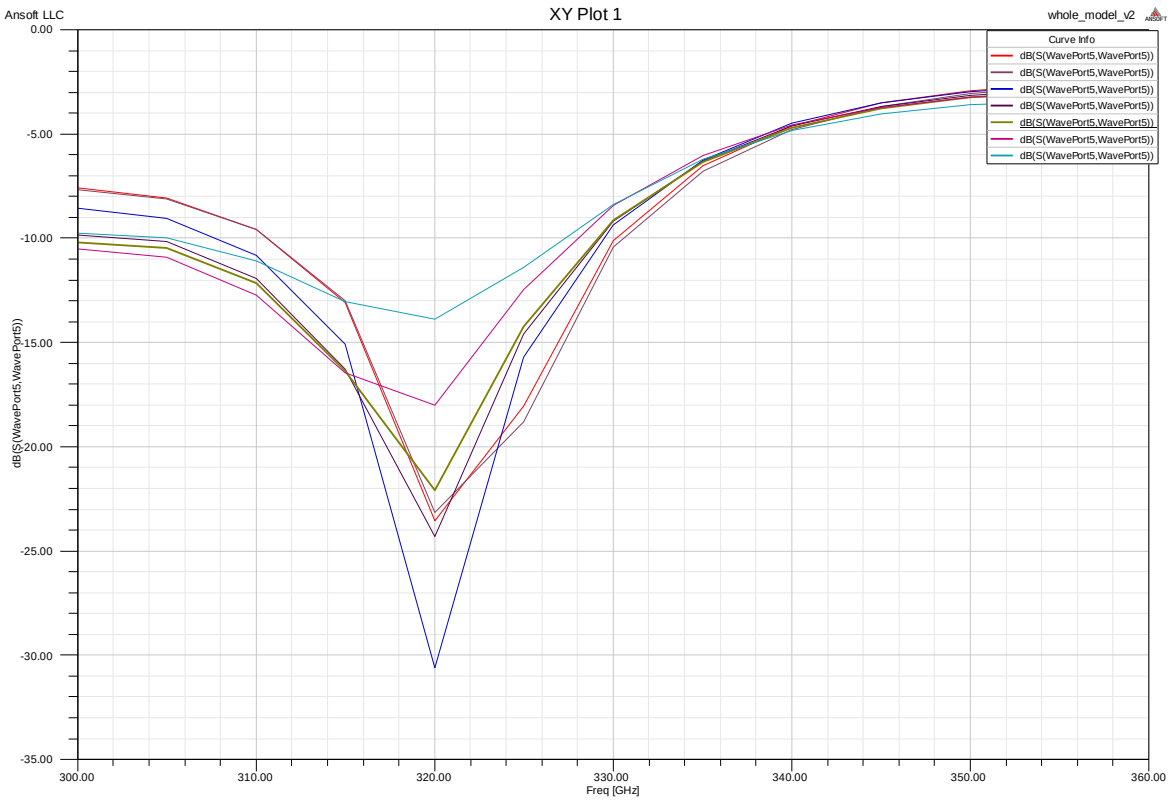

Figure 4-29 – optimisation of the LO backshort length to improve LO S11 reflection – top to bottom in the centre of dip 160, 105, 85, 40, 30, 70, 45 um

This shows that sweeping the backshort length in HFSS shows that the length used in the optimised model (85um) is a good compromise between peak depth and width.

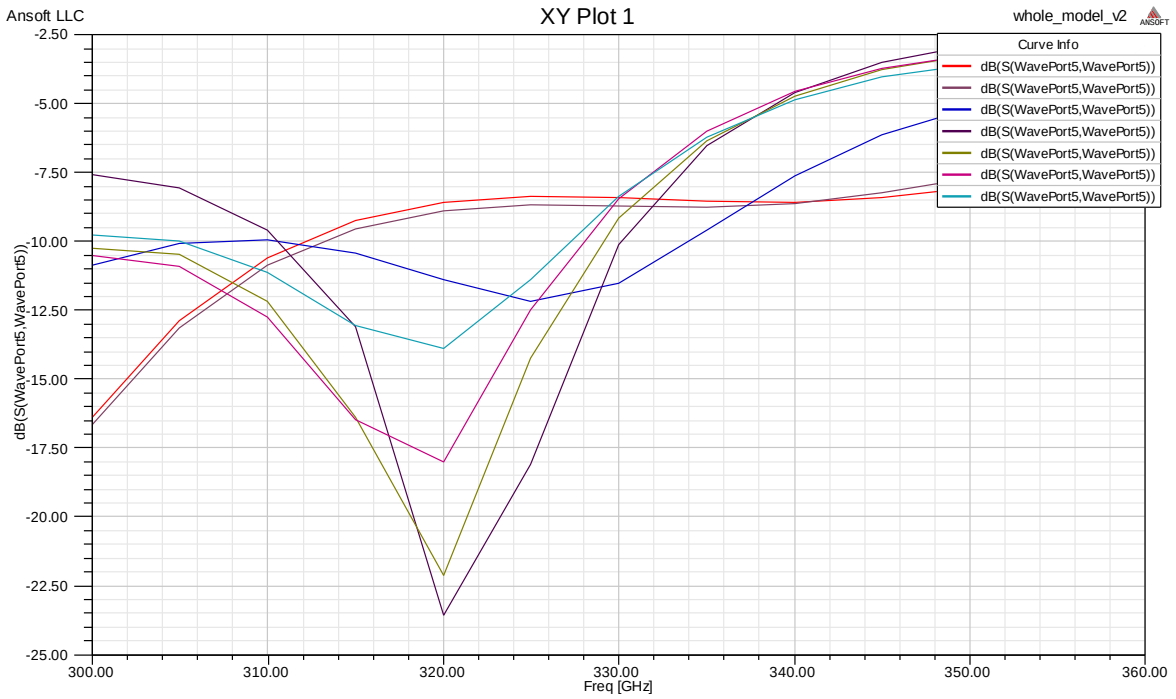

Figure 4-30 – Optimisation results from HFSS for both backshort and both waveguide lengths

Optimising both backshort lengths and both waveguide transition lengths over a 4 day period for the whole model in HFSS results in a wider but shallower peak for the LO (royal blue line above). Using these lengths in the non-linear ADS model results in similar S11 plots for the LO but with a shallower peak. Despite the fairly large difference in LO matching though, the conversion loss plot remains largely the same as before.

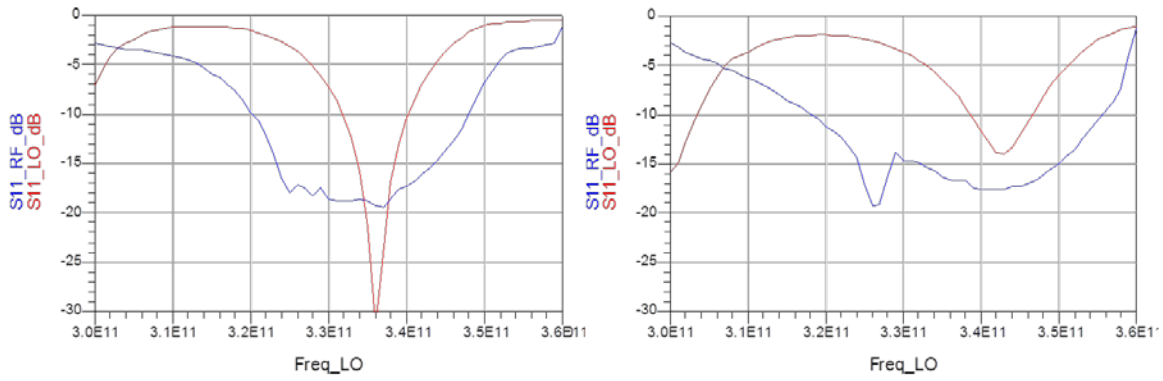

Figure 4-31 – Previous LO and RF reflection plots (left) and after optimisation in HFSS (right)

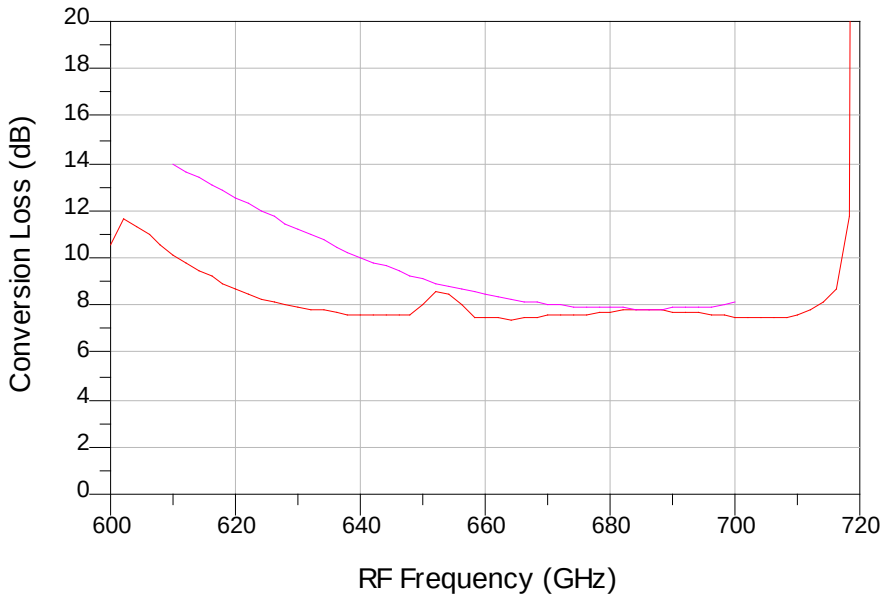

Figure 4-32 – Conversion loss after all optimisations. Distributed model in pink and whole model in red.

Parametric Analysis of finished design

Several parameters were swept to check performance. Diode resistance, ideality and junction capacitance gave similar results to the previous design. In the below figures, the double headed blue arrow indicates the desired range of operation for the mixer as set out in ESA Micromachined Receivers Technical Note 1 which are also replicated below in Figure 4-33.

664 GHz receiver front-end		
Parameter	Value	Comment
RF frequency range	655-675 GHz	Tuning the LO
Input band (IF)	2 GHz	
Mixer Noise Performance	<2,000K DSB	
Conversion loss	<10dB	
Nominal LO power	5mW	At half the RF frequency
Mass	50g	

Figure 4-33 – Technical requirements for mixer from ESA Technical Note.

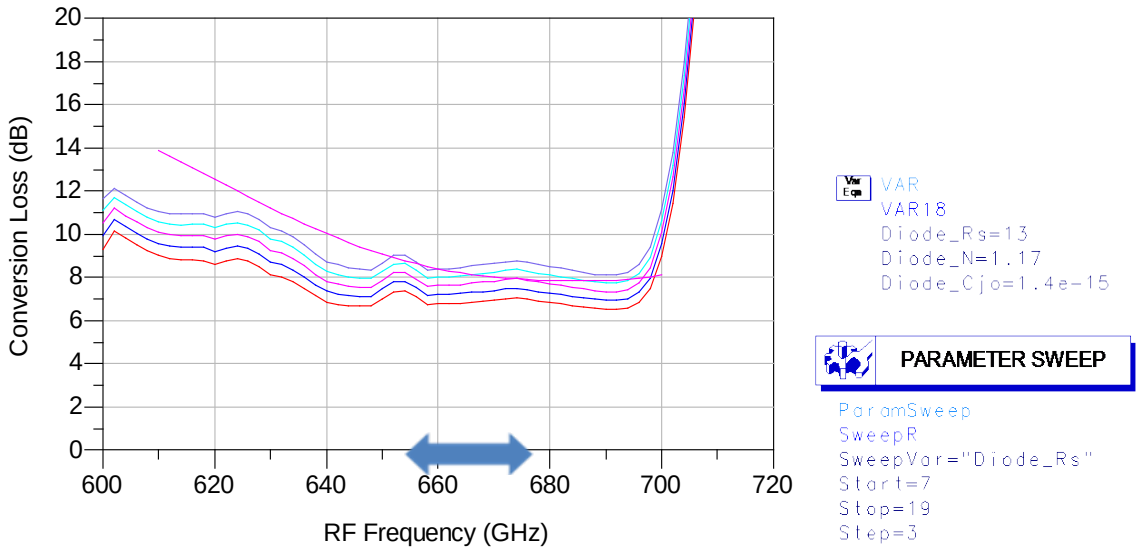

Figure 4-34 – Diode parameter sweep – resistance, both diodes

This sweep of diode resistance shows that the lower the resistance the better the performance of the mixer. Sweeping the ideality as below between 1.14 and 1.19 has little effect on the performance.

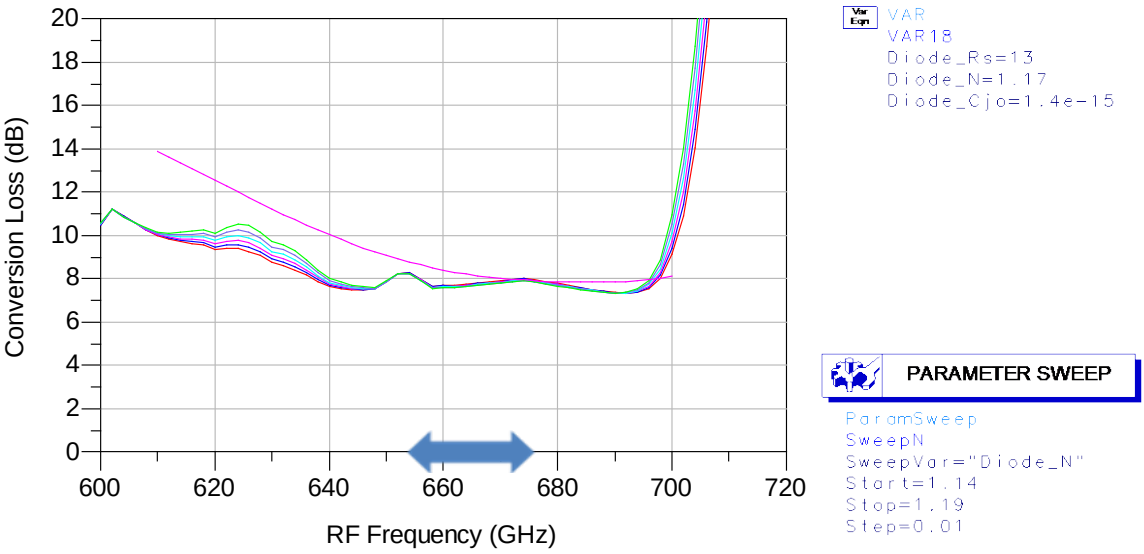

Figure 4-35 – Diode parameter sweep – ideality, both diodes

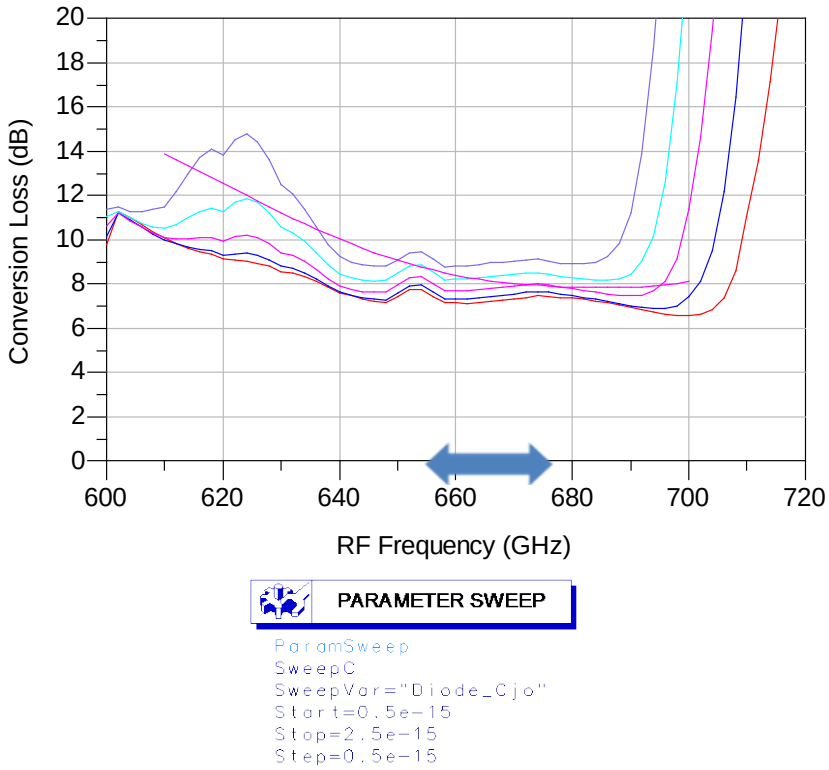

Figure 4-36 – Diode parameter sweep – Cjo, both diodes

As expected, the junction capacitance has a noticeable effect on the performance of the mixer with the bandwidth also being affected as well as the conversion loss across the area of interest.

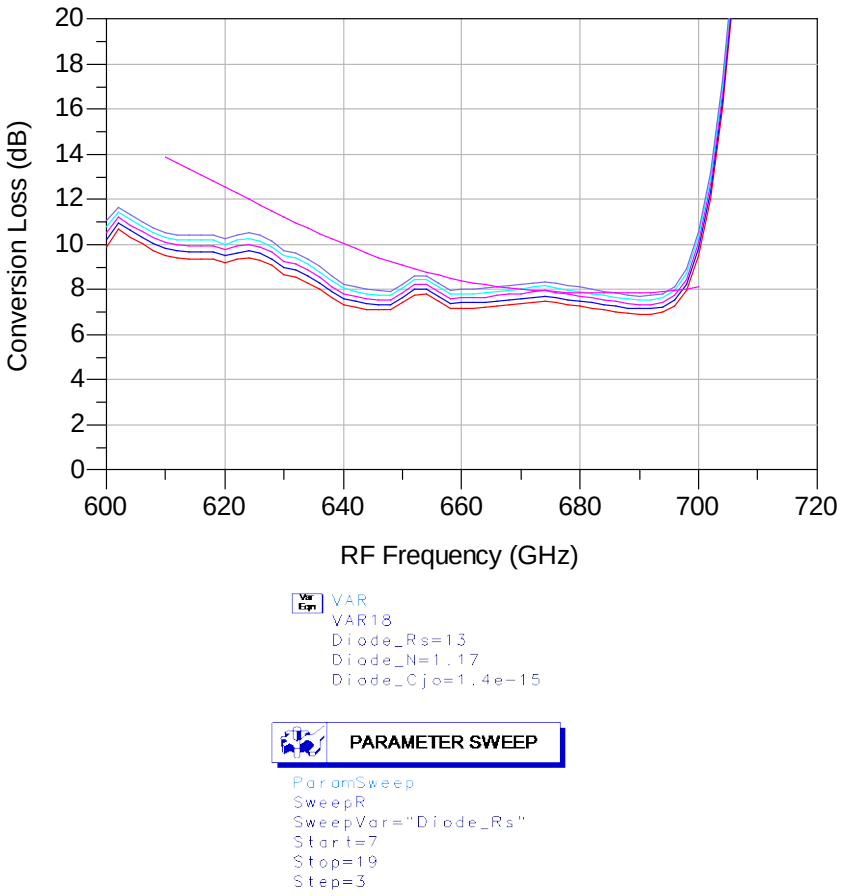

Figure 4-37- Diode parameter sweep – resistance, one diode

As expected, changing the resistance of a single diode has a smaller effect than changing the resistance of both, and no further unexpected results are seen. A similar effect is seen in the ideality changes in a single diode.

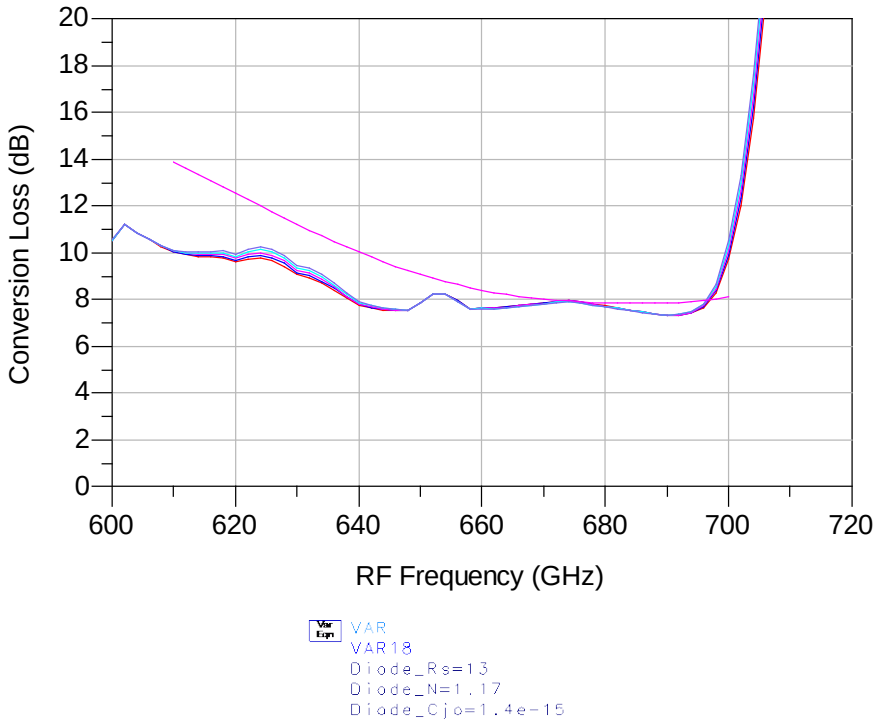

Figure 4-38 – Diode parameter sweep – ideality, one diode

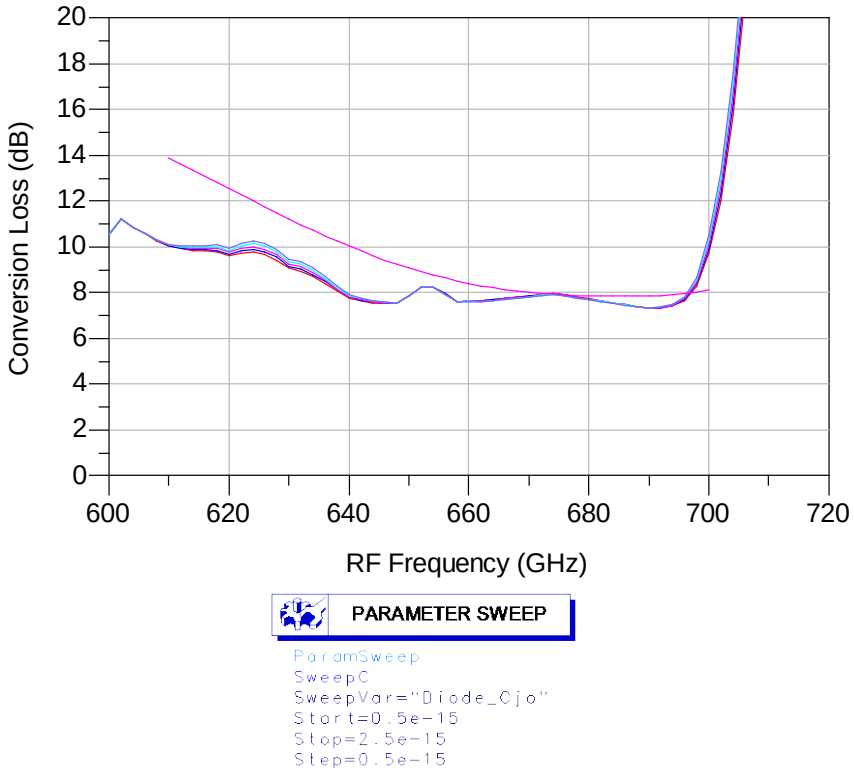

Figure 4-39 – diode parameter sweep – Cjo, one diode

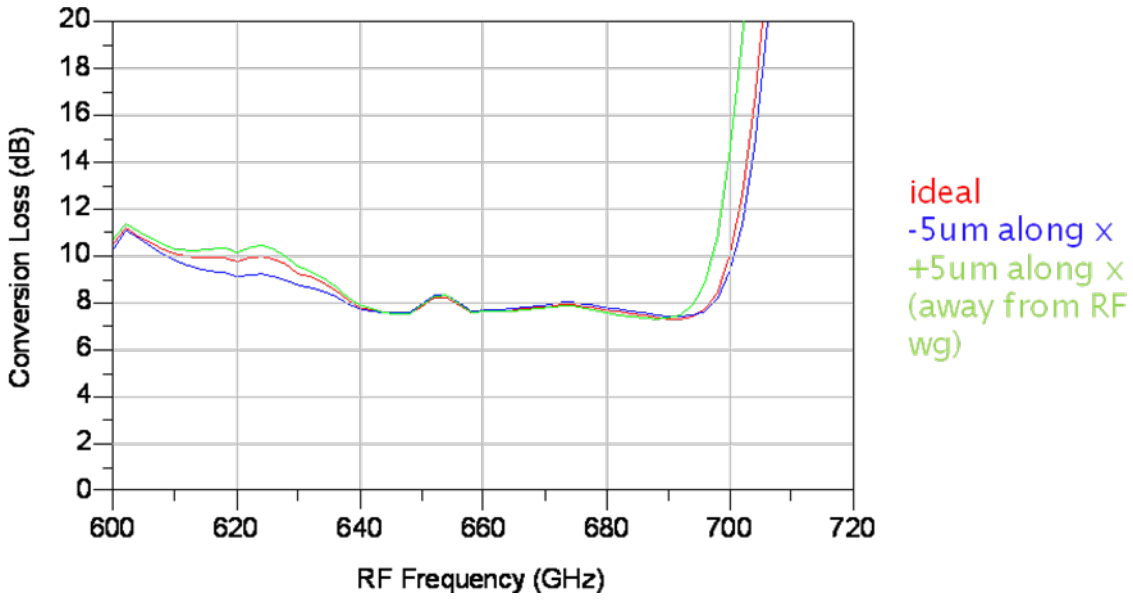

Figure 4-40 – parameter sweep – diode position along x axis (length of filter)

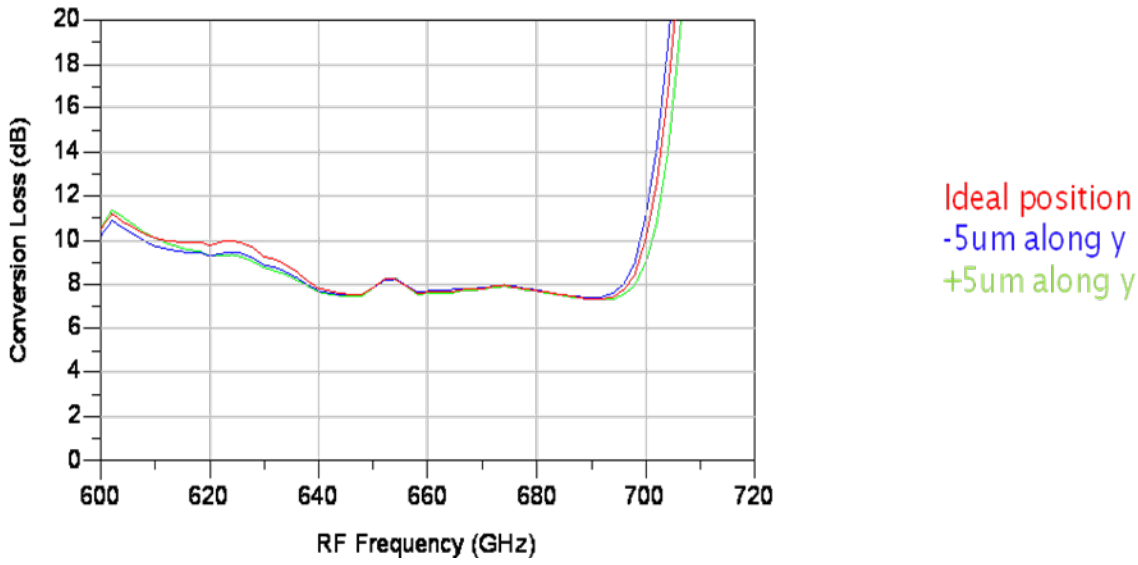

Figure 4-41 – parameter sweep – diode position along y axis

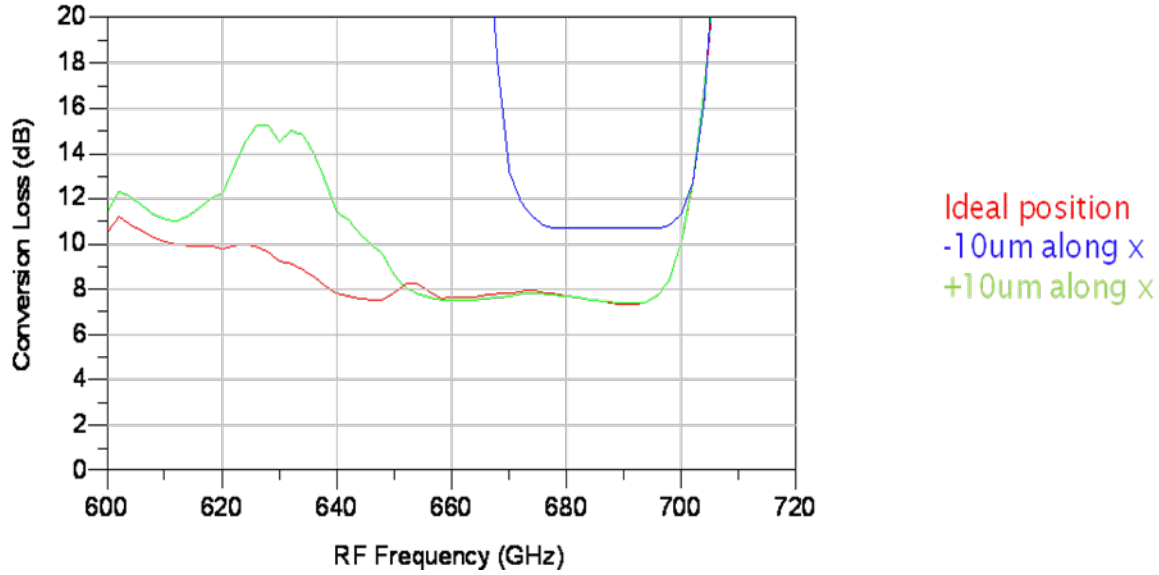

Figure 4-42 – parameter sweep – circuit position along x axis

Changing the position of the diode on the filter circuit by 5um each way has little effect on the mixer design performance. Changing the position of the filter circuit in the block has a much more noticeable effect, but the filter should be able to be positioned within 1um or so of the designed position without too much difficulty. This alignment is easy to see due to the low impedance sections of microstrip in the waveguide to microstrip transitions.

The filter thickness (below) also has a noticeable effect on the tuning of the mixer performance, but since this is created by an automated dicing machine, and can easily be accurately characterised using the SEM this is not expected to be a problem.

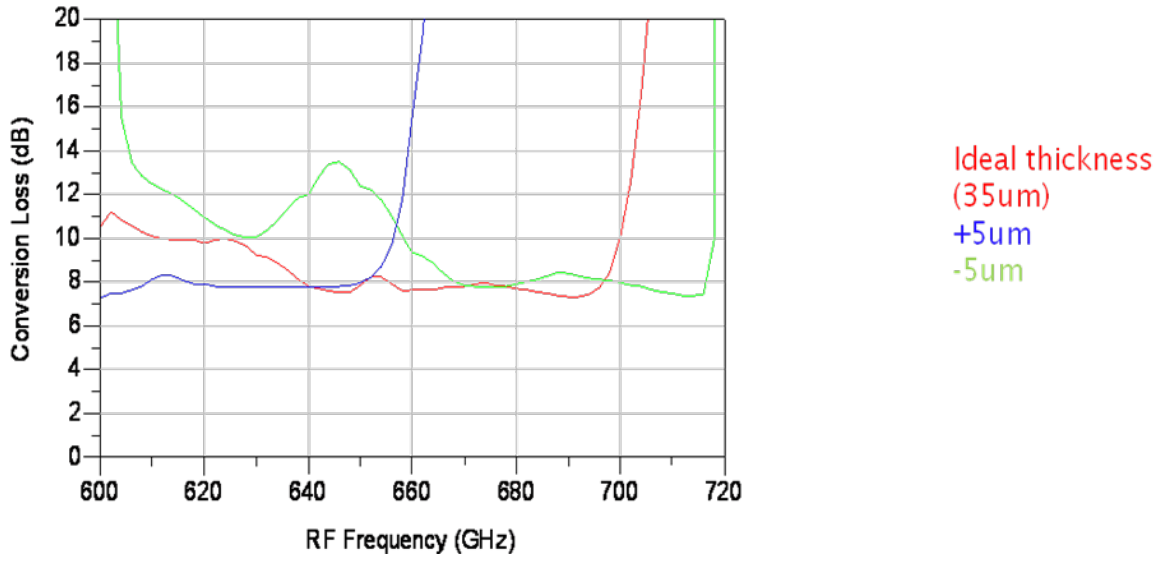

Figure 4-43 – parameter sweep – quartz filter thickness

A few final tweaks were added to make the block more practical to manufacture, so the final simulated performance for the whole model is shown below.

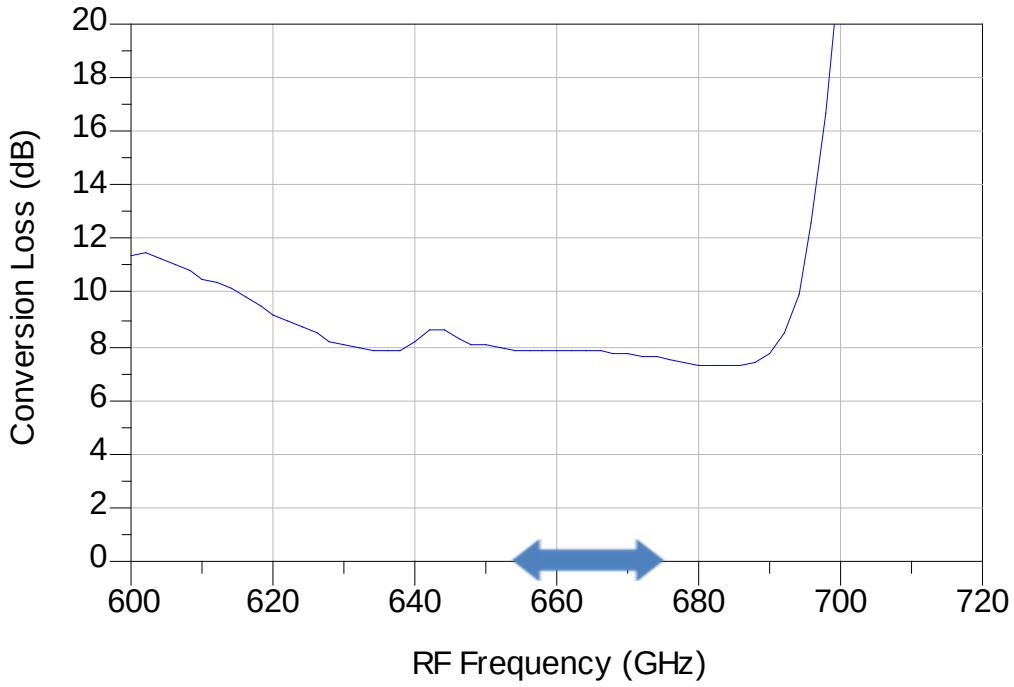

Figure 4-44 – final whole model conversion loss (double headed arrow shows desired range of operation)

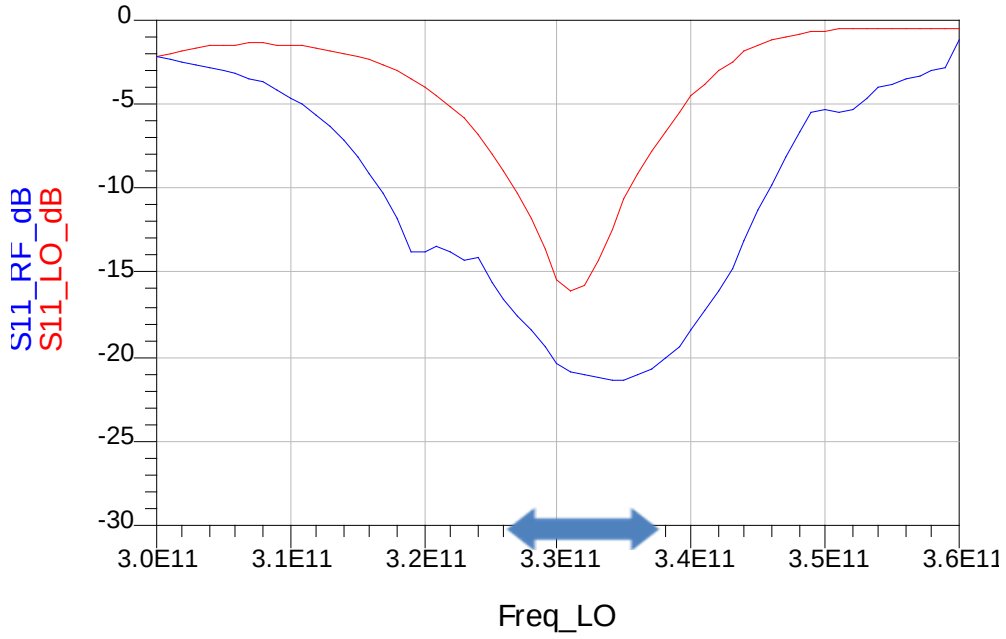

Figure 4-45 – final whole model input port reflections (double headed arrow shows desired range of operation)

The two new blocks have now been manufactured and the filter circuits are nearing completion using a new improved fabrication process. The diodes will be taken from stock so this means the assembly can be completed quickly.

Figure 4-46 – 664GHz_SHM_2 re-designed mixer blocks manufactured at RAL

The mixer will was tested at RAL using the new 332GHz doubler and also tested at RPG where they currently have more power available at 332GHz. The mixer is optimised for an LO power of around 4-5mW.

Chapter 5 – 664GHz Results

664GHz Mixer design results

The 332GHz RAL doubler was not completed in time for initial testing, so the mixer was sent to partners Radiometer Physics GmbH in Germany for testing. At the time this was the only place in Europe that had the required power at the LO frequency.

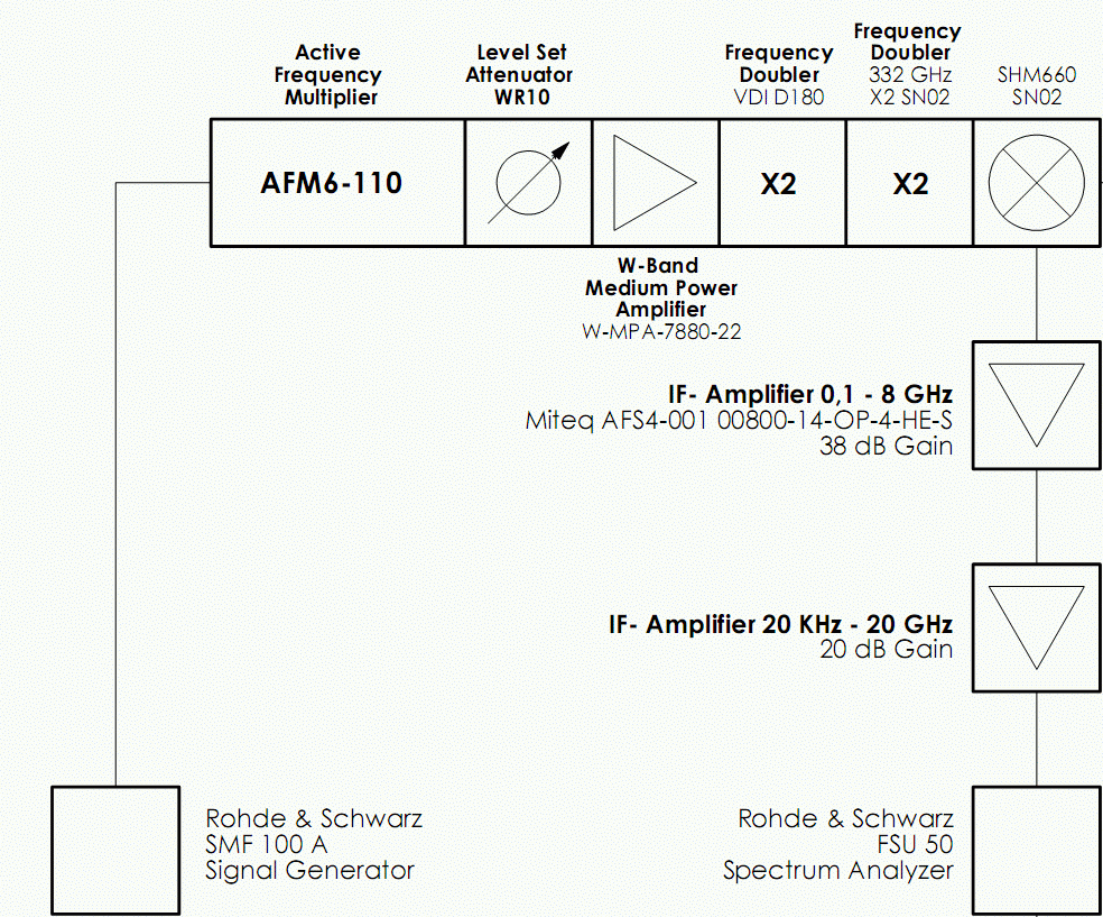

Figure 5-1 – Mixer test set up at Radiometer Physics GmbH (diagram from RPG).

The initial results gave a performance of 15-16dB for the conversion loss and a 9000K mixer noise temperature which is below the simulated performance levels. Whilst this is a lower performance than the target it is still a significant achievement to design a working device in this timescale, especially one that is only a little below the target, as these

devices are generally designed by a small group of people with significant experience in the field. Since this testing no other results at this frequency have been published.

When the measurements were taken an LO power of 7mW was available which should have been enough to draw out the peak performance of the design. Varying the LO frequencies with both mixer blocks showed standing wave behaviour between the multiplier and the mixer which was not consistent between the two blocks. This suggests that the diodes were being pumped successfully and that lack of LO power was not likely to be responsible for the performance. Further testing would show this but initially there was no LO power available to complete the tests and no commercial parts were available to build the required set up.

A doubler was being designed and manufactured at RAL in parallel to this work and further measurements were completed at RAL once the doubler was complete, giving LO power of 3-4mW at 332GHz. The LO return loss was measured using a 10dB directional coupler which gave the available LO power of around 1-1.5mW. This gave an LO return loss of -8dB which seemed reasonable given the fact that the LO return loss will degrade due to the under-pumping of the diode.

Bias was applied to one of the diodes in the mixer and varied to try and achieve a good IF match which was successful with a match of better than -10dB conversion loss achieved which suggests the IF matching circuit is ok.

After these diagnostics were unsuccessful in identifying the problem one of the mixer blocks was opened up and imaged in an SEM to look for physical problems. It was suspected that if the diode chip was larger than simulated or if the solder was thicker then there could have been RF coupling between the ohmic pads on the diodes and the channel wall.

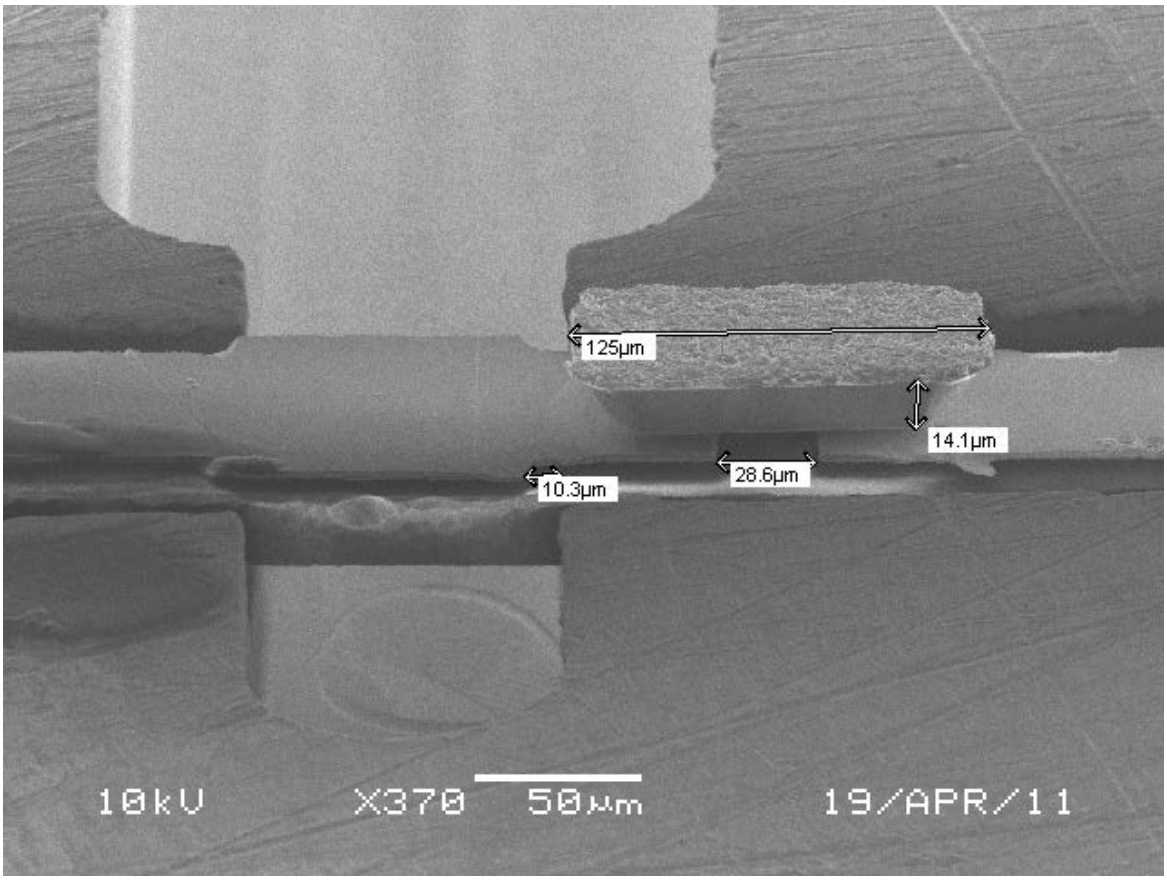

Figure 5-2 – SEM image of inside the mixer block

The only discrepancy which was found was the position of the quartz line in the block which was around 10um out of place making the diodes closer to the RF waveguide to microstrip transition The other dimensions are very close (~1um) to the design. As seen in Figure 5-3 below, this could definitely be responsible for at least some of the discrepancy between the simulated results and the observed performance.

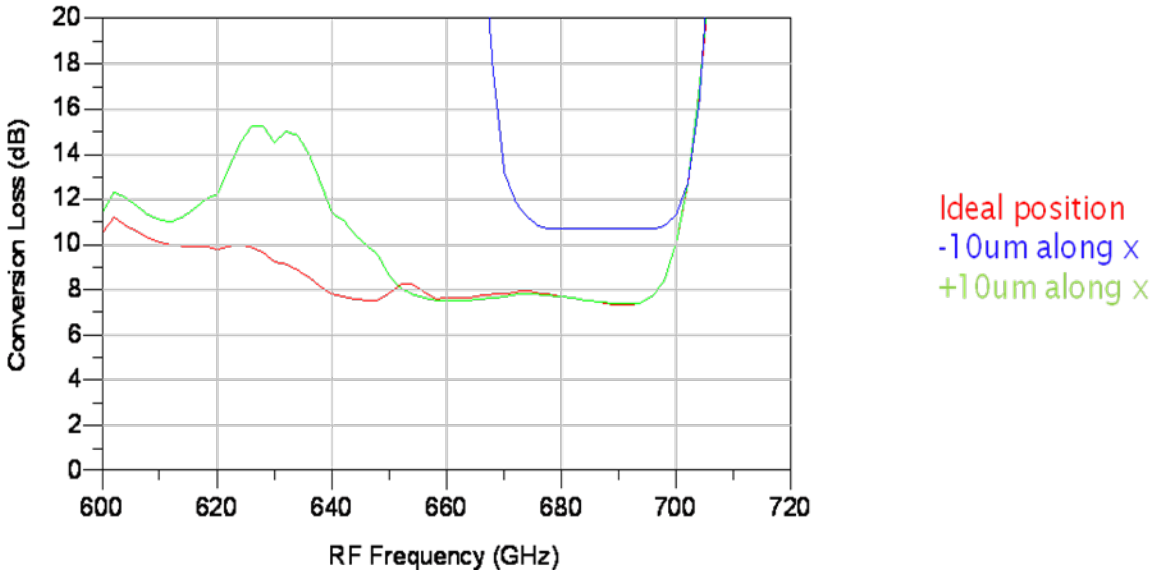

Figure 5-3 – parameter sweep – circuit position in block along x axis

This may seem like a simple adjustment to make, but the assembly of these devices is highly skilled and time consuming work and as a result there was not an opportunity to manufacture and assemble more devices for testing.

Diode results at 664GHz

The diodes optimised in chapter 2 were also used in a mixer design by RPG from which the performance is shown below. The diodes were the same design, but the substrate was thinned down from 15um to 8um for use in the mixer. Performance of around 11dB conversion loss and 3500K Tmix were seen which shows that the diodes are capable of better performance at 664GHz than was observed in the earlier mixer design. This result has not been published and shows that 10dB was an ambitious target in the ESA requirements. This in turn shows that the 15-16dB conversion loss in the mixer detailed in the earlier chapters is a significant achievement.

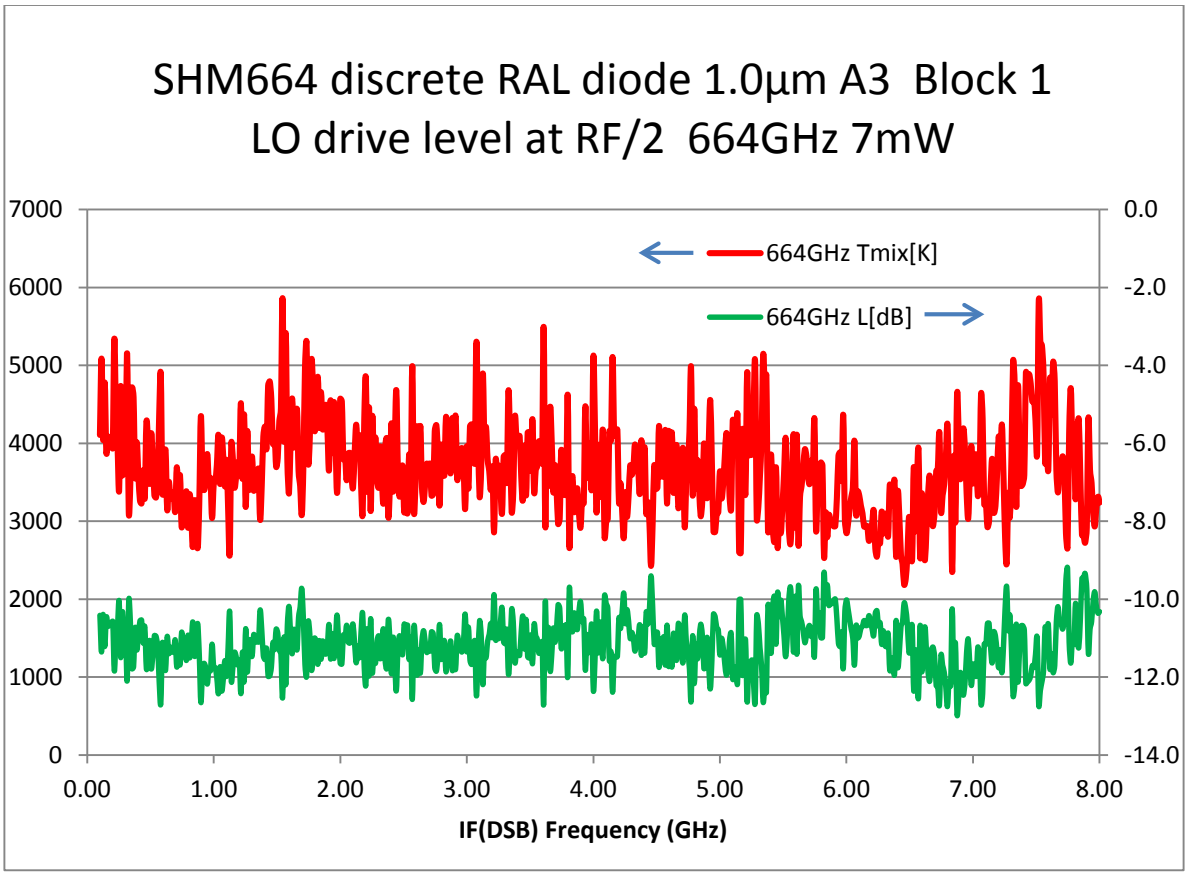

Figure 5-4 – Performance of RPG mixer containing optimised diode – red line is left hand scale and shows Mixer noise temperature, green line is right hand scale and shows mixer conversion loss [42].

Chapter 6 – Conclusion

The main objective of this study was to produce a 664GHz sub-harmonic mixer with state of the art performance. This target set in an earlier chapter has not been met, but the result of a mixer with 15dB conversion loss and 9000K mixer noise is still a significant achievement. Better performance was seen using the optimised diodes in other mixers though with a conversion loss of 11dB attained by an RPG designed mixer. The development of both mixers were funded by ESA as part of their competitive process to identify future instrumentation, so the improved diode designed in this work is very likely to be selected for future Schottky based receivers at this frequency.

The optimisation of the diodes was the first task and the decision to look at the inductance of the fingers first through the basic modelling and then through full 3D simulations paid off. The simulations showed significant performance benefits of the modified design using fingers which started wide and tapered to a point at the anodes.

This modified diode design showed good results when measured in a mixer designed by RPG (Figure 5-3) which is available commercially. The diodes themselves are also available commercially [43] through Teratech Components, a spin-out company from the research group at RAL where this work was completed.

The 664GHz mixer was designed using standard principles and techniques that have shown to be proven. The design choices explained in Chapter 3 should have resulted in a sub-harmonic mixer with state of the art performance that didn't pose any manufacturing hurdles that could not be overcome in a fairly straightforward manner. The 5 section filters were demonstrated to have adequate performance in simulations which would enable the correct signals to reach the correct parts of the circuits. The integrated feedhorn would enable the mixer to be characterised without the complexity (and expense) of manufacturing a corrugated feedhorn which would improve the signal sensitivity of the mixer in use in a scientific instrument.

The position of the filter strip in the block appears to be sensitive according to the analysis completed in Figure 4-42 and this combined with the 10um position error shown in Figure 5-2 seems the most likely reason for the under-performance of the measured mixer compared to the design's simulation results.

Better performance could be attained by re-building the mixers paying particular attention to the position of the filter strip in the block and characterising this properly before testing the high frequency performance of the device. This would enable the hypothesis above to be tested but this could not be completed as part of this thesis due to time constraints. Another iteration of the design may also lead to gains in performance but this would take months of work for the design, manufacture, assembly and testing so was not possible during the study period. It would be a good starting point for future work though.

Future work that would improve the performance would include better characterisation of the basic components of the mixer design and comparison to simulations. This is now possible due to the availability of Vector Network Analysers that operate at the very high RF frequencies in this work but which were not available at the time the design and testing were undertaken. Characterisation of the microstrip, waveguides, filters and waveguide to half height transitions at the appropriate frequencies would better inform the design of the mixer block and enable some of the standards of mixer design to be challenged or re-affirmed. Advances in micro-machining and computer aided manufacturing allow for new topologies using top-down manufacturing methods compared to topologies that are currently used though. New additive manufacturing production techniques like metal powder laser sintering would perhaps allow even more elaborate topologies although mounting the circuit in the block could be the limiting step. This would not be simple though, mainly due to the difficulty in measuring power transmitted through these structures at high frequencies because of the lack of signal power, receivers and other components like directional couplers.

References ..

[1] Low noise broadband fixed tuned SIS waveguide mixers at 660 and 800 GHz - C.E. Honingh et al, University of Cologne, APPLIED SUPERCONDUCTIVITY, VOL. 7, NO. 2, JUNE 1997

[2] E. R. Brown, J. R. Soderstrom, T. C. G. Sollner, L. J. Mahoney, K. M. Molvar, T. C. McGill. Appl. Phys. Lett. 1991, v. 58 (20), p. 2291

[3] Dual Gunn device oscillator with 10mW at 280 GHz, H. Eisele, Electronics Letters 24th May 2007 Vol. 43 No. 11

[4] GaN-based Gunn Diodes: Their Frequency and Power Performance and Experimental Considerations, Egor Alekseev and Dimitris Pavlidis

[5] The Quantum Cascade Laser as a Terahertz Local Oscillator, A.L. Betz, R.T. Boreiko, Nasa ESTC2006

[6] Long wavelength Terahertz Quantum Cascade Lasers, emitting down to 1.2 THz, Walther, C, 6-11 May 2007 Page(s):1 - 2

[7] Emission of Coherent THz Radiation from Superconductors, L. Ozyuzer, A. E. Koshelev, Science 23 November 2007: Vol. 318. no. 5854

[8] Nature Photonics 1, 97 - 105 (2007)

[9] THE MAIN BEAM EFFICIENCY OF CORNER CUBE REFLECTORS - B. Vowinkel, International Journal of infrared and Millimeter Waves, Vol 7, No. L 1986

[10] A dielectric hybrid-mode horn as a gaussian beam-mode antenna in 3-MM band - W. B. Dou, Z. L. Sun, Microwave and Optical Technology Letters Volume 6 Issue 8, Pages 475 - 478

[11] http://www.faqs.org/docs/electric/Semi/SEMI_3.html

[12] HP application Note 956-6 - Temperature dependence of Schottky Detector Voltage Sensitivity

[13] Dynamic Shape of the Depletion Layer of a Submillimeter-Wave Schottky Varactor – Jyrki T Louhi et al, IEEE TRANSACTIONS ON MICROWAVE THEORY AND TECHNIQUES, VOL. 44, NO. 12, DECEMBER 1996

[14] Characterisation and Reliability Testing of THz Schottky Diodes – Christopher M Price, 03 2007, University of Birmingham

[15] Characterisation of European Millimetre-Wave Planar Diodes – Ville S Mottonen et al, 34thEuropean Microwave Conference – Amsterdam, 2004

[16] Low-Noise Submillimeter Receivers Using Single-Diode Harmonic Mixers – N R Erickson, PROCEEDINGS OF THE IEEE, VOL. 80, NO. 11, NOVEMBER 1992

[17] Capability of THz sources based multiplier on Schottky diode frequency chains – J Ward et al, 2004 IEEE MTT-S Digest

[18] Limitations of Microwave and Millimeter-Wave Mixers Due to Excess Noise – Hegazi, G.M et al, Microwave Theory and Techniques, Volume 33, Issue 12, Dec 1985 Page(s): 1404 – 1409

[19] GaAs metallization: Some problems and trends – J M Woodall and J L Freeouf, J. Vac. Sci. Technol., 19(3), Sept. 1981

[20] Effects of the epitaxial layer thickness on the noise properties of Schottky barrier diodes – G. Gomila, JOURNAL OF APPLIED PHYSICS VOLUME 86, NUMBER 2 15 JULY 1999

[21] Advances in THz Heterodyne Detection Technology – Imran Mehdi, ESTC, June 27th, 2006, Maryland

[22] Opening the Terahertz Window With Integrated Diode Circuits – T Crowe et al, IEEE JOURNAL OF SOLID-STATE CIRCUITS, VOL. 40, NO. 10, OCTOBER 2005

[23] 200, 400 and 800 GHz Schottky Diode “Substrateless” Multipliers: Design and results – E Schelecht et al, 2001 IEEE MTT-S Digest

[24] A Monolithic 250 GHz Schottky-Diode Receiver - Steven S. Gearhart and Gabriel M Rebeiz, IEEE TRANSACTIONS ON MICROWAVE THEORY AND TECHNIQUES, VOL. 42, NO. 12, DECEMBER 1994

[25] 600 GHZ PLANAR-SCHOTTKY-DIODE SUBHARMONIC WAVEGUIDE MIXERS - I Mehdi et al, 1996 IEEE MTT-S Digest

[26] A 640 GHz Planar-Diode Fundamental Mixermeceiver - P H Siegel et al, 1998 IEEE M.TT-S Digest

[27] Fixed-Tuned Submillimeter Wavelength Waveguide Mixers Using Planar Schottky-Barrier Diodes - Jeffrey L Hesler et al, IEEE TRANSACTIONS ON MICROWAVE THEORY AND TECHNIQUES, VOL. 45, NO. 5, MAY 1997

[28] General-purpose Fifth-Harmonic Waveguide Mixer for 500-700 GHz, Ville S mottonen, 34thEuropean Microwave Conference - Amsterdam, 2004

[29] Submillimetre-wave receiver developments for ICI onboard MetOP-SG and ice cloud remote sensing instruments - Bertrand Thomas et al, RPG, IGARS Symposium 2012

[30] A broadband 440-590 GHz receiver - Jeffrey Hesler et al, IRMWW-Thz 2011

[31] A 200 GHz Broadband, Fixed-Tuned, Planar Doubler - David W Porterfield, Virginia Millimeter Wave, Inc.

[32] A 260-340 GHz Dual Chip Frequency Tripler for THz Frequency Multiplier Chains - Maestrini et al, THz Technology, Ultrafast Measurements, and Imaging, WedB1l-6

[33] A HIGH EFFICIENCY FREQUENCY DOUBLER FOR 100 GHz - Marek T. Fabert, 1985 IEEEMTT-S Digest

[34] Capability of THz sources based on Schottky diode frequency multiplier chains - John Ward et al, 2004 IEEE MTT-S Digest

[35] From Chips to (Space) Ships: Status of Solid State LO Sources for THz Receivers – Imran Mehdi

[36] On the Development of a High Efficiency 750 GHz Frequency Tripler for THz Heterodyne Systems – Anders Rydberg et al, IEEE TRANSACTIONS ON MICROWAVE THEORY AND TECHNIQUES, VOL. 40, NO. 5. MAY 1992

[37] Performance Evaluation of Multiplication Chains up to THz Frequencies – Jesus Grajal et al, 2004 Joint 29'" Int. Cont. on Infrared and Millimeter Waves and 12' Int. Conf. on Terahetiz Electronics

[38] Progress Toward Solid-state Local Oscillators at 1 THz – T W Crowe et al, IEEE MICROWAVE AND GUIDED WAVE LETTERS, VOL. 6, NO. 5, MAY 1996

[39] http://www.ee.scu.edu/eefac/healy/indwire.html from E.B. Rosa, "The Self and Mutual Inductances of Linear Conductors", Bulletin of the Bureau of Standards, Vol.4, No.2, 1908, Page 301ff.

[40] B. Thomas, A. Maestrini and G. Beaudin. A Low-Noise Fixed-Tuned 300-360 GHz Sub-Harmonic Mixer Using Planar Schottky Diodes. IEEE Micowave And Wireless Component Letters, vol. Vol. 15, no. No. 12, December 2005. 39, 42

[41]VNA frequency extenders to 1.1 THz – Thomas W Crowe et al, IRMMW-THz 2011

[42] M. Brandt, Radiometer Physics GmBH – Test Report (Document D3) Sub-Millimetre Wave Receiver Front-End for ESA Contract Nr: 22032/08/NL/JA – RPG/664FE/RP/2011-035

43 http://www.teratechcomponents.com/products-and-services/#AP2

Other Sources:

Microwave Mixers (Second Edition) – Stephen A Maas, Artech House

Semiconductor Devices, Physics and Technology (Second Edition) – S M Sze, Wiley

Mixers review paper – M Devlin, Plextek Communications Technology Consultants

HP Application Note 995 from http://cp.literature.agilent.com/litweb/pdf/5954-2073.pdf